63-3-6

406134

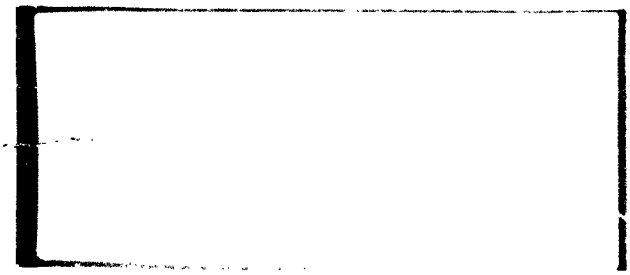

406134

DDC
RECEIVED
MAY 24 1963
TISIA A

Alkaline Battery Division

GULTON INDUSTRIES, INC.

Metuchen, N. J.

STATE OF CHARGE INDICATORS FOR NICKEL CADMIUM BATTERIES

TECHNICAL DOCUMENTARY REPORT
NO. ASD-TDR-63-191

February, 1963

Directorate of Aeromechanics
Aeronautical Systems Division
Air Force Systems Command
Wright-Patterson Air Force Base, Ohio

Project No. 8173, Task No. 817304-15

DDC
RECEIVED
MAY 24 1963
TISIA A

(Prepared under Contract No. AF 33(657)-8130
by the Gulton Industries, Inc., Metuchen, New Jersey;
M. Lurie, H. N. Seiger, R. C. Shair, authors.)

NOTICES

When Government drawings, specifications, or other data are used for any purpose other than in connection with a definitely related Government procurement operation, the United States Government thereby incurs no responsibility nor any obligation whatsoever; and the fact that the Government may have formulated, furnished, or in any way supplied the said drawings, specifications, or other data, is not to be regarded by implication or otherwise as in any manner licensing the holder or any other person or corporation, or conveying any rights or permission to manufacture, use, or sell any patented invention that may in any way be related thereto.

Qualified requesters may obtain copies of this report from the Armed Services Technical Information Agency, (ASTIA), Arlington Hall Station, Arlington 12, Virginia.

This report has been released to the Office of Technical Services, U.S. Department of Commerce, Washington 25, D.C., for sale to the general public.

Copies of this report should not be returned to the Aeronautical Systems Division unless return is required by security considerations, contractual obligations, or notice on a specific document.

FOREWORD

This Final Technical Report was prepared by Gulton Industries, Inc., Metuchen, N. J., for the Aeronautical Systems Division, Wright-Patterson Air Force Base, Ohio, under Contract No. AF 33 (657)-8130. Mr. J. E. Cooper and Mr. W. S. Bishop were task engineers for the Aeronautical Systems Division. We wish to acknowledge the helpful discussions held with them.

The studies reported cover the complete contract period from January 1962 to January 1963.

ABSTRACT

The variations of several electrical properties of nickel cadmium cells with state of charge were studied to determine the suitability of any of these for measuring state of charge. Three methods were originally proposed: measurements of ohmic resistance, microsecond transients and double layer capacitance. During the investigations two additional parameters were measured, a. c. impedance and phase shift.

Double layer capacitance and a. c. impedance and transient behavior are not useful properties for determining state of charge.

A phase shift system is described which when properly calibrated predicted state of charge with an average deviation of $\pm$ 10%. Ohmic resistance measured under correct conditions showed a closer correlation to state of charge but is difficult to measure.

PUBLICATION REVIEW

The publication of this report does not constitute approval by the Air Force of the findings or conclusions contained herein. It is published for the exchange and stimulation of ideas.

TABLE OF CONTENTS

		Page
1.	Introduction	1
2.	Analysis of Electrical Properties of Cells	4
3.	Double Layer Capacitance	7
4.	Transient Peak Height	10
5.	Impedance at Audio Frequencies	11
6.	Phase Shift	13
7.	Internal Resistance	21
8.	Conclusions and Recommendations	28
	References	30
Appendix I.	Operation of Breadboard State-of-Charge Indicator	31
Appendix II.	Calculation of Time and Current Dependence of Resistance of a Cell	35
Appendix III.	Calculation of Resistance of Mercury Switch	37

LIST OF TABLES

		Page
1.	Double Layer Capacitance, F, at Various Residual Capacities	40
2.	Impedance of 4 A-H Cells at Various States of Charge	43
3.	Predicted and Actual Residual Capacities for Batteries on Manual Cycle	44
4.	Predicted and Actual Residual Capacities for Batteries on Automatic Cycle	48
5.	Predicted and Actual Residual Capacities for Batteries on Shelf Stand	49
6.	Predicted and Actual Residual Capacities for Batteries Charged at Modified Constant Potential	50
7.	Predicted and Actual Residual Capacities for KO-35 Cell and 4KO15 Battery	51
8.	Effective Resistance at Various States of Charge	52
9.	Predictions of Residual Capacity from Resistance	54
10.	Resistance of Rotary Switch and Components	57

LIST OF TABLES

		Page
1.	Double Layer Capacitance, F, at Various Residual Capacities	40
2.	Impedance of 4 A-H Cells at Various States of Charge	43
3.	Predicted and Actual Residual Capacities for Batteries on Manual Cycle	44
4.	Predicted and Actual Residual Capacities for Batteries on Automatic Cycle	48
5.	Predicted and Actual Residual Capacities for Batteries on Shelf Stand	49
6.	Predicted and Actual Residual Capacities for Batteries Charged at Modified Constant Potential	50
7.	Predicted and Actual Residual Capacities for KO-35 Cell and 4KO15 Battery	51
8.	Effective Resistance at Various States of Charge	52
9.	Predictions of Residual Capacity from Resistance	54
10.	Resistance of Rotary Switch and Components	57

LIST OF FIGURES

		Page
1.	Equivalent Circuit for Nickel Cadmium Cell	58
2.	Equivalent Circuit for Half-Cell	59
3.	Circuit for Demonstrating Transient	60
4.	Initial Transient, 4 A-H Cell	61
5.	Mechanical Switch for Pulse Measurements	62
6.	Schematic for Electronic Switch	63
7.	Variation of Double Layer Capacitance with Residual Capacity	64
8.	Variation of Double Layer Capacitance with Residual Capacity	65
9.	Transient Peak Height at Various Residual Capacities	66
10.	Transient Peak Height for Two Cycles on Three Cells	67
11.	A.C. Kelvin Double Bridge	68
12.	Impedance Vs. Frequency for 4 A-H Cells	69
13.	100 cps. Impedance at Various States of Charge	70
14.	Apparatus for Measuring Resonant Frequency	71
15.	Apparatus for Measuring Phase Shift at 60 cps	72
16.	Diagram of Phase Measuring System	73
17.	Resonant Frequency Vs. Residual Capacity	74
18.	Resonant Frequency Vs. Residual Capacity	75
19.	Phase Shift at Several Frequencies Vs. Residual Capacity	76
20.	40 Cycle Phase Shift Vs. Residual Capacity	77

LIST OF FIGURES (Cont'd)

		Page
21.	Calibration Curve at Room Temperature	78
22.	Calibration Curves at Fixed Temperatures	82
23.	Calibration Curve Showing Extreme Points	83
24.	Distribution of Deviation, Histogram	84
25.	Mechanical High Current Switch	85
26.	Wiring Diagram of Mechanical Switch	86
27.	Oscilloscope Display to Measure Resistance During High Current Pulse	87
28.	Effective Resistance Vs. Current and Time	88
29.	Four Methods of Connecting Voltage Leads to a Cell	89
30.	Average Curve of R_0 Vs. R. C.	90
31.	Resistance of Cell Permanently Connected to Apparatus	91
32.	Design of Ultra-Low Resistance Switch	92
33.	Block Diagram of Breadboard State of Charge Meter	93
34.	Layout of Breadboard State of Charge Meter	94
35.	Schematic of 40 Cycle Power Amplifier	95

ABBREVIATIONS USED IN REPORT

A-H	Ampere-Hours
C	Capacitance
CRO	Oscilloscope
cps	Cycles per Second
E	Electromotive Force
f	Frequency in Cycles per Second
F	Magnitude of double layer capacitance in Farads
H	Henries
I	Current
j	$\sqrt{-1}$
L	Inductance
R	Resistance, subscript indicates patticular resistor
RC	Residual capacity, in Ampere-Hours
ω	Angular frequency = $2\pi f$
v,V	Voltage
Z	Impedance

1. INTRODUCTION

The purpose of the work reported here has been to investigate several proposed methods of measuring state of charge of Ni-Cd batteries. These investigations were to lead to a breadboard state-of-charge indicator. This report covers the contract period from commencement in February 1962 to January 1963. The required breadboard design has been completed and preliminary evaluation tests show that the device can predict the remaining capacity in batteries that have been used recently as well as batteries that have been stored for some time. For favorable conditions, an average error of $\pm$ 10% has been consistently obtained.

There have been several previous efforts to find a method for measuring state of charge of Ni-Cd batteries. Recent efforts have included studies of (i) dyes, (ii) charge and discharge characteristics and (iii) impedance at audio frequencies by Fleischer, (1) and (iv) a very extensive study of charge-discharge tests by Kordesch and Kornfeil.[2] Fleischer concluded that none of the techniques he studied were acceptable state-of-charge indicators. Kordesch and Kornfeil devised a means of measuring the polarization resulting from charge or discharge without the effect of the internal ohmic resistance of the cell. Kordesch incorporated this technique into a battery tester based on charge-discharge characteristics.[3] Prototypes of this tester were built by the Vitro Corporation and were put through extensive tests by Gulton Industries under contract to the Signal Corps (Contract No. DA 36-039 SC-85066). The conclusion reached at the end of those tests was that the device was not an acceptable battery tester.[4] To be acceptable, a device would generally have to:

1) Have an accuracy of $\pm$ 5% (although a larger error might still prove very useful).

2) Not discharge the battery appreciably during the measurement.

3) Give a reading independent of cell history.

4) Be operable by an unskilled person and not require more than a few minutes for a measurement.

Since the simplest access to a cell and the only access to a sealed cell is via the terminals, it would be most desirable to find some electrical property of a cell, one that could be measured at the terminals, that depends on state of charge. For this reason,

Manuscript released by the authors January 1963 for publication as an ASD Technical Documentary Report.

1. INTRODUCTION

The purpose of the work reported here has been to investigate several proposed methods of measuring state of charge of Ni-Cd batteries. These investigations were to lead to a breadboard state-of-charge indicator. This report covers the contract period from commencement in February 1962 to January 1963. The required breadboard design has been completed and preliminary evaluation tests show that the device can predict the remaining capacity in batteries that have been used recently as well as batteries that have been stored for some time. For favorable conditions, an average error of $\pm$ 10% has been consistently obtained.

There have been several previous efforts to find a method for measuring state of charge of Ni-Cd batteries. Recent efforts have included studies of (i) dyes, (ii) charge and discharge characteristics and (iii) impedance at audio frequencies by Fleischer, (1) and (iv) a very extensive study of charge-discharge tests by Kordesch and Kornfeil.(2) Fleischer concluded that none of the techniques he studied were acceptable state-of-charge indicators. Kordesch and Kornfeil devised a means of measuring the polarization resulting from charge or discharge without the effect of the internal ohmic resistance of the cell. Kordesch incorporated this technique into a battery tester based on charge-discharge characteristics.(3) Prototypes of this tester were built by the Vitro Corporation and were put through extensive tests by Gulton Industries under contract to the Signal Corps (Contract No. DA 36-039 SC-85066). The conclusion reached at the end of those tests was that the device was not an acceptable battery tester.(4) To be acceptable, a device would generally have to:

1) Have an accuracy of $\pm$ 5% (although a larger error might still prove very useful).

2) Not discharge the battery appreciably during the measurement.

3) Give a reading independent of cell history.

4) Be operable by an unskilled person and not require more than a few minutes for a measurement.

Since the simplest access to a cell and the only access to a sealed cell is via the terminals, it would be most desirable to find some electrical property of a cell, one that could be measured at the terminals, that depends on state of charge. For this reason,

Manuscript released by the authors January 1963 for publication as an ASD Technical Documentary Report.

the approach used in this work was to study those electrical characteristics of cells that were shown to vary with state of charge. Many such properties were found, but for reasons involving their measurability, consistency and form of variation, most of these properties were unsuitable. Many electrical characteristics are appreciably different for fully charged and discharged cells, but remain nearly constant as a cell is discharged from 100% to 20% of capacity, most of the change occurring abruptly between 20% c arge and complete discharge. Two of the properties studied were found to vary with state of charge in such a way that useful information could be obtained. These were the phase shift and ohmic resistance to be discussed in Sections 6 and 7.

The work was divided, logically and chronologically, into three general phases:

1) Observe any properties that vary with state of charge.

2) Devise equipment to measure these properties.

3) Using 2, examine the variation closely, noting in particular,

   a) How small a change in state of charge is detectable

   b) How consistent is the variation? From cell to cell? Cycle to cycle?

Following this approach, five properties of cells were studied carefully:

1) Phase shift of cell voltage compared to current

2) Internal resistance during a short, high current pulse

3) Double layer capacitance

4) Height of transient following a sudden change in current.

5) Impedance at audio frequencies

The last three were eliminated after experiments showed that these properties did not depend of state of charge in a consistent, useful manner. Detailed studies of the first two properties account for the largest part of the exploratory phase of this work. The variation of phase shift was first observed while the impedance was being measured. Its dependence on state of charge was then established empirically.

Although the term "state of charge" is widely used in battery literature, the residual capacity -- the actual number of ampere-hours available from the battery at a particular time -- is a more useful number because it can be measured directly by simply discharging the battery. In this report the results of measurements and predictions of battery condition are given as residual capacity in ampere-hours. Because the term occurs so frequently, the authors have taken the liberty of using the abbreviation RC.

2. ANALYSIS OF ELECTRICAL PROPERTIES

A brief theoretical discussion of the electrical prcperties of Ni-Cd cells is now given to show the relation of the various properties studied. The electrical model shown in Figure 1 has a sine and transient response close to that of a cell and, therefore, is a good heuristic device for providing an understanding of cell properties.

The circuit of Figure 1 can be arrived at on purely physical grounds by considering the half-cell in Figure 2. Let there be a current flowing into the negative terminal and through the electrolyte to some other electrode. The current first encounters resistance and inductance due to the terminal hardware and electrode material. Next the current sees a rise in potential between the electrode and the main body of the electrolyte. In the electrolyte, the current encounters more resistance. There is a capacitance between the electrode and the layer of charged ions in the electrolyte near the electrode. This is the double layer capacitance. The dashed line parallel to the electrode in Figure 2 indicates the effective position of the layer, though it is really diffuse. The double layer can be considered as a capacitance with one end connected to the electrode and the other end somewhere in the electrolyte. Following the discussion above, the half-cell equivalent circuit in Figure 2 (a) was drawn. In the same manner, a mirror image circuit can be obtained for a positive electrode in the same electrolyte. These will connect as in Figure 2(b). Combining all similar series elements, e.g. adding all series resistors to form one larger resistor, yields the circuit in Figure 2 (c). If the time constants of the two RC sections are nearly the same, these can be combined into one RC section yielding the equivalent circuit in Figure 1. The resonant frequencies of the positive and negative electrodes compared to an Hg/HgO reference were measured and found to be of the same magnitude so this is a satisfactory approximation.

Certainly the above discussion is descriptive, not rigorous. Its justification and utility lies in its ability to explain the sinusoidal and transient properties of a cell. The element values can be found from high and low audio frequency measurement. For a V04 nickel-cadmium cell, these values are, approximately,

$$L \sim 10^{-6}\ \text{H}$$

$$R \sim 10^{-3}\ \text{Ohms}$$

$$R \sim 10^{-3}\ \text{Ohms}$$

$$C \sim 10\text{F}$$

$$E \sim 1.3\ \text{V}.$$

Using these values, the approximate resonant frequency can be predicted.

The impedance of the equivalent circuit is given by:

$$Z = R_L + j\omega L + \frac{-\frac{jR_C}{\omega C}}{R_C - \frac{j}{\omega C}} \qquad (1)$$

Separating real and imaginary parts

$$Z = \frac{R_L R_C^2 + \frac{R_L + R_C^2}{\omega^2 C^2} + j\left[-\frac{R_C^2}{\omega C} + \omega R_C^2 L + \frac{L}{\omega C^2}\right]}{R_C^2 + \frac{1}{\omega^2 C^2}} \qquad (2)$$

For resonance, the imaginary part of Z is zero, so

$$\frac{R_C^2}{\omega C} = \omega R_C^2 L + \frac{L}{\omega C^2} \qquad (3)$$

$$\omega^2 = \frac{R_C^2 C - L}{R_C^2 C^2 L} \qquad (4)$$

$$\text{Resonant frequency, } f = \frac{1}{2\pi} \sqrt{\frac{R_C^2 C - L}{R_C^2 C^2 L}} \qquad (5)$$

Substituting the orders of magnitude given for the components above,

$$f = \frac{1}{2\pi} \sqrt{\frac{10^{-5} - 10^{-6}}{10^{-10}}} \cong 50 \text{ cps} \qquad (6)$$

Actual resonant frequencies for 4 A-H cells were measured from 60 to 150 cps. Clearly this is within the accuracy of the order of magnitude calculation.

The transient behavior observed when a cell is short circuited can also be predicted from this circuit. The actual calculations are lengthly and not relevant in this report so the result will be given without derivation. The current, I, when a cell is short circuited is given by,

$$I = \frac{E}{R_L + R_C} (1 - e^{-bt}) \quad (7)$$

Figure 3 is a schematic representation of the various switch circuits used to measure cell transients. When S is open, the oscilloscope sees the open circuit cell voltage. When S is closed, the current I rises according to the equation above. The voltage displayed is IR_s, where R_s is the resistance of the switch when it is closed. After S is closed this voltage drops to zero then rises exponentially as I rises. The voltage does not rise to the open circuit voltage because of the drop across R_L and R_C and polarization. This is just the transient behavior observed in Figure 4.

The state-of-charge dependence of the five electrical properties mentioned in the Introduction will now be discussed in detail.

3. DOUBLE LAYER CAPACITANCE

At any solid-liquid interface there exists a double charged layer. On the solid, the electrode in our case, the charge is gotten either by absorption or ionization. Ions of opposite charge are distributed near the electrode and are held there by an electrostatic attraction. The layer of charge in the solution is not discrete, but is diffuse. By assuming that there is a plane representing the locus of the charges in this diffuse layer, the double layer is seen. Since the electrodes with which we are dealing are flat plates the capacitance per unit area is given by:

$$C = \frac{k}{4\pi d} \qquad (8)$$

In sintered plate nickel-cadmium cells this capacitance is very large, in the order of 10 Farads for a VO4 cell.

The voltage across the double layer is given by:

$$V = \frac{4\pi d\sigma}{k} \quad , \qquad (9)$$

so that one may write the well-known equation,

$$V = \frac{\sigma}{C} \, . \qquad (10)$$

Multiplying the surface charge and the capacitance per unit area by the total surface area and differentiating, one obtains,

$$F = \frac{I}{dv/dt} \qquad (11)$$

This equation was the basis for measurement of the double layer capacitance in these experiments. A know discharge current was passed through the cell and the time rate of change of voltage was measured. Because F is very large this slope is small even for large currents. Furthermore, the time interval during which the slope can be measured is fixed at about 3 milliseconds because the measurement must be made after the transient has decayed and before polarization sets in further depressing the voltage.

TECHNIQUE

The voltage decay and current were measured simultaneously using a Tektronix 502 dual beam oscilloscope. A resistive load was placed across a cell by means of a switch and the ensuing current and voltage decay were photographed with an oscilloscope camera. To determine I from the oscillogram, the zero current level had to be recorded as well as the current after the resistor was connected across the cell. This was accomplished by triggering the oscilloscope before the switch was closed. The switch shown in Figure 5 was first used for this measurement. The small spring contact triggered the oscilloscope before the main contacts closed. Thus, the short trace before the current flowed indicated the zero current level. For the small slope found - about 0.3 mV/msec - the noise superimposed on the voltage trace because of contact bounce in the switch caused a large error. To produce a cleaner pulse and provide a more controllable trigger pulse, an electronic switch, shown in Figure 6, was built. This switch used a silicon controlled rectifier, (SCR) to turn on the current. The oscilloscope was triggered 0.2 millisecond before the gate was applied to turn on the SCR. Once the SCR is turned on, the cell discharged until the circuit was opened.

Using this electronic switch, the current and voltage displays were completely free of noise and ripple. The photograph in Figure 4 was made with this switch. The elimination of noise in the trace halved the errors in determining the double layer capacitance. Furthermore, to take full advantage of the quality of the oscilloscope trace, the camera was critically focussed and the oscillograms were measured under magnification. Thus, double layer capacitance measurements were made in three stages namely:

1) Mechanical knife switch

2) Electrical switch

3) Electrical switch and critical camera focussing plus measurements with magnification.

Each stage halved the error of the previous one. Typical data are given in Table 1. With the best technique, the capacitance could be measured to about 1 Farad.

RESULTS

The double layer capacitance, F, varies as shown in Figure 7. For 4 A-H cells, F varied from a maximum of 23 Farads for a fully charged cell to 3 Farads for a discharged cell. The slope of capacitance

vs. RC is not as large as this would indicate, though, because F for any one cell did not vary from 3 to 23 Farads. The actual slope of F vs. RC is about 3 F/A-H. With an estimated uncertainty of 1 Farad in measuring F, the RC should be determined within 1/3 A-H. However, variations from cell to cell and cycle to cycle were so great that little was learned about RC by measuring the double layer capacitance. For cell No. 21 in Figure 7, for example, F was 23.5 at 5 A-H for one cycle and 23.5 at 2.8 A-H on the next cycle. Figure 8 again shows the displacement of the F vs. RC curves for two cycles.

Although the errors in measuring the double layer capacitance were halved by each of two improvements in the measuring technique, no improvement in the ability to predict state of charge resulted because of large variations among cells and cycles. As a result, double layer capacitance can not be used to indicate state of charge.

4. TRANSIENT PEAK HEIGHT

When a current is suddenly passed through a cell the terminal voltage shows an initial transient which decays in a few milliseconds. This behavior was predicted in Section 2 for short circuit currents and demonstrated in Figure 4. A decrease in transient peak height with decreasing RC was observed so investigations were started to see if the transient could indicate state of charge.

TECHNIQUE

The transient peak height was measured from photographs of oscilloscope displays of voltage and current. Figure 4 shows such an oscillogram. Two parameters of the transient were measured. The first was the voltage difference between the open circuit voltage and the minimum voltage, P_1 in the figure. The second was the voltage difference between the minimum voltage and the maximum return voltage, P_2 in the figure. The electronic switch used to produce the discharge is shown in Figure 6. This switch does two things:

1) Triggers the oscilloscope just before the pulse begins.

2) Connects a resistor across the cell thereby drawing current and producing the pulse.

No additional batteries were used to drive the current through the cell so any effects observed were due to the cell itself. The switch produced a smoothly rising current with a rise time of less than 0.1 milliseconds. The current was generally about 7 Amps, the transient peak height in the range of 20 millivolts.

RESULTS

Neither interpretation of the peak height of the transient showed a reliable dependence on state of charge. Many cells showed a marked increase in both P_1 and P_2 with increasing residual capacity while some showed no change, or, in a few cases an opposite change. Data for one cell could not always be reproduced several cycles later. Transient peak height P_1 at various values of RC are shown in Figure 9. Figure 10 shows the variation of P_1 from cell to cell and from cycle to cycle. P_2 shows a more random distribution.

Since no reproducible variation of transient peak height with state of charge was found, this technique cannot be used in a state of charge indicator.

5. IMPEDANCE AT AUDIO FREQUENCIES

The effective internal impedance of a cell, i.e. the change in terminal voltage due to a change in current through the cell, can be considered as a sum of an electrical impedance and a chemical impedance. The chemical impedance is, in turn, made up of the concentration polarization, activation polarization and double layer charging. The electrical impedance is produced by the plate materials, hardware and terminals and is expected to depend on the state of charge since the resistivity of the active materials in the plates is different from that of the inactive materials. In particular, Cd is a good conductor and $Cd(OH)_2$ is a poor one. Therefore, measuring the ohmic-electrical-component of the internal resistance could indicate the state of charge.

TECHNIQUE

Two techniques were used to measure impedance. The first, known as the direct method, is simply the application of Ohm's Law. The cell voltage and current are measured simultaneously; the impedance is the voltage divided by the current. Much higher precision was obtained using the second technique, a bridge. The apparatus is shown in Figure 11. It is an a.c. version of the Kelvin Double Bridge. Current is passed through the cell (½ Amp. p-p) via one set of leads and the voltage is sensed with a separate set of leads. The voltage across the slide wire is balanced against the cell voltage to obtain a null. Once the bridge is calibrated, the length of the slide wire uses, S, varies directly with the cell impedance. Using a one meter wire with knife contacts to adjust the length S, impedance was measured $\pm$.05 milliohms.

RESULTS

Figure 12 shows that at 100 cps, a fully discharged cell (1.0 V end point at C/2 rate) had an appreciably higher impedance than a charged cell. However, at 1Kc and higher, there was no detectable difference in impedance. For this reason, bridge measurements were made of impedance of three VO4 cells at frequencies from 50 to 500 cps for varying states of charge. These data are given in Table 2. For VO4 cells containing more than 1 AH no predictable dependence of impedance on state of charge was found. Figure 13 is a plot of data for the three VO4 cells at 100 cps. The short horizontal lines indicate the uncertainty in impedance. Note that the random variation of impedance is well outside the range of error with the exception of a marked rise in impedance at zero residual capacity. These results agree with those found by Fleischer.[1]

Since impedance measurements apparently indicate only whether a cell has more or less than 20% capacity, impedance is not a useful indicator of state of charge.

6. PHASE SHIFT

During the investigation of the impedance of cells at audio frequencies, a phase shift produced by the cells was observed. When the impedance was measured by the direct method, the magnitude of Z, the impedance, was determined by dividing the magnitude of the voltage by the magnitude of the current, but the voltage and current were not in phase. Furthermore, the difference in phase was found to vary with state of charge. Because observing a phase shift of zero, i.e. resonance, was easier than actually measuring an unknown phase angle with the equipment available, the resonant frequency was measured and this, too, was found to depend on state of charge. Let us now carefully define these terms for this particular application:

Phase Shift - difference in phase between the sinusoidal component of cell voltage and the sinusoidal current through the cell. The shift is taken as positive when the voltage leads the current.

Resonant Frequency - frequency at which the phase shift is zero. The peak in voltage or current usually associated with resonance is not found here because the resonance is very highly damped.

Accurate measurements of the resonant frequency were difficult because the Q of the cells was very low, i.e. the phase shift varied slowly with frequency so the exact minimum in phase shift was hard to find. Measuring the phase shift at a particular frequency proved to be more accurate once the proper equipment was obtained. Phase shift measurements are more desirable than resonance measurements from the point of view of building apparatus because the phase measurements are made at one frequency only. Therefore, the various oscillators, amplifiers, filters, and other components in the apparatus have to operate at only one frequency greatly simplifying their design.

Phase and frequency measurements, in general, have an advantage over measurements of the magnitudes of voltages or currents. When measuring small voltages, for example, interference and losses due to poor contacts and long leads produce large errors. However, when measuring phase or frequency, only a time must be measured so changes in the magnitudes of the signals cause no errors.

RESONANT FREQUENCY APPARATUS

Figure 14 shows the apparatus used to determine the resonant frequency. The voltage across the shunt is in phase with the current. When the sine component of the cell voltage, v, is out of phase with the current it is also out of phase with the voltage across the shunt,

V. For this situation the trace on the oscilloscope is an ellipse. At the frequency for which the cell produces no phase shift, V and v are in phase and the ellipse degenerates to a straight line. A phase difference of about 1/2" could be detected under the best conditions.

To determine the resonant frequency, the frequency of the oscillator was changed until the ellipse became a straight line. The error in determining the resonant frequency was $\pm$ 5 cps.

PHASE SHIFT APPARATUS

Preliminary phase measurements were made at frequencies of 60, 400 and 1000 cps. The apparatus used for the 60 cycle measurements is shown in Figure 15. The voltage across the cell is fed to the vertical input of the oscilloscope. The voltage across the resistor is fed through a phase shift circuit to the horizontal input. When the oscilloscope trace is a straight line, indicating zero phase angle, the shift produced by the phase shifter must be equal and opposite to that produced by the cell. For 60 cycles, which is below the resonant frequency, a monotonic variation of phase shift with state of charge was found. For 400 and 1000 cycles, both above the resonant frequency, the variation was not monotonic.

Because the results obtained with the apparatus in Figure 15 were encouraging, a system was built to make more accurate phase shift measurements. This consisted of a Waveforms 401C oscillator to provide any required frequency and an Ad-Yu 405 Precision Phase Meter to measure phase shift. Several amplifiers and small parts were also required to provide the proper signals. After several changes in design the system in Figure 16 was evolved. This system provided a current whose frequency could be set within 1%, and measured phase shifts within 0.25°.

The alternating current from the output of the audio amplifier passed through the cell. The amplitude and frequency were adjusted using the controls on the oscillator. Probes touched to the cell terminals fed the cell voltage through a D.C. blocking filter to a balanced pre-amplifier then to the phase meter. The voltage across the 4 Ohm non-inductive resistor (capacitance can be neglected for such a low value resistor) in series with the cell was also fed to the phase meter as a reference since that voltage was in phase with the current through the cell. The phase meter read the difference in phase between the cell voltage and the current.

This phase shift was the combined shifts of the cell and all the leads and components in the system. The shift produced by everything except the cell was determined by substituting a 1.0 milliohm shunt for the cell and reading the phase shift. The shunt was known to produce no measurable shift. The required phase angle was the difference between that read with the cell and that read with the shunt. In the later portions of the work when all the measurements were restricted to one frequency, the RC network labelled "Phase Shifter" in Figure 16, was added. This network introduced a phase shift equal

but opposite to the shift of the system at 40 cycles. Therefore, at 40 cycles, the meter read cell phase shift directly.

The details of operating the final breadboard version of the phase shift system are given in Appendix I.

For cells of 4 and 9 A-H capacities a current of 1 A p-p gave a sufficient signal (IV. p-p) at the output of the pre-amplifier to operate the phase meter within its rated accuracy. Frequent adjustment of the phase meter was required when it was first used but, as the device has aged, the intervals between re-adjustments have extended to about a week. The adjustment takes about 20 minutes. The Ad-Yu Co., manufacturer of the phase meter, claim that these adjustments are necessary for the low input levels because of tube aging.

RESULTS

The resonant frequency was found to vary with state of charge. However, the range of values of RC at a particular resonant frequency was about 25% of the nominal capacity. This means that if the resonant frequency were used to predict RC there would be an uncertainty of 25% in the prediction. At first it was thought that the spread of values might be due to variations among cells and that once a cell was known to yield high or low values of resonant frequency the necessary corrections could be added to the resonant frequency to yield consistent, accurate results. However, more extensive data showed that the variations are random. Approximately the same range of values was obtained by recording several cycles on one cell or one cycle on each of several cells. Note that the spread of values in Figure 17 which shows several cycles on four cells is not greater than that in Figure 18 which shows eight (8) cycles on only one cell.

Phase measurements at various states of charge were made at fixed frequencies of 40, 60, 100, 120 and 200 cycles. Figure 19 shows the phase shift at each of these frequencies versus RC. For the 40 cycle curve, the spread of points above and below the curve is about 0.3 A-H. This is an uncertainty of 8% since the cells have a nominal capacity of 4 A-H. Because the change of phase shift with RC is larger for 40 cycles than for the other frequencies, further tests were run at 40 cycles only. This simplified the measuring procedure and, of course, would simplify construction of future measuring systems; the VFO and amplifier could be replaced by a 40 cycle power oscillator and all the other components would have to operate at 40 cycles only. Forty (40) cycle phase shift measurements for six (6) cycles on each of three cells are shown in Figure 20. The spread in RC at a particular phase shift is 15%. Having established the variation of 40 cycle phase shift with RC, the applicability of

this technique to a practical state of charge indicator had to be determined. This involved finding the exact dependence of phase shift on RC, determining the uncertainty in RC at a given phase shift and testing the reproducibility of the data for batteries with varied histories.

Up to this point, measurements were made on cells because it was felt that the simplest systems should be studied first. A practical state-of-charge indicator, of course, would be used on batteries so the problem of testing an entire battery was considered in the light of the cell data. When testing a battery of any number of cells, the 40 cycle current leads were attached to the main battery terminals, but the voltage of each cell had to be picked off at the terminals of that cell. Thus, an operator would connect one set of current leads, then read the shift of each cell in turn. This is necessary because the phase angle of a sum of sinusoidal voltages depends not only on the angle of each voltage, but on their relative amplitudes, the larger signals, from cells with higher 40 cycle impedance, dominating the total signal. To demonstrate this, three cells were connected to form a 3.9 V battery. The total phase shift showed no significant relationship to RC or to the phase shift of each cell. However, the angles read for each cell were the same before and after assembly into the battery. Apparently data on cells can be applied directly to batteries made up of the same type of cells.

CALIBRATION

To determine RC using the phase shift method, a curve of RC versus phase shift was made. This curve calibrates the phase meter in terms of RC. Referring to the calibration curves, Figure 21 for room temperature, and Figure 22 for 19°C and 30°C, RC is determined by locating on the abscissa the phase shift indicated by the phase meter, then finding the corresponding ordinate for the drawn calibration curve. This ordinate is the RC of the cell tested, within the errors of the method.

Before going on, a definition of the RC of a battery is required. The severest definition is that which states that the RC of a battery is the RC of the weakest cell in the battery. This definition has been adopted here. Since phase shift increases (considering sign) with increasing RC, the smallest phase shift is used to predict the RC of the battery. Thus, when phase shift versus RC data are given for a battery, the phase shift is the smallest measured among the cells of the battery and the RC is the residual capacity of the weakest cell.

The calibration curves were determined from actual measurements of RC at many values of phase shift. The curves shown in Figure 21 were determined from measurements made at room temperature, approximately 25°C, while those in Figure 22 were made at carefully controlled temperatures.

Since the phase shift is temperature dependent, batteries were allowed to stand for at least 4 hours following charge or discharge before their phase shifts were measured. Temperature measurements on an insulated VO4 cell showed that several hours are probably required for a battery of VO4 cells to come to room temperature after a 2A charge.

For the data in Figure 21, the phase shift of a cell or battery -- the smallest shift when a battery was used -- was measured after the cell or battery was charged to approximately the desired state of charge and left on open circuit for at least four hours to cool. After the phase shift was measured a discharge was run at the C/2 rate to 1.0V end point to determine the actual RC. Measurements were made at states of charge from 0-100% by varying the number of ampere-hours put into the test battery. The calibration curve was drawn as the best smooth curve fitting the measured points. This procedure would be followed when calibrating the indicator for any type of battery.

For the second set of curves, Figure 22 at fixed temperatures, the batteries were in a temperature controlled oil bath, and the wait between the charge and the phase measurement was increased to 10 hours to insure accurate temperature equilibrium. The spread among the curves at various temperatures shows that the phase shift is definitely temperature dependent. However, for moderate fluctuations in room temperature, say from 22°C to 28°C (approximately 10°F), a single curve at 25°C would not appreciably increase the error in predicting RC.

The phase shift measuring system and the associated calibration curves form a complete laboratory residual capacity indicator. Preliminary tests to determine the limitations on the device and the accuracy of its predictions are described next.

TESTS

The accuracy of the RC measurements is simply the difference between the actual RC and the predicted RC. The scatter of points on the RC versus phase shift plots used to arrive at the calibration curves indicates the expected uncertainty in predicting RC from these curves. As shown in Figure 23, the maximum deviation of points from the calibration curve is about 25% of the RC indicated by the curve. These points are extremes; all data lie within these limits. As will be shown later, the errors encountered in predicting RC fall well within these limits. For manually cycled 6 VO4 batteries, the average deviation was 9%.

The tests were divided into five groups. Each group was designed to evaluate the accuracy of the phase shift method of predecting RC under a different set of conditions. The first three tests

were to determine whether the accuracy of this method depends on history. These tests are described below. Data and intepretation follow the descriptions.

1. Batteries on manual cycle. Batteries were charged at various rates and for various times. Then RC was predected with the indicator. The actual RC was determined by a timed discharge at the C/2 rate to 1.0 V.

2. Battery on shelf stand. Batteries were put on shelf stand fully charged, at room temperature and at 50°C (122°F); for periods ranging from 7 to 32 days. After the required stand, the RC was predicted with the phase shift indicator. The actual RC was determined by a timed discharge at the C/2 rate.

3. Batteries on automatic cycle. Four 6 V04 batteries were put on automatic cycle. The cycling was interrupted approximately every 50 cycles and RC predicted with the indicator. Again, actual RC was determined by timed discharge at the C/2 rate. The cycle routine was:

   Discharge 2 h at 1.0 A = -2.0 A-h

   Charge 4 h at 0.60 A = +2.4 A-H

   Depth of discharge = 50%

The first 24 cycles were slightly different (charge 4 h at 0.70 A) but the end of charge voltages were too high so the charge rate was reduced. For the cycle routine given here, end of charge voltages were typically 1.42 and end of discharge voltages were typically 1.22. To obtain the most information from the given number of batteries and a given number of cycles, the batteries were removed for test at various times during a given discharge cycle. Thus, each battery came off automatic cycle at a different state of charge. Furthermore, any one battery was removed at a different state of charge each time the cycle was interrupted for measurements. This process yielded the greatest number of different conditions for a given number of cycles and batteries.

4. Batteries charged on constant potential. Batteries were put on a modified constant potential charge. They were charged at 1.45V per cell but the initial surge current was limited to 6 Amps. After floating at 1.45V per cell for several hours, they were discharged to some arbitrary capacity at the C rate. After the batteries cooled to room temperature, they were tested with the phase meter then discharged to 1.0V at the C/2 rate.

For the tests above, two different size batteries of similar construction were used, Gulton 6 V04 and 6 V09 batteries. These are

six cell, sealed batteries of 4 A-h and 9 A-h, respectively. Data for individual VO4 cells and four and six cell batteries are the same; apparently battery voltage has no effect on these measurements. This was to be expected since a.c. is used and readings are taken cell by cell.

5. Batteries of <u>various types</u>. The fourth test was to demonstrate that this method could be applied to predicting RC for other than VO series batteries. Room temperature calibration curves for a KO-35 cell and a 4KO15 battery (vented and in nylon case, as opposed to the VO cells which are sealed and in steel cases) were drawn, using the procedure described on p. 17. The curves were drawn, the cells were brought to various states of charge and RC was predicted. As with the other cells, a C/2 discharge was used to determine the actual RC.

The results of these tests are given in Tables 3 to 7, respectively. The average deviation of the predicted residual capacity for the manually cycled 6VO4 batteries was ± .35 A-h as shown at the end of Table 3. Since the nominal capacity of 6VO4 battery is 4 A-h, ± 0.35 A-h represents an average deviation of 9%. For similar measurements on 6VO9 batteries the average deviation was 13%. For the 6 VO4 and 6 VO9 batteries that had been on shelf stand at 50°C (112°F) and at room temperature, the average deviation was 16%. Table 4 shows the results of measurements of RC after automatic cycles. All four batteries appeared to indicate more than their nominal capacity when measured with the phase meter. However, they were known to have less than full charge because they were taken off cycle during discharge as discussed above. After the phase measurements were made, the cells were discharged at C/2 to 1.0 V. The capacities removed are listed as actual RC in the Tables.

The tests conducted so far indicate that RC can be predicted from phase shift for different types of cells and batteries. at various temperatures. All that is needed in addition to the measuring equipment is the appropriate calibration curves.

The manual cycle tests show that an average deviation of 9% has been realized. The phase shift apparatus predicted the residual capacities of batteries that had been standing at 50°C and at room temperature ($\sim$25°C), batteries that were charged on constant current and batteries that were charged at constant potential. The most accurate results were obtained when batteries were charged on constant current. The phase shift gave no valid indication of the RC of batteries that had been on automatic cycle.

The results of all the tests are summarized below.

TEST	BATTERIES USED	AVERAGE ACCURACY OF PREDICTIONS
1. Manual cycle	6 V04; 6 V09	10%
2. Shelf Stand	6 V04; 6 V09	16%
3. Automatic cycle	6 V04	No valid predictions
4. Constant potential charge followed by C rate discharge	6 V04; 6 V09	20%
5. Other types of batteries	KO-35;4 KO-15	16%

ANALYSIS OF DATA

The data for all manual cycles including the VO-4, VO-9, KO-15 and KO-35 cells and batteries were collated in order to determine the validity of RC predictions based on the phase shift data. These pooled data are shown as a histogram in Figure 24. The bell shaped curve suggests a normal distribution of errors. It is only for the 6 V04 batteries that a large enough sample was tested for the conclusions to have statistical significance.

The analysis in the accompanying table gives the probability that the RC is within the indicated accuracy. For example, the probability that the predicted RC is within ± 20% of the actual RC is 0.84. Expressed in another way, of 100 batteries tested, 84 would have predictions of RC correct within ± 20%.

DESIRED ACCURACY	% OF MEASUREMENTS HAVING DESIRED ACCURACY
±5%	27%
±10%	50%
±20%	84%

7. EFFECTIVE INTERNAL RESISTANCE

It can be shown theoretically, that the internal resistance R_o of a galvanic system is given by

$$R_o = \lim_{\substack{t \to o \\ I \to \infty}} \frac{\Delta V}{I} \text{ minimum value of } R_{eff} \qquad (12)$$

where

R_o = ohmic resistance

t = length of time the current I flows

V = change in terminal voltage during time t

R_{eff} = effective resistance

This relation is derived in Appendix II. As $t \to o$ and $I \to \infty$, the effects of concentration polarization and activation overpotentials are minimized or eliminated so the effective resistance approaches R_o, the ohmic resistance. This is the lowest possible value of effective resistance since the ohmic resistance is a property of the cell material and configuration and cannot be eliminated. As discussed in Section 5, Impedance at Audio Frequencies, the ohmic resistance is expected to depend on state of charge because the composition of the electrodes varies with state of charge. However, the A.C. method measured all contributions to effective resistance, and it turned out that the ohmic portion was small compared to the others. With a D.C. method, under the prescribed conditions, the ohmic contribution to resistance should be large.

APPARATUS

To obtain the conditions of high current and short time intervals required by the equation above, a specialized switch was required. The switch resistance had to be low so that currents as high as 100C (400 Amps for the cells used) could be drawn from a single 1.2 V cell. Furthermore, the total "on" time of the switch had to be low to prevent appreciable discharge of the cell by the 100C current. Last, some means of measuring both current and cell voltage had to be provided. A switch and circuit fulfill the above requirements as shown in Figures 24 and 25. A copper disk, turned by a synchronous motor opens and closes two sets of contacts with each rotation. As the disk rotates, a light set of contacts close

first. This supplies a trigger signal to a dual beam oscilloscope used to observe cell voltage and current simultaneously. At this stage no current is drawn from the cell so the oscilloscope displays zero current and the open circuit cell voltage. Within a millisecond after the oscilloscope is triggered the heavy duty contacts close, shorting the cell. These contacts carry up to 400 Amps. One terminal of the cell is connected to the stationary contact and the other terminal is connected to the rotating disk through a mercury reservoir as shown in Figure 25. The dimensions of the contacts and the speed of the motor are such that the cell is shorted for approximately 30 milliseconds. Drawing a current of 100 C from a cell for 30 milliseconds lowers the state of charge by only .08% because

$$(100\ \text{C Amps})\ (.030\ \text{sec})\ \left(\frac{1}{3600}\ \frac{\text{Hrs.}}{\text{Sec}}\right)\left(\frac{1}{\text{C}}\right) = .0008 = .08\% \tag{13}$$

As shown in Figure 26, a shunt is used to measure the current. The lower beam of the oscilloscope displays the current while the upper beam displays the cell voltage. A Tektronix 502 Dual Beam Oscilloscope was used. An oscilloscope camera recorded the displays so accurate measurements could be made. A typical photograph is shown in Figure 27.

Currents of 50 to 100 Amps were easily obtained from a single VO4 cell. By using 1/2" wide ground strap for the leads to the cell, shortening these leads to 2 to 3 inches and being careful to keep all contacts clean and tight, currents of 400 Amps could be drawn from a VO4 cell. The total resistance of the switch in the "on" position, including leads and contacts, was 1.8 milliohms. This was determined by sending 20 Amp through the switch and measuring the voltage drop across it with a potentiometer.

RESULTS

The first experiments were performed to verify the relation at the beginning of this section, namely

$$R_o = \lim_{\substack{t\to o \\ I\to\infty}} \frac{\Delta V}{I} \tag{14}$$

If this is true, then the measured resistance $\frac{\Delta V}{I}$ should increase with time and should be smaller for larger currents. Measurements were made using the rotary switch. Resistance was determined for currents from 170 to 360 Amps and at times ranging from 1.5 milliseconds to 21.5 milliseconds. The time stated, t* in Figure 28, is the length of the interval from the current turn-on time to the moment the

resistance was measured. Figure 28 clearly shows the increase in resistance with time t* and the decrease with increasing current I. Since the minimum effective resistance is the desired quantity, Figure 28 indicates that the resistance should be measured as soon as possible after the current is turned on and that a current of at least 300 Amps should be used. The current would be proportionally larger for a larger cell because the current density in the cell must be kept high. A discharge rate of at least 75 C would be required in general according to Figure 28. The resistance cannot be determined less than 1.5 milliseconds after the current is turned on because the voltage transient masks the ohmic voltage drop during that time. To measure resistance as a function of state of charge, then, currents of at least 75 C -- usually about 350 Amps for VO4 cells -- were used and the resistance was determined from the voltage drop and current 1.5 milliseconds after the current was turned on.

The procedure was similar to those followed in the previous studies reported here. A group of twelve cells were measured after a full charge, then after discharges to various residual capacities. After a resistance measurement, RC was determined by a C/2 discharge to 1.0 V. It was clear that the position and type of voltage probe had an effect on the measured value. Because of the very high currents and relatively small voltage drops ($\sim$0.6V) measured, voltage drops in the terminals as well as inductive coupling between voltage leads and current leads produced large errors in the measured resistance. Even so, a variation in R_o with state of charge was definitely established. Table 8 gives measured values of effective resistance at various residual capacities for two different VO4 cells. The leads were attached as indicated in Figure 29 (A). The two values of resistance given for each RC in Table 8 were measured consecutively, without changing the positions of the leads. The column labeled dev. R_o gives the deviation between the two values of R_o. The average of these deviations is .013 milliohms indicating a repeatability of $\pm$ .013 milliohms for R_o measurements when the leads were not moved. When the leads were removed and replaced, the measurements were less consistent.

An average curve of resistance vs. RC was drawn for the VO4 cells after about ten cycles on four cells. This curve, shown in Figure 30, was used as a basis for predicting RC from resistance measurements. A series of measurements was made on the same four cells using each of the connections shown in Figure 29 (A-D). To remove the current leads when the configuration in A, B and D were used, the upper nut was removed and the current lead taken off. For the configuration in C the terminal nut was left in place and the current lead was detached from the end of the extension. The resistances measured were used to predict RC from the average curve in Figure 30. With connections as in C and D of that figure, results were so scattered that no meaningful predictions were possible. With the connections as in A and B, RC

was predicted with average deviations of ± 23% and ± 25%, respectively. These data are given in Table 9.

To demonstrate that the errors in the resistance measurements and, hence, the errors in the RC predictions, were largely due to the placement of the leads, three cycles were run on one cell permanently connected to the pulsing switch. The leads were attached as in Figure 29A and were not removed or disturbed during the three cycles. Any variations in the measured resistance were produced by changes in the cell. The results were very consistent. Figure 31 shows the data at various states of charge during the three cycles. An average curve and the variations from that curve are indicated in the figure. If this average curve was used for predicting RC from resistance for this cell, the average deviation would be ± 0.2 A-h or ± 5%. This indicates strongly that the internal resistance of a cell has a consistent relation to the state of charge and could be a good indicator if accurate measurements could be made in a practical manner.

ANALYSIS OF RESULTS

A statistical analysis of the data just discussed and the data taken with connections as in Figure 29A further emphasizes that the measurement technique and not the properties of the battery are responsible for most of the error. The correlation factors, r, were calculated for both sets of data and these were found to be:

PERMANENT CONNECTIONS	FIGURE 29A CONNECTIONS
$r = 0.992$	$r = 0.615$
$r^2 = 0.98 = 98\%$	$r^2 = 0.38 = 38\%$

This means that with connections as in Figure 29A 38% of the predicted value of RC was actually due to a change in resistance of the cell with RC but 62% was due to random variations, presumably due to the placement of the leads. When the connections were left permanently on the cell 98% of the variation was due to a change in resistance with RC and only 2% of the change was random.

This information indicates strongly that a practical resistance measuring device having the same repeatability as the device above with permanent connectors, would be an accurate state-of-charge indicator. It is also significant that a method using ohmic resistance as its indicator should be free from the undesirable polarization effects that plague most other methods of predicting state of charge. A brief calculation shows that the contribution of the electrolyte to the ohmic resistance is only a few per cent of the total value. If this fraction of the resistance varies by

a few per cent due to, say, temperature, then the total change in resistance will be negligible. The resistance of the electrolyte can be estimated by considering the total plate area, separator thickness, and porosity, and the conductivity of the electrolyte. For a V04, the resistance due to the electrolyte is of the order 10^{-4} ohms, or less than 10% of the ohmic resistance of the cell.

Designing a resistance measuring device to read a cell resistance of a few milliohms within about 1% poses several problems. First, the resistance of the device must be, at most, 3 milliohms. If it is more, then a 1.2V cell could not possibly drive enough current through the device. This upper limit of resistance eliminates commercial milli-ohmmeters. Clearly, a device must be designed specifically for this application.

DESIGN OF NEW SWITCH

Because small voltages are hard to measure in the presence of high currents, it would be desirable to eliminate the voltage measurement and find R_o from current only. This is practical if the resistance of the switch is less than the resistance of the cell, R_o. However, this is quite difficult to realize experimentally because the resistance of the cells tested so far are about 1.5 milliohms. A switch is required that has a total resistance, including connections to the cell, of less than 1.5 milliohms, that can carry several hundred amperes, and provide an accurate way of measuring peak current (to give minimum resistance). Furthermore, the turn on time of the switch must be less than one millisecond if the resistance is to be measured 1.5 milliseconds after the current begins to flow.

As a starting point in the design of such a switch -- here "switch" refers to the entire device, connectors, shunt, on-off mechanism -- the resistance of each of the sections of the mechanical switch used for the previous work was measured, as well as the resistance of each of several types of connectors. The resistances were measured by passing a high current (10 to 100 A) through the components and measuring the voltage drop with a potentiometer. The results are given in Table 10.

A goal of 0.5 milliohms was set for the resistance of the new switch to be designed. From Table 10 it is clear that a completely new type of switch was required. Shunt resistance had to be reduced, leads virtually eliminated, and the resistance of the on-off mechanism kept to a minimum. To eliminate leads, the switch had to take the form of a fork. This meant that the shunt and on-off mechanism had to be small enough to fit between the terminals of a cell, yet carry several hundred amperes.

Several designs were analyzed theoretically, considering total resistance, reproducibility of resistance and turn on time. The best of these is shown in Figure 32. A switch was constructed according to that design. Because of the required low resistance of the switch, the friction connections used in any mechanical switch could not be tolerated. Furthermore, because of the absence of leads, the unit is rigid and incorporating any moving parts would be awkward. A mercury switch avoids both of these problems. However, the resistivity of mercury is high (ρ = 95 x 10^{-6} ohm-cm) so the geometry of the electrodes had to be considered carefully to get minimum resistance when the switch was in the "on" position. At first thought, the way to get the lowest resistance is to use the largest electrodes possible, put them as close as possible, then fill the space between them with mercury. Although this will, indeed, give a low resistance, the viscosity of mercury makes it impossible to turn such a switch on or off very quickly. Also, with very close plates as electrodes, there is a possibility of drops of mercury "hanging" between the electrodes, preventing the switch from being turned off. The calculations given in Appendix III predict a resistance of 0.02 milliohms between sections 2 and 4 when they are separated by 0.005 inches. The actual measured resistance of this device was 0.025 milliohms in excellent agreement with the predicted value. When the final version of the device was constructed, a layer of epoxy was used instead of the 0.005 nylon. The epoxy also bound sections 2 and 4 together without using clamps. Apparently the epoxy layer was slightly more than 0.005 inches thick because the resistance increased to 0.037 milliohms when the nylon was replaced by the epoxy.

CONSTRUCTION

Referring to Figure 32, sections 1 and 2 are one-inch cubes of copper, each with a small projection on one face. The shunt is a thin rectangular wafer of constantan brazed to these projections. After the brazing was done, the constantan and the projecting copper parts were filed to give the required resistance. Filing the constantan and copper at one time insured a sharply defined edge on the constantan and eliminated any shorts caused by brazing material bridging across the constantan. Constantan was used for the shunt metal because it is a poor conductor for a metal and, more important, has the lowest thermal coefficient of resistivity of any known metal or alloy. For constantan, ρ = 44.1 x 10^{-6} ohm-cm and $\frac{\Delta\rho}{\rho C}$ = 2 x 10^{-6}. To be able to measure the current accurately, the shunt should give a voltage drop of about 5 mV per 100 A. Therefore, the shunt resistance was set to 0.05 milliohms by filing. Sections 3 and 4 are female "Supercon" connectors rated at 250 Amps continuous. They are gold plated brass. Section 3 is soldered to section 1. Sections 2 and 4 are held together by the layer of insulating epoxy. Furthermore, the entire space between the left and right halves of the switch is filled with epoxy for strength.

The surfaces of the on-off section of the switch that come in contact with the mercury were treated with $Hg(NO_3)_2$, forming an amalgam on those surfaces. This made the mercury wet the surfaces assuring minimum resistance. The same switch had six times the resistance when the surfaces were nickel plated to prevent an amalgam from forming.

TESTING

The resistance of the entire unit from the end of one connector to the end of the other was 0.087 milliohms. Assuming a resistance of 0.11 milliohms for each of the connections to the cell, as indicated in Table 10, the entire resistance of the switch would be 0.31 milliohms, better than the goal of 0.5 milliohms.

When the switch was being tested, it was turned on and off by adding mercury and removing it. During the tests, a small amount of mercury crept out of the reservoir and appeared at the interfaces between sections 2 and 4 and the insulating epoxy layer. Probably the epoxy did not form an adequate bond to the copper and brass. After several days, the mercury apparently formed a continuous path from 2 to 4 because the switch remained on even after as much mercury as possible was removed. With the switch always in the on state, no cell measurements could be made. However, the difficulty is one of fabrication since the electrical properties of the device were even better than anticipated. Rebuilding the switch according to the original plan using a nylon insulator should solve the mechanical problem. Certainly the data indicating a 5% error inherent in a resistance type state of charge indicator, coupled with the early success in designing the ultra-low resistance switch with the required electrical properties call for further efforts on this most promising technique.

8. CONCLUSIONS AND RECOMMENDATIONS

Of the five electrical properties of Ni-Cd cells studied -- phase shift, ohmic resistance, double layer capacitance, transient peak height and impedance at audio frequencies -- only the first two were found to depend on state of charge in a useful manner. The variations of phase shift and ohmic resistance with state of charge are measurable and reproducible enough to provide an indication of state of charge.

The phase shift apparatus described in this report, together with the required calibration curves, measured the residual capacity of cells and batteries with average errors from ± 10% to ± 20%. A statistical analysis showed that 84% of all readings should have errors of less than ± 20%. The batteries included one to six cell packs with nominal capacities from 4 A-H to 35 A-H, both sealed and vented types. The tests conducted so far show that this technique can predict the residual capacity of batteries with various histories and at different temperatures. These tests are strong evidence of the value of the phase shift method, and were as complete as the duration of this work allowed. More extensive supplementary evaluation is required. A variety of batteries of many sizes from various manufacturers should be tested under all possible conditions. History, temperature, method of charge, and method of discharge should all be varied for a complete evaluation of the method. Only three drawbacks were found during the testing of this method. First, the Ad-Yu phase meter is not ruggedized and requires weekly calibration. This could probably be eliminated by designing a meter specifically for this system. Second, a battery must be allowed to come to the ambient temperature before it is measured or else a temperature compensation is required. Third, no valid state of charge indication is given for batteries that have been on continuous repetitive automatic cycling.

The ohmic resistance was shown to vary in a very reproducible way with residual capacity. In a carefully controlled experiment the variation of ohmic resistance with residual capacity was reproducible within 5%. Although a device to measure ohmic resistance of cells must meet severe requirements of resistance, switching time and current capability, a great deal of progress was made in the design of such a device. The ultra-low resistance switch discussed in Section 7 not only met all the electrical requirements but surpassed them. A short developed preventing the switch from being turned off. Considering the almost complete success of the first design, it is apparent that the required device can be built since the failure was mechanical. Resistance measurements would not only be possibly the most accurate method of measuring state of charge

found so far, but would be the simplest technique to use.

To take full advantage of the possibilities of this method, the variations of cell resistance should be studied thoroughly and new resistance measuring devices should be investigated and constructed.

A variation of the method described, recommended by the contracting agency, to get around the variability of contacts is to force the 100 C current from an external supply and merely supply appropriate contact points for measuring voltage changes that are inside the measuring loop.

REFERENCES

1. Fleischer, A., Research Studies on the Development of Testing Methods for Nickel-Cadmium Alkaline Storage Batteries, Final Report, Signal Corps Contract No. DA 36-039-SC-42657, 15 February, 1955.

2. Kordesch, K., and Kornfeil, F., Method and Device for Testing Ni-Cd Batteries, Signal Corps Project No. 162A, Technical Memorandum No. M-1578, 1 June 1954.

3. Kordesch, K., A Method for the Determination of the State of Charge of Alkaline Storage Batteries, Signal Corps Project No. 20558, Technical Memorandum No. M-1664, 9 June 1955.

4. Cherdak, A., and Shair, R. C., Evaluation of Nickel-Cadmium Battery Testers, Gulton Industries, Metuchen, New Jersey, Signal Corps Contract No. DA 36-039-SC-85066, 30 July 1961.

5. Fleischer. A., op. cit., Fourth Quarterly Report, 15 January 1954, p. 48.

APPENDIX I.

OPERATION OF BREADBOARD STATE OF CHARGE INDICATOR

Figures 33, 34 and 35 show the complete breadboard phase measuring system. This system, with the calibrations curves, is the breadboard state of charge indicator.

DISCUSSION

The A.C. power source is a Waveforms Oscillator #401C set at 40 cps. The frequency can be switched easily to 400 cps as required for part of the adjustment procedure. The output of the oscillator is amplified to the required level by the transistor amplifier. The 40 cycle output is fed to the test battery through the CURRENT LEADS. An ammeter indicates the r.m.s. current through the battery. A D.C. blocking capacity prevents discharge of the battery through the amplifier output circuit. Polarity must be observed when connecting the CURRENT LEADS because the capacity is polarized. A resistor and a shunt in series with the test battery provide voltages in phase with the current through the battery. The voltage across the resistor is fed through an RC phase shifter to E_2 on the phase meter. The voltage across the shunt is about two millivolts and is used for a zero check as described later. The current through the battery produces a 40 cycle component in the voltage of each cell. The cell voltage picked up with the VOLTAGE LEADS is fed to a high pass (40 cps) filter. The signal coming out of the filter is amplified approximately 1000 times in the balanced pre-amplifier. A low noise pre-amplifier is required because the signal from the cell is about a millivolt. To achieve its low noise characteristics, the pre-amplifier uses D.C. on the filaments and five (5) 45V batteries for B and C voltages. The 6 VDC supply uses a Ni-Cd battery as a filter and achieves very low ripple in a minimum of space. The output of the pre-amplifier is fed to E1 on the phase meter. An r.m.s. voltmeter reads this voltage. It is essential that this voltage be at least 0.4 volts r.m.s. Otherwise the accuracy of the phase meter is reduced.

To prevent the phase meter from reading random and sometimes violent fluctuations when connecting and disconnecting batteries, a relay has been inserted to open the meter movement circuit. A button on the positive voltage lead closes the relay so that the meter can be read.

OPERATION

The zero reading of the phase meter should be checked daily.

ZERO CHECK

1) Adjust 40 cycle current to about 0.5 Amp. r.m.s.

2) Touch VOLTAGE LEADS to ZERO CHECK terminals. Voltage E1 should read at least 0.4 V r.m.s.

3) Set RANGE to 180°, ADD switch to 180°. Touch VOLTAGE LEADS to ZERO CHECK terminals. Adjust reading to 180° with DEFLECTION control.

4) Set the RANGE to 12°, ADD to 0. Read phase shift at ZERO CHECK as in 3. ...e reading should be less than 15'.

If the reading is greater than 15' the phase meter must be adjusted, See p. 33.

MEASURING RESIDUAL CAPACITY

All readings are taken on the 12° range of the phase meter.

1) Connect the CURRENT LEADS to the main battery terminals, being careful to observe polarity. Batteries up to 15 V can be measured. (Any voltage could be handled by using a DC blocking capacitor of the appropriate working voltage.)

2) Adjust the current to about 0.5 amps. This adjustment will rarely be changed. For very large batteries, a larger current may be required. Use a current that gives an E1 voltage as read on the voltmeter of 0.4 V or more.

3) Touch VOLTAGE LEADS to the terminals of the first cell in the battery, wait a few seconds for E1 to become steady, then push the READ button and read the phase shift. Repeat the procedure for each cell in the battery, releasing the READ button whenever a reading is not being taken.

4) A brief look at the curve for the type of cell tested will show whether the largest or smallest phase shift (ignoring signs since these are unnecessary) will give the smallest capacity. This smallest capacity is the predicted residual capacity of the battery.

ADJUSTMENT OF PHASE METER

If the zero reading measured during ZERO CHECK above is greater than 15', it is more likely that the Ad-Yu phase meter requires adjustment than the phase shifter.

The adjustment described below is quoted from the manufacturers manual.

"BIAS ADJUSTMENT:

Bias controls R_1 to R_8, on top of the chassis, should be adjusted if meter reading varies with change of signal amplitudes or is off zero when a single signal is applied to both inputs, or when tubes are changed in the limiter stages. The procedure for adjusting the bias control, R_1, for the limiter stage, T_1, is as follows:

1. Apply a single signal (available at CAL OUT on panel) to both "E_1 IN" and "E_2 IN".

2. Set the "RANGE" switch to "TEST" and the "STAGE" switch at rear to T_1. Take reading on meter.

3. Remove the input signal and short the input binding post to ground. Take meter reading again.

4. Adjust R_1 until the meter reading of step 3 equals that of step 2.

5. Repeat the above steps several times to insure that the output plate current of T_1 remains unchanged when the input signal varies from zero to over 10 volts.

The procedure for adjusting R_2 for the second limiter stage, T_2, is the same as described above, with the following exceptions: In step 2, set the "STAGE" switch to T_2; in step 3, push the "GR" switch and remove the input signal. Use a similar procedure to adjust R_3. The procedure for adjusting R_5 is similar to that of R_1. The procedure for adjusting R_6, R_7, is similar to that of R_2 and R_3. The order of adjustment must be from first to the second, to the third, to the fourth stage. This will insure that the input to the stage under adjustment (namely, the output of the previous stage) is a signal symmetrical with respect to the zero axis."

Usually, only resistors 1, 2, 3, 5, 6 and 7 must be adjusted. The procedure for adjusting R4 and R8 can be found in the Ad-Yu operation manual. These have never required adjustment during six months of operation.

If the phase meter is adjusted as above, and the ZERO CHECK is still not correct, then the PHASE SHIFTER must be adjusted. Note that this rarely happens. The adjustment is made by tuning the potentiometer through the small hole in the front panel just above the 40 cps current meter.

NOTE: In general, it is better to leave the 110V 60 power on continuously where possible. Otherwise, at least one hour warm-up should be allowed for the phase meter. The preamplifier power should be turned off when no readings are being taken to conserve battery power.

APPENDIX II.

CALCULATION OF TIME AND CURRENT DEPENDENCE OF RESISTANCE OF A CELL

The open circuit potential of a cell V_o is given by the sum of two half cell potentials. Each half cell potential may be obtained from a thermodynamic or a kinetic treatment of the electrode processes. Although the latter is less precise, the kinetic treatment allows an understanding of procedures necessary to determine the state of charge.

For the electrochemical reaction

$$A^{+m} + Ze^- \underset{k_r}{\overset{k_f}{\rightleftharpoons}} A^{-(Z \mp m)}, \tag{15}$$

the electrode flux is given by

$$j = ZF\, k_f^o C_o^\sigma \exp\left(-\frac{F_f^\ddagger + \alpha \eta ZF}{RT}\right) - \tag{16}$$

$$ZF\, k_r^o C_r^o \exp\left(-\frac{F_r^\ddagger - (1-\alpha)\eta ZF}{RT}\right),$$

where j is current density, C_o^σ and C_r^σ are the concentrations of $A^{\pm m}$ and $A^{-(Z \mp m)}$ at the electrode/electrolyte interface, $F_f^\ddagger$ and $F_r^\ddagger$ are the activated free energy barriers, and α is the fraction of the overpotential η ($=V_o - V_\tau$) which accelerates the cathodic electrode process. Now, if the time interval of current passage is short enough then the surface concentrations will not change so that the surface activities are equal to bulk activities.

If we consider the discharge of the electrode then the last exponential term will be negligible, and the flux equation may be written as,

$$i_{t\to o} = i_o e^{-\frac{\alpha \eta ZF}{RT}} \tag{17}$$

Rearranging,

$$\eta = \frac{RT}{\alpha ZF} \ln i_o - \frac{RT}{\alpha ZF} \ln i. \tag{18}$$

The above equation deals with only the electrochemical processes at an electrode so that one must add to it the ohmic drops,

$$\eta = \frac{RT}{\alpha ZF} \ln i_o - \frac{RT}{\alpha ZF} \ln i - iR_o, \tag{19}$$

where R_o is the ohmic resistance.

Differentiating with respect to current to obtain the effective resistance,

$$\frac{d\eta}{di} = R_{eff} \underset{t\to o}{} = -\frac{RT}{\alpha ZF} \cdot \frac{1}{i} - R_o. \qquad (20)$$

If the discharge current is very high then the first term on the right may be neglected yielding,

$$\lim_{\substack{t\to 0 \\ i\to \infty}} R_{eff} = R_o. \qquad (21)$$

APPENDIX III.

CALCULATION OF RESISTANCE OF MERCURY SWITCH

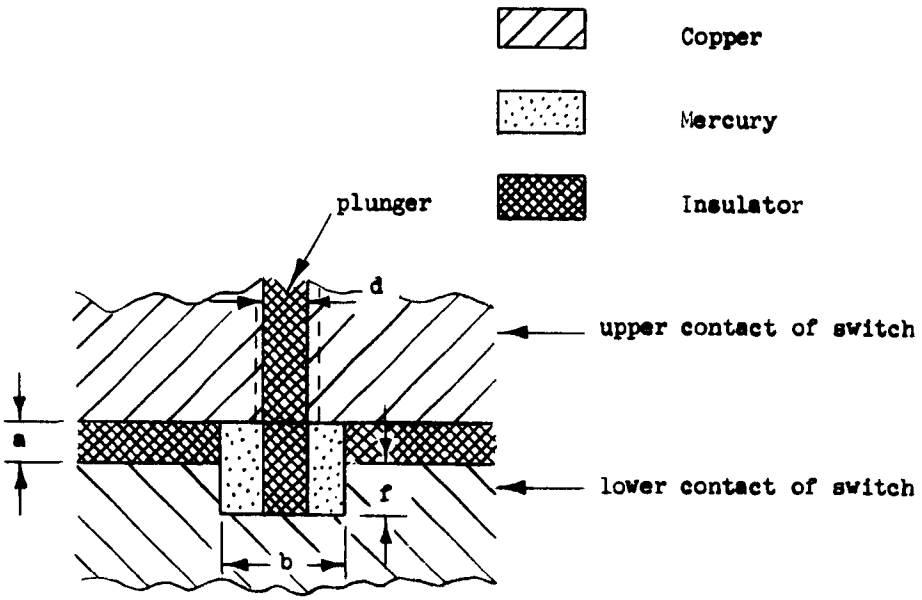

Consider the two dimensional problem below.

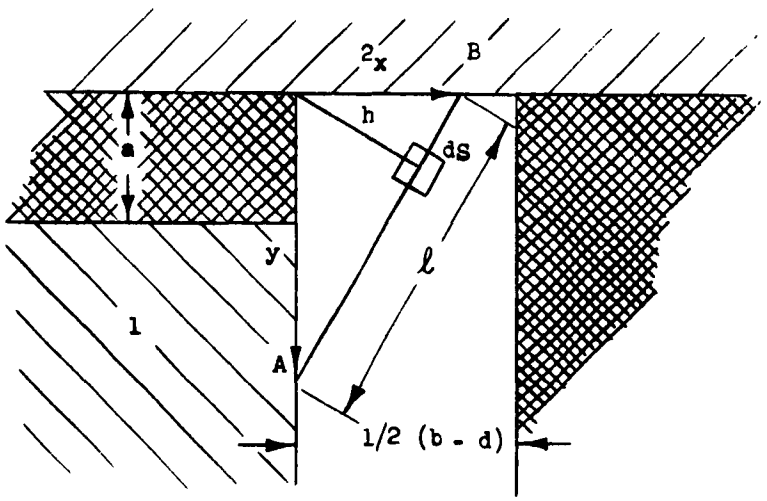

(1) and (2) are sheets of conductor, e.g. copper. For current to pass from (1) to (2) it must go through the mercury. The element of conductance for the path

from point A on (1) to point B on (2) is

$$dG = \frac{\sigma\, dS}{l} \tag{22}$$

where dS is an element of area whose normal is along the line from A to B. Assuming unit thickness for the sheets of conductor

$$dS = dh \tag{23}$$

$$dG = \frac{\sigma\, dh}{l} \tag{24}$$

Approximating the lines of current flow as straight lines parallel to l

$$G = \sigma \int_{h_{min}}^{h_{max}} \frac{dh}{l} \tag{25}$$

By similar triangles,

$$\frac{l}{h} = k = \frac{(f + a)^2 + 1/4\,(b-d)^2}{1/2\,(f + a)\,(b-d)} \tag{26}$$

so

$$G = \frac{\sigma}{k} \int_{h_{min}}^{h_{max}} \frac{dh}{h} = \frac{\sigma}{k} \ln \frac{h\ max}{h\ min} \tag{27}$$

Again by similar triangles, $\frac{h\ max}{h\ min} = \frac{Y\ max}{Y\ min}$ (28)

so

$$G = \frac{\sigma}{k} \ln \frac{Y\ max}{Y\ min} \tag{29}$$

In the actual switch the electrodes are not flat sheets of unit thickness but are cylinders. If $b-d \ll b$ a good approximation is to let G' for the cylindrical problem be πb times G for the flat sheet problem. Although $b-d \approx 1/2\ b$ for the actual switch, a valid result is obtained here. Therefore,

$$G' = \pi b \frac{\sigma}{k} \ln \frac{Y\ max}{Y\ min} \tag{30}$$

Putting in numbers

$b = 0.5" = 1.3$ cm
$f = .25" = 0.6$ cm
$d = 5/16" = 0.8$ cm
$a = .005" = .013$ cm
$\sigma = 10^4 (\text{ohm-cm})^{-1}$ for mercury

whence

$$G' = \pi (1.3) \frac{10^4}{2.9} \ln \frac{.61}{.013} = 5 \times 10^4 \text{ mhos} \qquad (31)$$

Then

$$R = \frac{1}{G'} = .02 \text{ milliohms} \qquad (32)$$

TABLE 1

DOUBLE LAYER CAPACITANCE, F,
AT VARIOUS
RESIDUAL CAPACITIES
4 AMP-HR CELLS

Measurements Using Mechanical Switch

F FARADS	R. C. A-H	F FARADS	R. C. A-H
12	2.4	12	2.5
12	1.9	11	2.0
11	1.1	9.3	1.2
7	0.6	9.0	0.7
15	2.6	15	2.7
12	1.6	14	1.7
9	0.6	9.3	0.7

Measurements Using Electronic Switch

F FARADS	R. C. A-H	F FARADS	R. C. A-H
CELL #18		CELL #20	
16	3.6	15	3.6
12	3.1	11	3.1
13	2.6	11	2.6
11	2.1	10	2.1
9	1.6	9	1.6
CELL #22		CELL #24	
16	3.7	15	3.4
14	3.2	12	2.9
11	2.7	13	2.4
11	2.2	10	1.9
10	1.7	10	1.4

TABLE 1 (CONT'D)

CELL #7		CELL #8	
19	4.3	19	4.1
19	3.8	18	3.6
18	3.3	15	3.1
16	2.8	17	2.6
15	2.3	15	2.1
14	1.8	14	1.6
13	1.3	14	1.1
20	4.3	22	3.1
17	3.8	16	2.6
16	3.3	16	2.1
16	2.8	15	1.6
14	2.3	14	1.1
15	1.8	13	0.6
14	1.3	8	0.1
13	0.8		
11	0.3		

CELL #9		CELL #10	
19	4.4	15	3.8
18	3.9	14	3.3
16	3.4	12	2.8
16	2.9	12	2.3
15	2.4	11	1.8
15	1.9	11	1.8
14	1.4	10	0.8
20	3.9	16	3.8
18	3.4	13	3.3
16	2.9	13	2.8
15	2.4	11	2.3
15	1.9	11	1.8
15	1.4	10	1.3
13	0.9	9	0.8
17	0.4	8	0.3

CELL #11		CELL #12	
23	4.4	22	4.4
21	3.9	23	3.9
19	3.4	19	3.4
17	2.9	18	2.9
18	2.4	18	2.4

TABLE 1 (CONT'D)

CELL #11 (Cont'd)		CELL #12 (Cont'd)	
17	1.9	17	1.4
19	1.4	23	4.5
25	4.5	22	4.0
21	4.0	21	3.5
21	3.5	20	3.0
18	3.0	19	2.5
17	2.5	18	2.0
18	2.0	17	1.5
17	1.5	17	1.0
15	1.0	13	0.5

Measurements Using Electronic Switch
and
Magnification of Photographs

F FARADS	R. C. A-H	F FARADS	R. C. A-H
CELL #20		CELL #21	
15.3	5.0	24.3	5.0
17.3	4.5	18.8	4.5
13.5	4.0	18.5	4.0
11.8	3.5	21.3	3.5
11.8	3.0	18.0	3.0
14.4	2.5	16.1	2.5
12.8	2.8	23.4	2.8
10.2	2.3	13.1	2.3
9.3	1.8	10.3	1.8
2.8	1.3	4.2	1.3
CELL #22			
20.0	4.8		
15.8	4.3		
14.9	3.8		
12.5	3.3		
12.8	2.8		
13.8	2.3		
14.4	2.8		
11.6	2.3		
9.1	1.8		
2.3	1.3		

TABLE 2

IMPEDANCE OF 4 A-H CELLS AT VARIOUS STATES OF CHARGE

Calibration of Bridge:

FREQ. cps	MILLIOHMS/CM of S
50	.032
100	.032
200	.032
300	.032
400	.033
500	.035

Residual Capacity AH	Cell No.	Bridge Setting (cm ± 1 cm) 50 cps	100 cps	200 cps	300 cps	400 cps	500 cps	Milliohms @ 100 cps ± 0.5 milliohms
3.3	2	49	49	45	44	44	44	1.6
2.3	2	--	48	45	43	43	43	1.5
1.3	2	--	45	45	44	44	44	1.4
3.7	3	46	44	42	42	42	43	1.4
2.7	3	--	44	39	--	39	39	1.4
1.7	3	--	44	40	40	39	--	1.4
2.2	4	60	60	58	56	56	57	1.9
1.2	4	--	52	48	47	47	46	1.6
0	4	--	76	63	58	51	50	2.4
		Measurements Using Direct Method						
3.2	2							2.0
1.2	2			(100 cps only)				1.8
0	2							3.2
3.3	3							2.0
1.3	3							1.6
0	3							3.4

TABLE 3

RESIDUAL CAPACITY MEASUREMENTS, BATTERIES ON MANUAL CYCLE

BATTERY TYPE	PREDICTED RESIDUAL CAPACITY A-H	ACTUAL RESIDUAL CAPACITY A-H	DEVIATION A-H
6 VO 4	4.0	3.8	0.2
	2.6	2.8	0.2
	2.0	1.8	0.2
	1.4	0.8	0.6
	3.8	3.7	0.1
	2.4	2.7	0.3
	1.6	1.7	0.1
	1.1	0.7	0.4
	3.5	3.7	0.2
	2.3	2.7	0.4
	1.4	1.7	0.3
	0.8	0.7	0.1
	3.7	3.8	0.1
	2.2	2.8	0.6
	1.6	1.8	0.2
	1.1	0.8	0.3
	4.1	3.9	0.2
	2.4	2.9	0.5
	1.1	1.9	0.8
	0.8	0.9	0.1
	4.0	3.8	0.2
	2.3	2.8	0.5
	0.8	1.8	1.0
	0.5	0.8	0.3
	3.6	3.9	0.3
	2.0	2.9	0.9
	0.7	1.9	1.2
	0.5	0.9	0.4
6 VO 4	4.2	3.7	0.5
	2.3	2.7	0.4
	1.0	1.7	0.7
	0.6	0.7	0.1

TABLE 3 (CONT D)

RESIDUAL CAPACITY MEASUREMENTS, BATTERIES ON MANUAL CYCLE

BATTERY TYPE	PREDICTED RESIDUAL CAPACITY A-H	ACTUAL RESIDUAL CAPACITY A-H	DEVIATION A-H
6 VO 4	3.9	3.7	0.2
	2.3	2.7	0.4
	1.3	1.7	0.4
	0.5	0.7	0.2
	3.9	3.6	0.3
	2.1	2.6	0.5
	1.2	1.6	0.6
	0.5	0.6	0.1
	3.5	3.6	0.1
	1.7	2.6	0.9
	0.6	1.6	1.0
	0.4	0.6	0.2
	3.9	3.5	0.4
	2.1	2.5	0.4
	1.2	1.5	0.3
	0.5	0.5	0
	3.8	3.4	0.4
	2.2	2.4	0.2
	0.8	1.4	0.6
	0.4	0.4	0
	3.6	3.3	0.3
	1.8	2.3	0.5
	0.6	1.3	0.7
	--	0.3	--
	4.2	3.3	0.9
	2.5	2.3	0.2
	1.2	1.3	0.1
	0.4	0.3	0.1
	4.1	3.4	0.7
	2.3	2.4	0.1
	1.1	1.4	0.3
	0.4	0.4	0

TABLE 3 (CONT'D)

RESIDUAL CAPACITY MEASUREMENTS, BATTERIES ON MANUAL CYCLE

BATTERY TYPE	PREDICTED RESIDUAL CAPACITY A-H	ACTUAL RESIDUAL CAPACITY A-H	DEVIATION A-H
6 VO 4	3.4	3.3	0.1
	2.1	2.3	0.2
	1.0	1.3	0.3
	--	0.3	--
	3.9	3.6	0.3
	2.5	2.6	0.1
	1.4	1.6	0.2
	0.9	0.6	0.3
	4.0	3.4	0.6
	2.6	2.4	0.2
	1.5	1.4	0.1
	1.0	0.4	0.6
	3.8	3.6	0.2
	2.4	2.6	0.2
	1.3	1.6	0.3
	0.9	0.6	0.3
	3.8	3.3	0.5
	1.4	2.2	0.8
	0.7	1.2	0.5
	4.0	3.5	0.5
	1.8	2.4	0.6
	1.3	1.4	0.1
	0.7	0.4	0.3
	4.2	3.7	0.5
	2.2	2.6	0.4
	1.6	1.6	0
	1.1	0.6	0.5
	4.2	4.0	0.2
	2.5	2.9	0.4
	1.8	1.9	0.1
	1.3	0.9	0.4
	3.4	3.7	0.3
	3.8	3.7	0.1
	3.8	3.8	0.0
	2.4	2.6	0.2

TABLE 3 (CONT'D)

RESIDUAL CAPACITY MEASUREMENTS, BATTERIES ON MANUAL CYCLE

BATTERY TYPE	PREDICTED RESIDUAL CAPACITY A-H	ACTUAL RESIDUAL CAPACITY A-H	DEVIATION A-H
6 VO 4	3.1	1.8	1.3
	0.7	0.7	0.0
	3.6	3.6	0.0
	1.7	1.6	0.1
	1.5	2.2	0.7
	3.6	3.1	0.5
		AVG. DEV. =	± 0.35 A-H
		FOR 6 VO 4	
		=	± 9%
6 VO 9	9.0	9.5	--
	9.0	7.1	1.9
	7.7	7.6	0.1
	9.0	6.4	2.6
	9.0	6.3	2.7
	7.5	6.8	0.7
	6.1	6.0	0.1
		AVG. DEV. =	± 10%
		FOR 6 VO 9	

TABLE 4

PREDICTED AND ACTUAL RESIDUAL CAPACITY OF FOUR 6 VO 4 BATTERIES ON AUTOMATIC CYCLE

BATTERY TYPE	PREDICTED RESIDUAL CAPACITY A-H	ACTUAL RESIDUAL CAPACITY A-H	DEVIATION A-H	% DEVIATION
AFTER 100 CYCLES				
CB-1	4.6	2.9	1.7	40%
CB-2	4.3	2.9	1.4	35%
CB-3	4.0	2.5	1.5	40%
CB-4	3.3	1.5	1.8	45%
AFTER 275 CYCLES				
CB-1	0	0	--	--
CB-2	3.5	1.7	1.8	45%
CB-3	2.5	1.1	1.4	35%
CB-4	1.3	0.5	0.8	20%

TABLE 5

PREDICTED AND ACTUAL RESIDUAL CAPACITY
BATTERIES ON SHELF STAND

STAND	BATTERY TYPE	PREDICTED RESIDUAL CAPACITY (A-H)	ACTUAL RESIDUAL CAPACITY (A-H)	% DEVIATIONS
3 DAYS, 50°C	6 VO 4	3.6	2.9	-18%
7 DAYS, 50°C	6 VO 4	1.1	1.3	+ 5%
7 DAYS, 50°C	5 VO 9	4.7	2.8	-21%
26 DAYS, 50°C	6 VO 4	0	0	0
26 DAYS, 50°C	6 VO 9	0	0	0
32 DAYS, 25°C	6 VO 4	0	0	0
32 DAYS, 25°C	4 VO 4	1.1	1.3	+ 5%
32 DAYS, 25°C	6 VO 9	3.7	0.8	-32%

AVG. DEV. EXCLUDING PREDICTIONS OF ZERO A-H = 16%

TABLE 6

PREDICTED AND ACTUAL RESIDUAL CAPACITY
6 VO 4 BATTERIES CHARGED AT MODIFIED CONSTANT POTENTIAL

PREDICTED RESIDUAL CAPACITY (A-H)	ACTUAL RESIDUAL CAPACITY (A-H)	% DEVIATION
> 4	4.2	5%
2.9	3.4	13%
2.9	1.9	25%
2.8	1.0	45%
2.5	1.2	33%
3.9	3.5	10%
3.9	2.9	25%
3.6	2.9	18%
3.2	3.2	0%

AVG. DEV. = 20%

TABLE 7

PREDICTED AND ACTUAL RESIDUAL CAPACITIES
GULTON KO 35 CELL

PREDICTED RESIDUAL CAPACITY A-H	ACTUAL RESIDUAL CAPACITY A-H	DEVIATION A-H
5	5	0
14	18	4
16	24	8
20	18	2
38	32	6
32	24	8
28	18	10

AVG. DEV. = ± 16%

PREDICTED AND ACTUAL RESIDUAL CAPACITIES
GULTON 4 KO 15 BATTERY

9.0	13.0	4.0
6.1	6.6	0.5
9.8	8.5	1.3
8.4	5.3	3.1
10.1	10.5	0.4
9.7	6.9	2.8
5.1	8.1	3.0
9.5	8.8	0.7
8.8	10.9	2.1
8.6	12.4	3.8
2.6	2.6	0.0
13.8	14.0	0.2

AVG. DEV. = ± 12%

TABLE 8

EFFECTIVE RESISTANCE VS. RESIDUAL CAPACITY

CELL #16

ACTUAL RESIDUAL CAPACITY A-H	R_o (MILLIOHMS)	DEV. R_o (MICRO-OHMS)
5.13	1.460 1.455	5
4.63	1.422 1.423	1
4.13	1.460 1.449	11
3.63	1.448 1.452	4
3.13	1.464 1.477	13
2.63	1.480 1.481	1
2.13	1.525 1.530	5
0	2.410 2.440	30

CELL #17

4.54	1.470 1.495	25
4.04	1.465 1.484	19
3.54	1.510 1.512	2
3.04	1.538 1.542	4

TABLE 8 (CONT'D)

EFFECTIVE RESISTANCE VS. RESIDUAL CAPACITY

CELL #17

2.54	1.602 1.602	0
2.04	1.614 1.640	26
1.54	1.656 1.652	4
0	2.280 2.340	60

TABLE 9

PREDICTION OF RESIDUAL CAPACITY FROM RESISTANCE, CONNECTIONS AS IN FIGURE 29A

PREDICTED RESIDUAL CAPACITY A-H	ACTUAL RESIDUAL CAPACITY A-H	DEVIATION A-H	
5.7	4.6	1.1	
4.5	3.6	0.9	
4.2	5.1	0.9	
4.1	4.1	0.0	
3.8	3.1	0.7	
3.7	4.0	0.3	
3.5	2.6	0.9	
3.0	4.5	0.5	
2.9	3.5	0.6	
2.7	3.7	1.0	
2.6	3.5	0.9	
2.6	2.1	0.5	
2.5	3.0	0.5	
2.5	3.8	1.3	
2.3	2.8	0.5	
2.2	3.6	1.4	
2.0	2.0	0.0	
2.0	4.0	2.0	
1.9	2.5	0.6	
1.9	2.7	0.8	
1.9	3.0	1.1	
1.9	2.5	0.6	
1.7	3.7	2.0	
1.7	2.7	1.0	
1.7	3.9	2.2	
1.7	1.7	0.0	
1.7	2.6	0.9	
1.6	1.8	0.2	
1.5	2.0	0.5	
1.5	1.0	0.5	
1.5	2.9	1.4	
1.4	1.5	0.1	
1.4	1.5	0.1	
1.3	1.7	0.4	
1.3	3.5	2.2	
1.3	1.9	0.6	
1.2	3.8	2.6	
1.2	2.8	1.6	AVG DEV.= $\pm$0.9 A-H
1.2	2.5	1.3	= $\pm$ 23%
1.1	1.5	0.4	
1.1	1.6	0.5	MAX. DEV. = 3.5 A-H
1.0	1.8	0.8	

TABLE 9

PREDICTION OF RESIDUAL CAPACITY FROM RESISTANCE, CONNECTIONS AS IN FIGURE 29A

PREDICTED RESIDUAL CAPACITY A-H	ACTUAL RESIDUAL CAPACITY A-H	DEVIATION A-H	
5.7	4.6	1.1	
4.5	3.6	0.9	
4.2	5.1	0.9	
4.1	4.1	0.0	
3.8	3.1	0.7	
3.7	4.0	0.3	
3.5	2.6	0.9	
3.0	4.5	0.5	
2.9	3.5	0.6	
2.7	3.7	1.0	
2.6	3.5	0.9	
2.6	2.1	0.5	
2.5	3.0	0.5	
2.5	3.8	1.3	
2.3	2.8	0.5	
2.2	3.6	1.4	
2.0	2.0	0.0	
2.0	4.0	2.0	
1.9	2.5	0.6	
1.9	2.7	0.8	
1.9	3.0	1.1	
1.9	2.5	0.6	
1.7	3.7	2.0	
1.7	2.7	1.0	
1.7	3.9	2.2	
1.7	1.7	0.0	
1.7	2.6	0.9	
1.6	1.8	0.2	
1.5	2.0	0.5	
1.5	1.0	0.5	
1.5	2.9	1.4	
1.4	1.5	0.1	
1.4	1.5	0.1	
1.3	1.7	0.4	
1.3	3.5	2.2	
1.3	1.9	0.6	
1.2	3.8	2.6	
1.2	2.8	1.6	AVG DEV.= $\pm$0.9 A-H
1.2	2.5	1.3	= $\pm$ 23%
1.1	1.5	0.4	
1.1	1.6	0.5	MAX. DEV. = 3.5 A-H
1.0	1.8	0.8	

TABLE 9 (CONT'D)

PREDICTION OF RESIDUAL CAPACITY FROM RESISTANCE, CONNECTIONS AS IN FIGURE 29A

PREDICTED RESIDUAL CAPACITY A-H	ACTUAL RESIDUAL CAPACITY A-H	DEVIATION A-H
0.9	0.9	0.0
0.9	3.1	2.2
0.6	4.1	3.5
0.5	2.1	1.6
0.5	1.1	0.6

TABLE 9

PREDICTION OF RESIDUAL CAPACITY FROM RESISTANCE, CONNECTIONS AS IN FIGURE 29B

PREDICTED RESIDUAL CAPACITY A-H	ACTUAL RESIDUAL CAPACITY A-H	DEVIATION A-H
6.2	4.3	1.9
5.6	5.3	0.3
4.9	3.3	1.6
3.6	2.3	1.3
2.9	5.0	2.1
2.5	6.0	3.5
2.5	4.0	1.5
2.5	1.3	1.2
2.2	2.5	0.3
2.1	2.3	0.2
1.9	3.0	1.1
1.9	2.8	0.9
1.9	1.8	0.1
1.9	1.8	0.1
1.6	3.0	1.4
1.6	1.5	0.1
1.5	2.0	0.5
1.5	0.8	0.7
1.0	1.0	0.0

AVG. DEV. = $\pm$ 1.0 A-H = $\pm$ 25%

MAX. DEV. = 3.5 A-H

TABLE 10

RESISTANCE OF ROTARY SWITCH AND COMPONENTS

ITEM	RESISTANCE IN MILLIOHMS
Entire Switch in Figure 25	1.75
Cu-Cu Mechanical Contact in above switch	0.14
Cu lead in mercury reservoir in above switch	0.1
Cu lug bolted to cell terminal	0.32
8" length of 1/2" wide ground strap	0.37
1" length of 1" x 1/4" Copper	$<$ 0.005
Superior Connector (50 A rating)	0.11

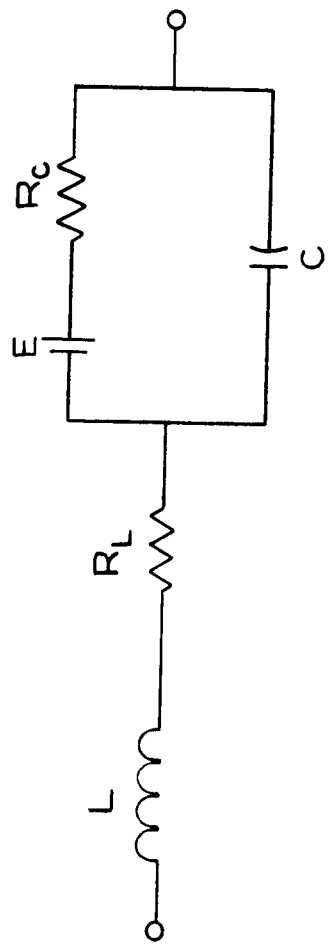

Figure 1 Equivalent Circuit for Nickel-Cadmium Cell

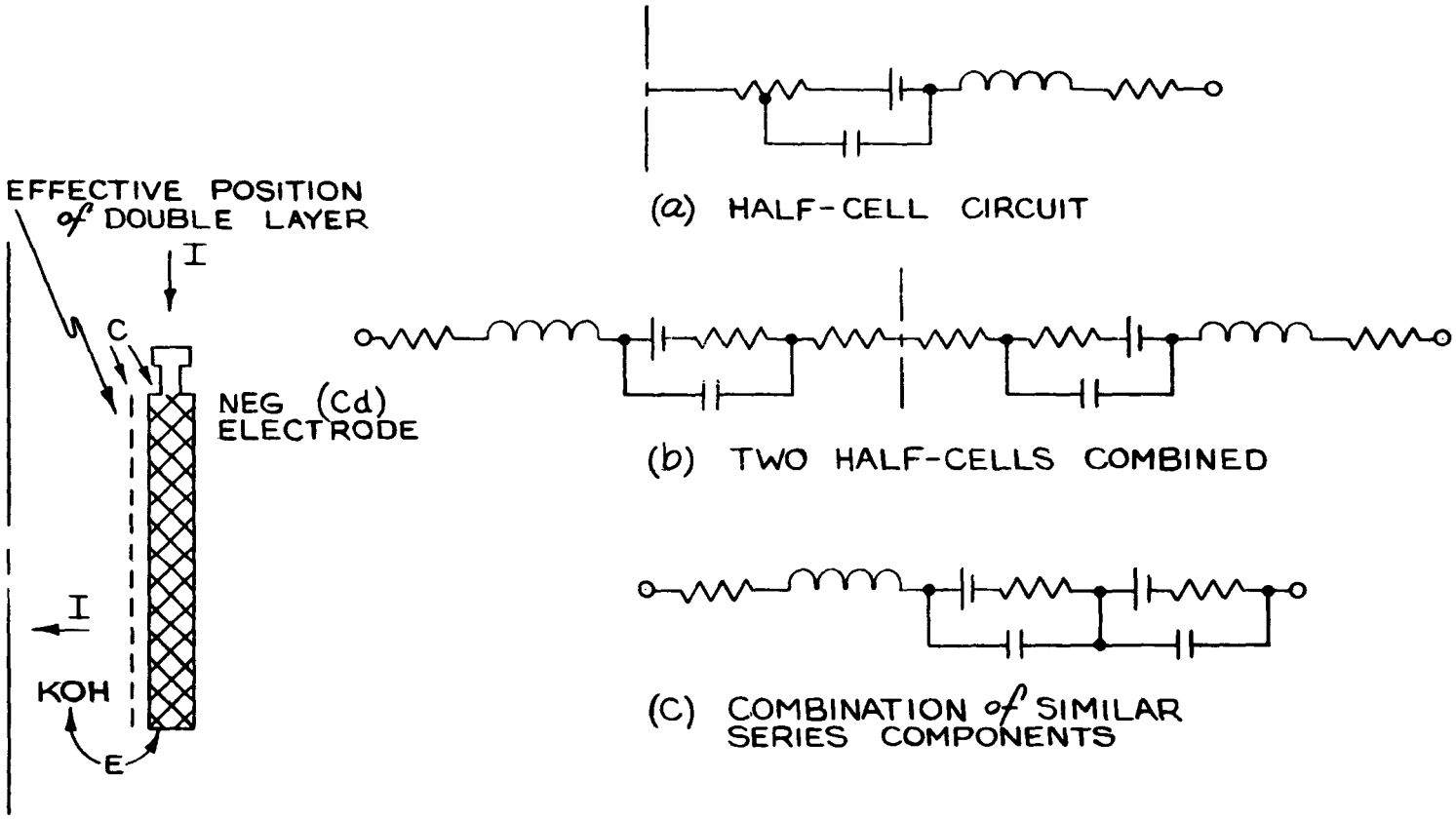

Figure 2 Equivalent Circuit for Half-Cell

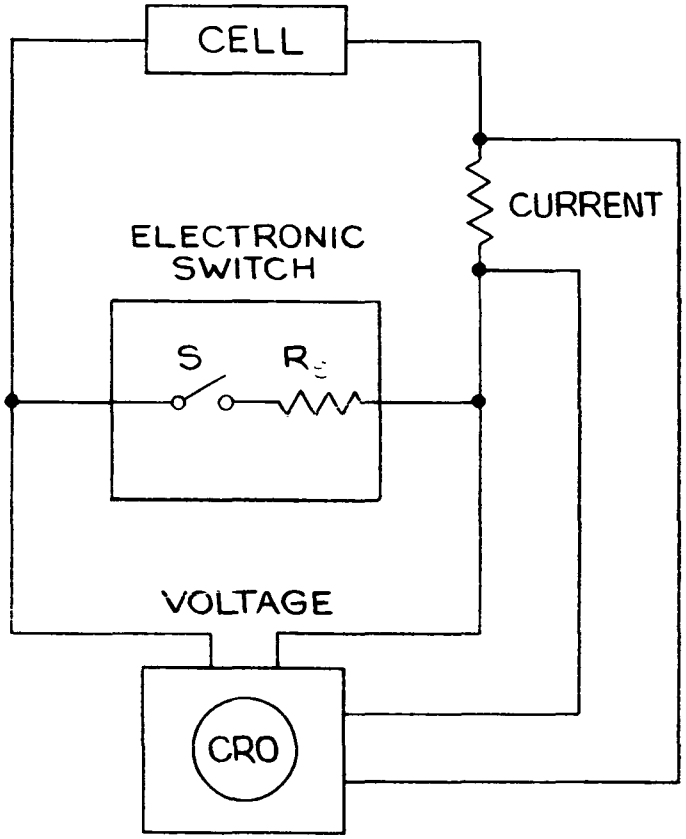

Figure 3 Circuit for Demonstrating Transient

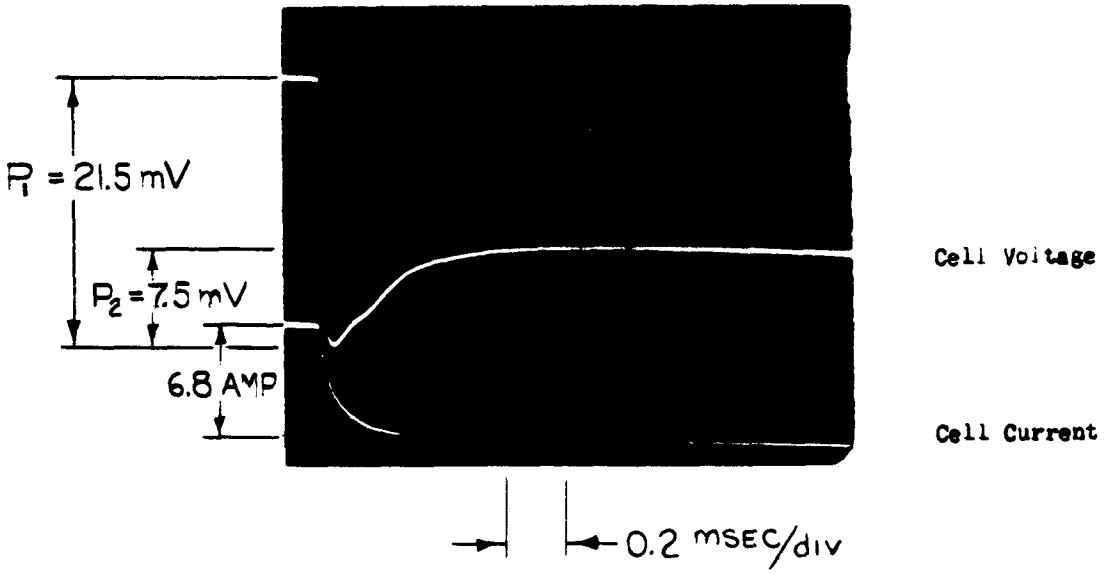

Initial transient and post transient slope. Short horizontal lines at extreme left show open circuit voltage and zero current before switch is closed.

Figure 4 Initial Transient, 4 A-H Cell

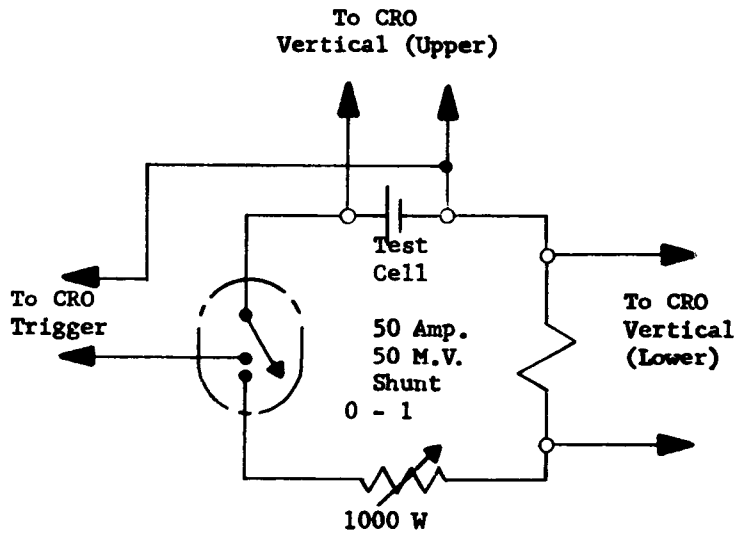

CRO = Tektronix 502
Dual Beam Oscilloscope

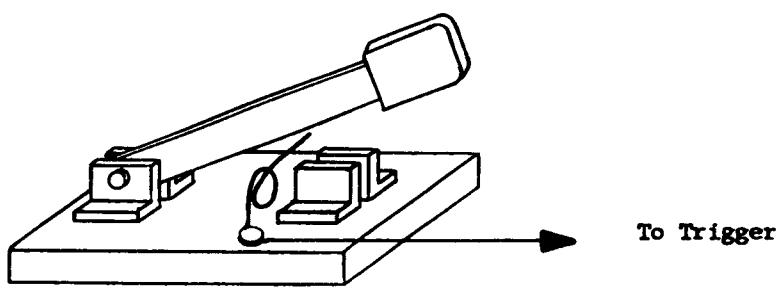

Knife Switch, 50 Amp. Rating

Figure 5 Mechanical Switch for Pulse Measurements

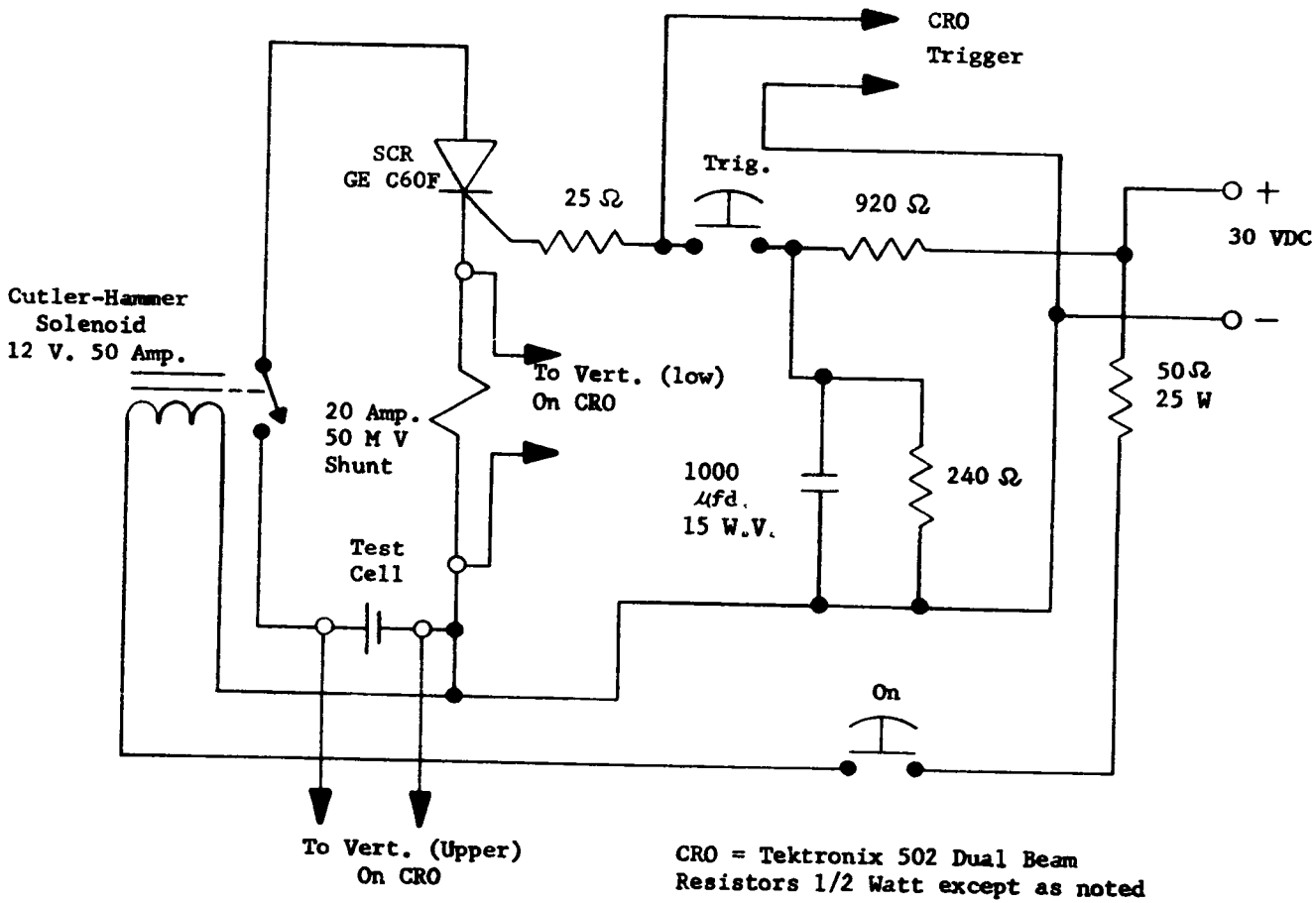

Figure 6 Schematic for Electronic Switch

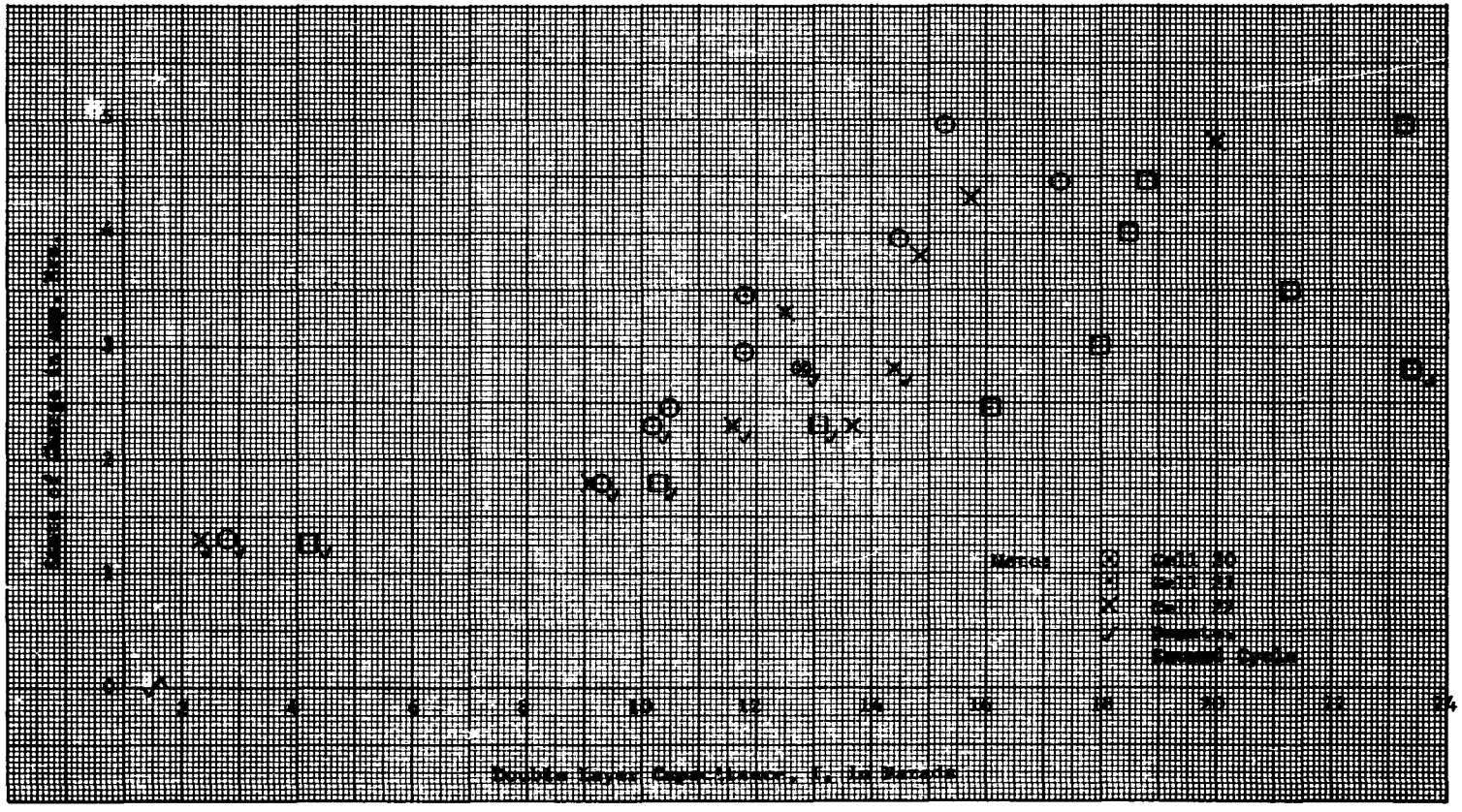

Figure 7 Variation of Double Layer Capacitance With Residual Capacity

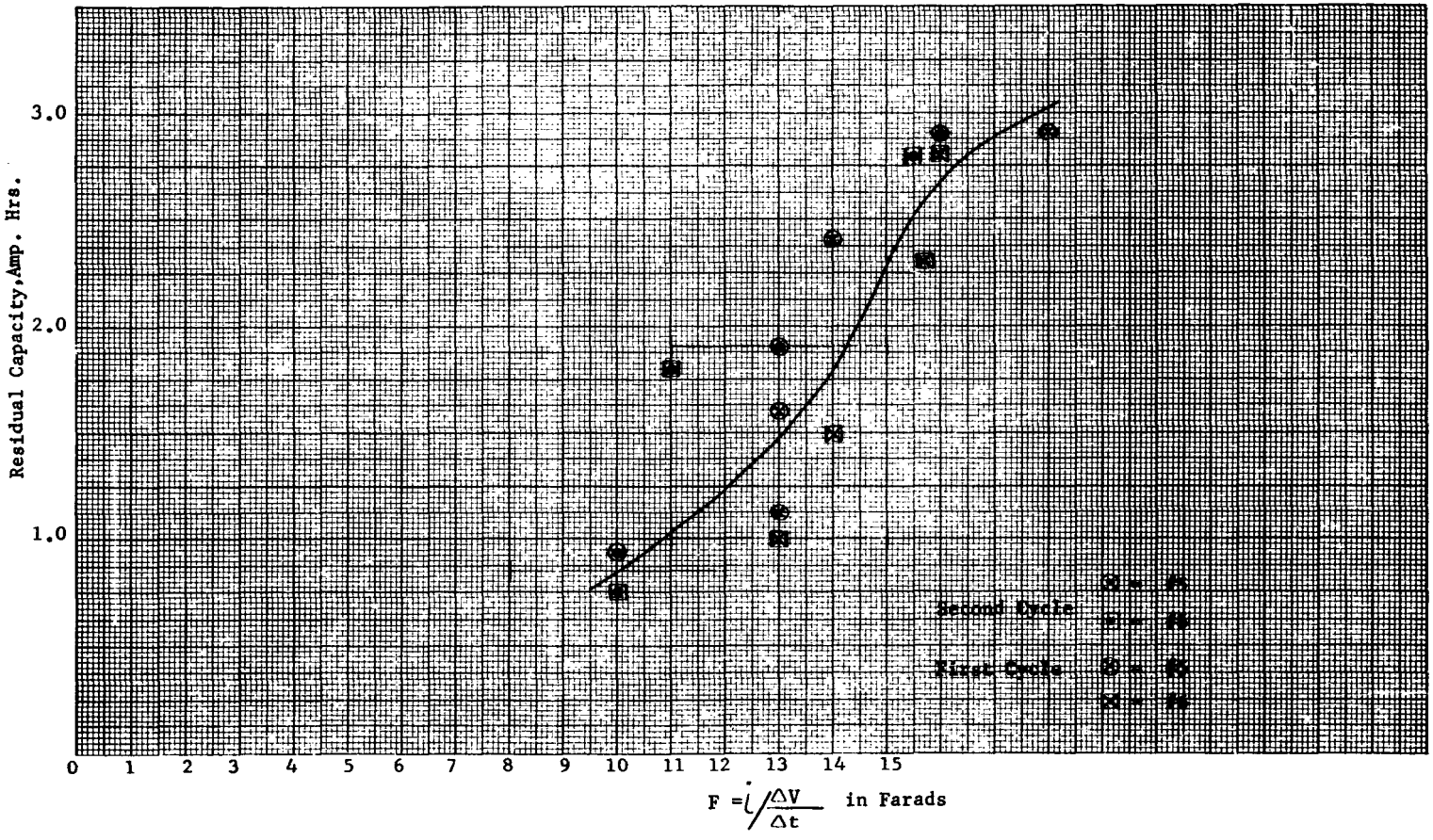

Figure 8 Variation of Double Layer Capacitance With Residual Capacity

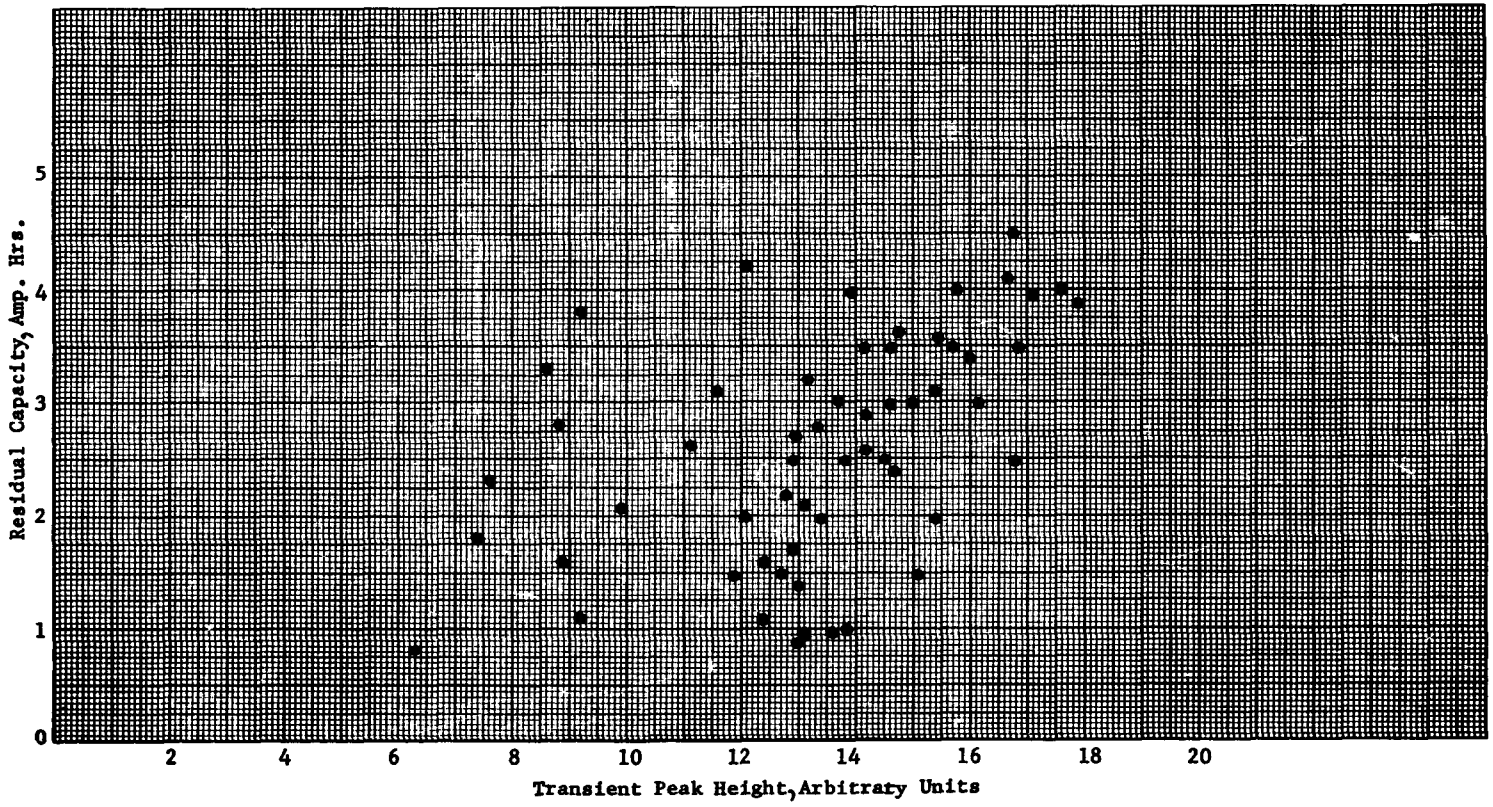

Figure 9 Transient Peak Height at Various Residual Capacities

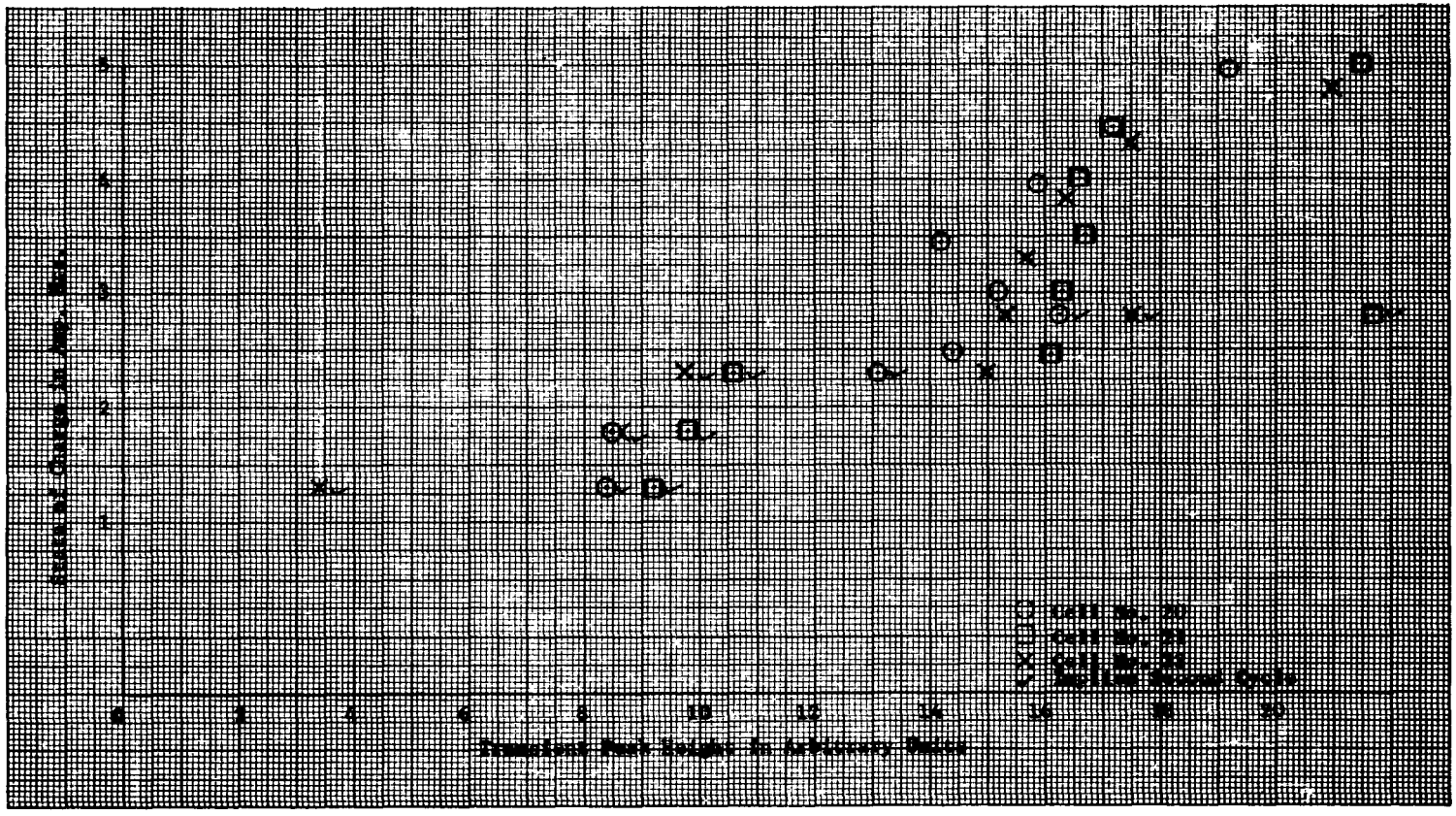

Figure 10 Transient Peak Height For Two Cycles on Three Cells

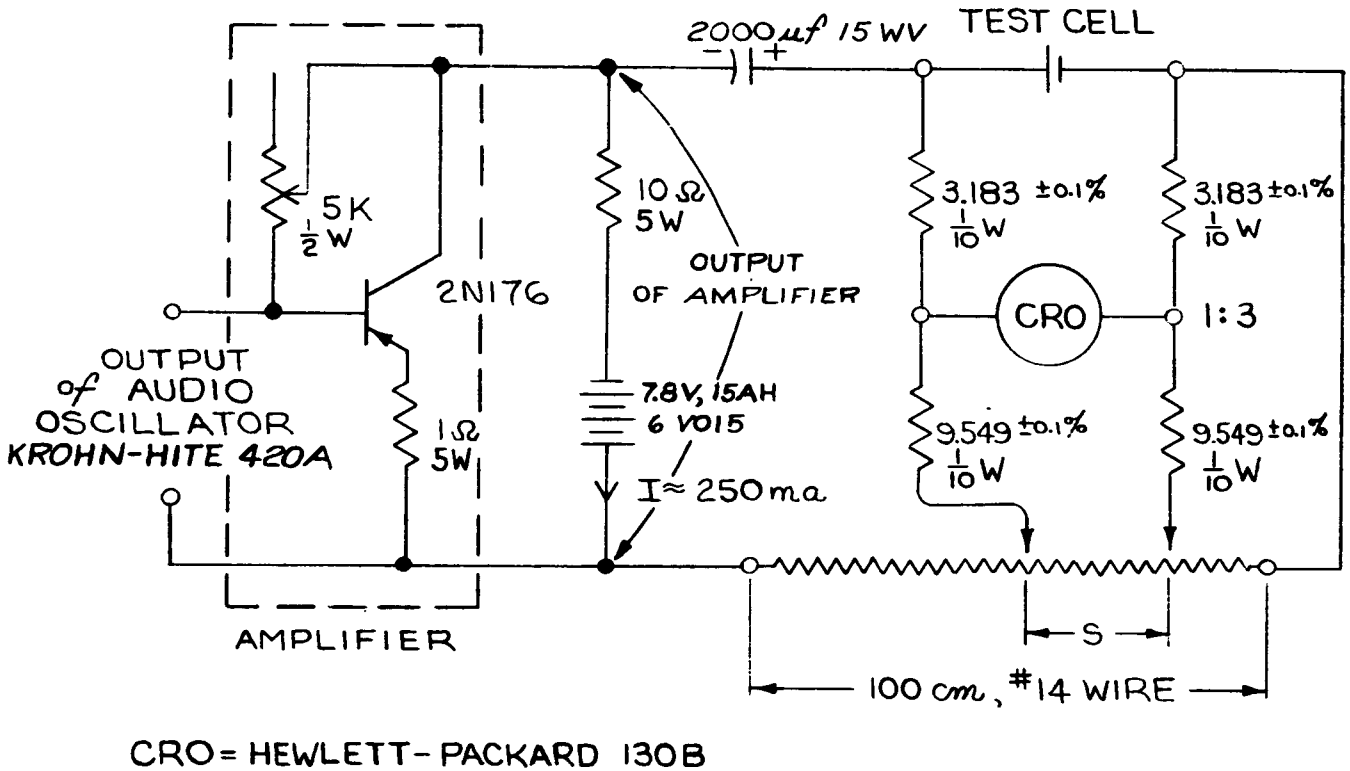

CRO = HEWLETT-PACKARD 130B

Figure 11 A. C. Kelvin Double Bridge

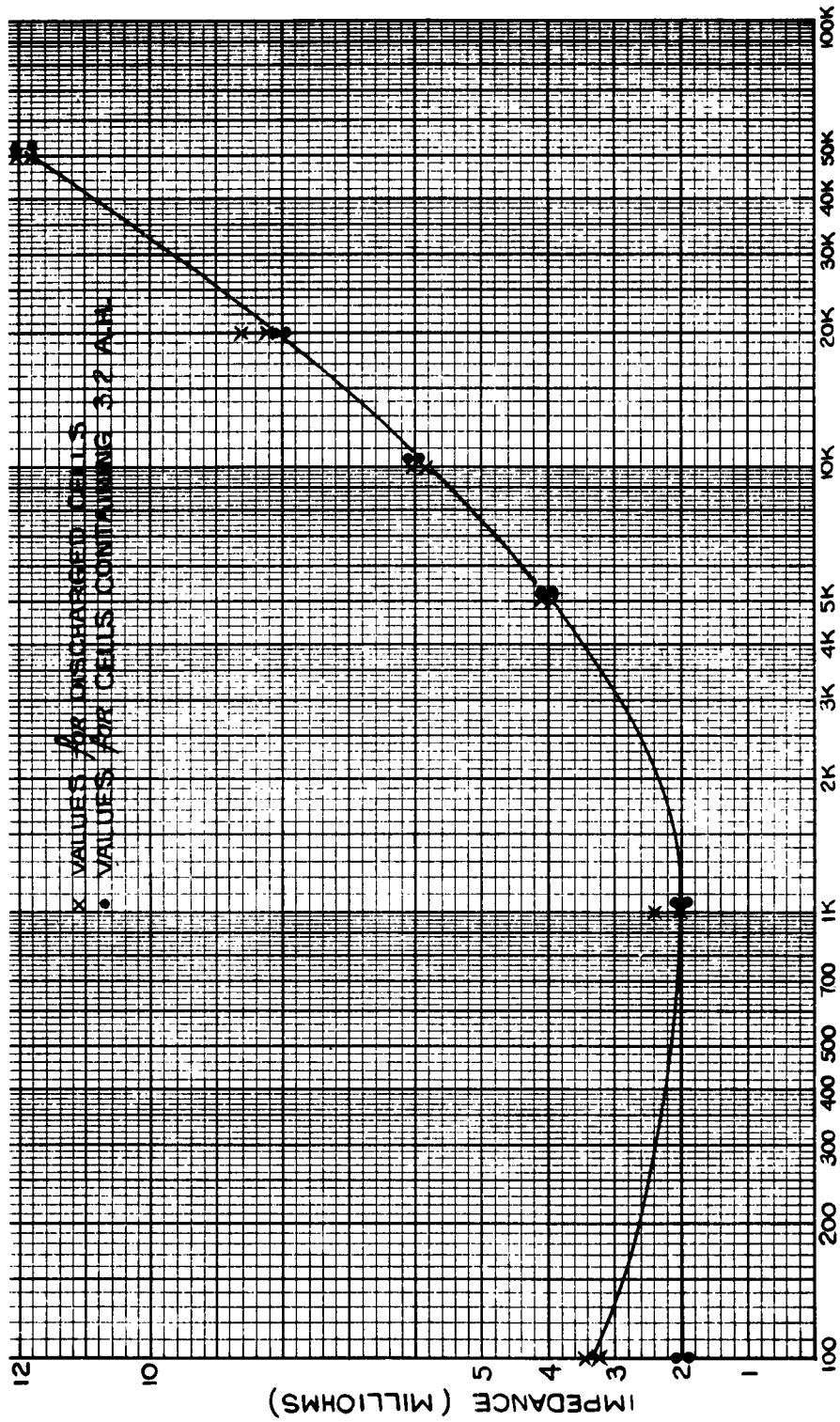

Figure 12 Impedance Vs. Frequency For 4 A-H Cells

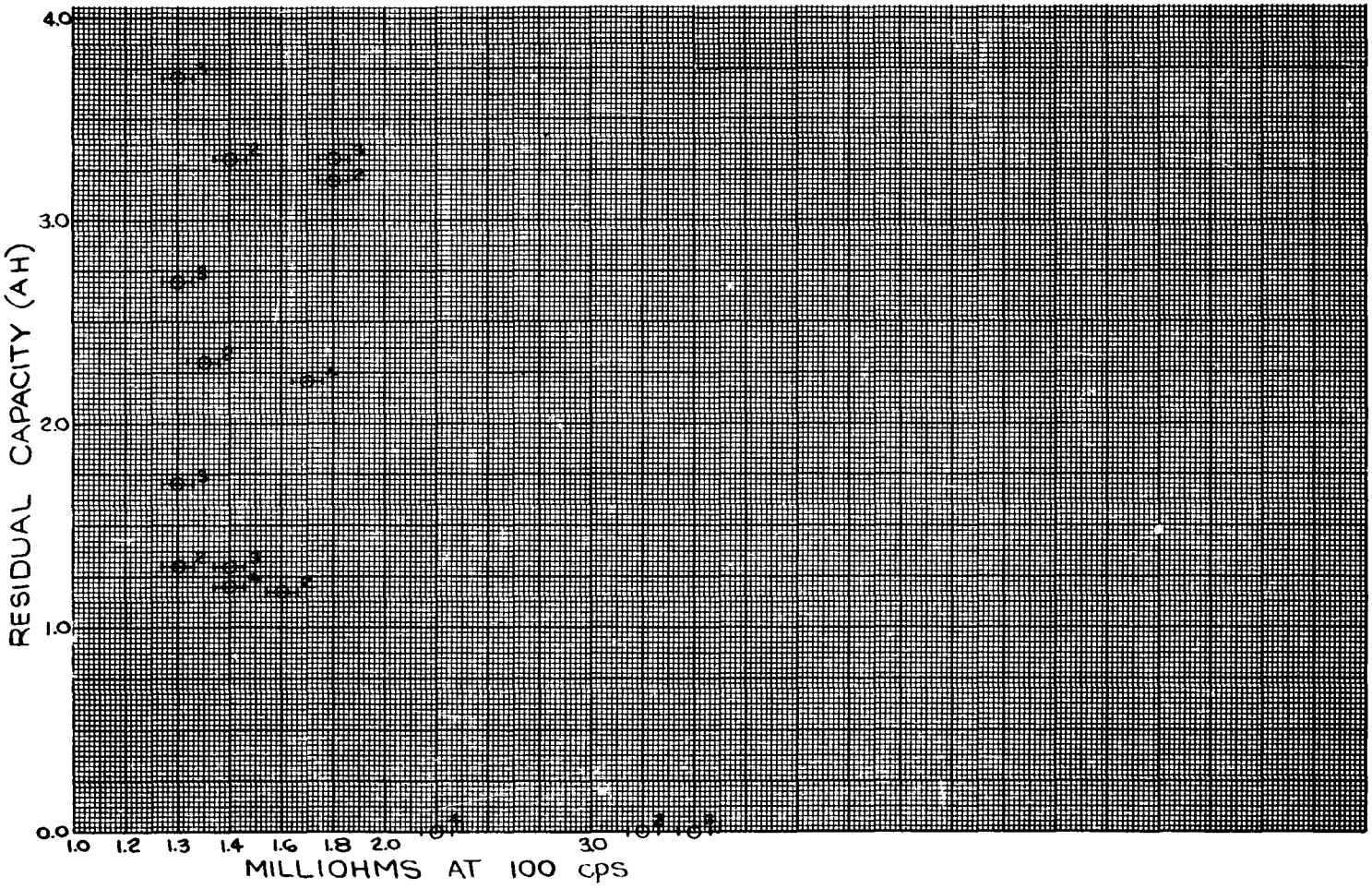

Figure 13 100 CPS. Impedance At Various States of Charge

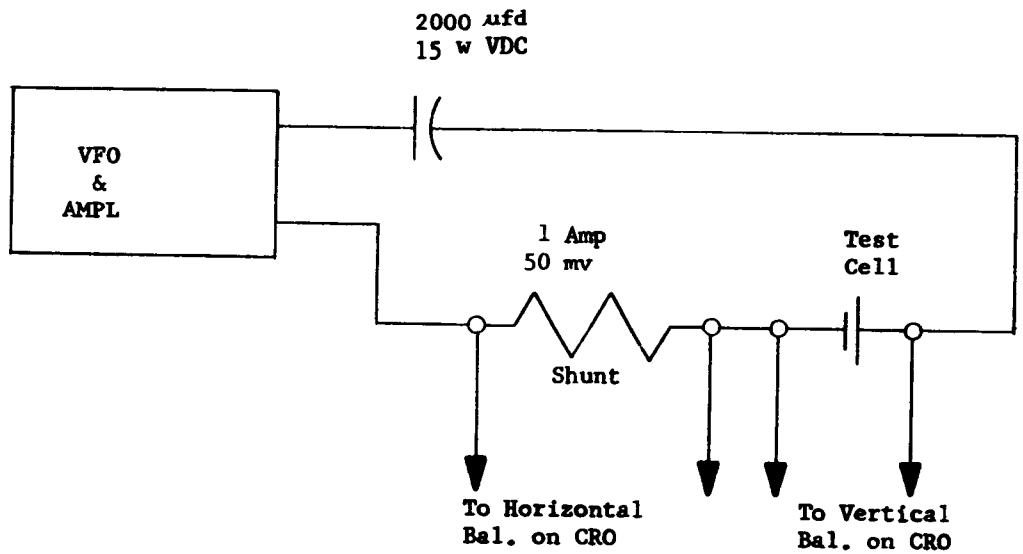

CRO = Tektronix 502

VFO = Krohn-Hite 420A

AMPL = McIntosh 50w

Figure 14 Apparatus For Measuring Resonant Frequency

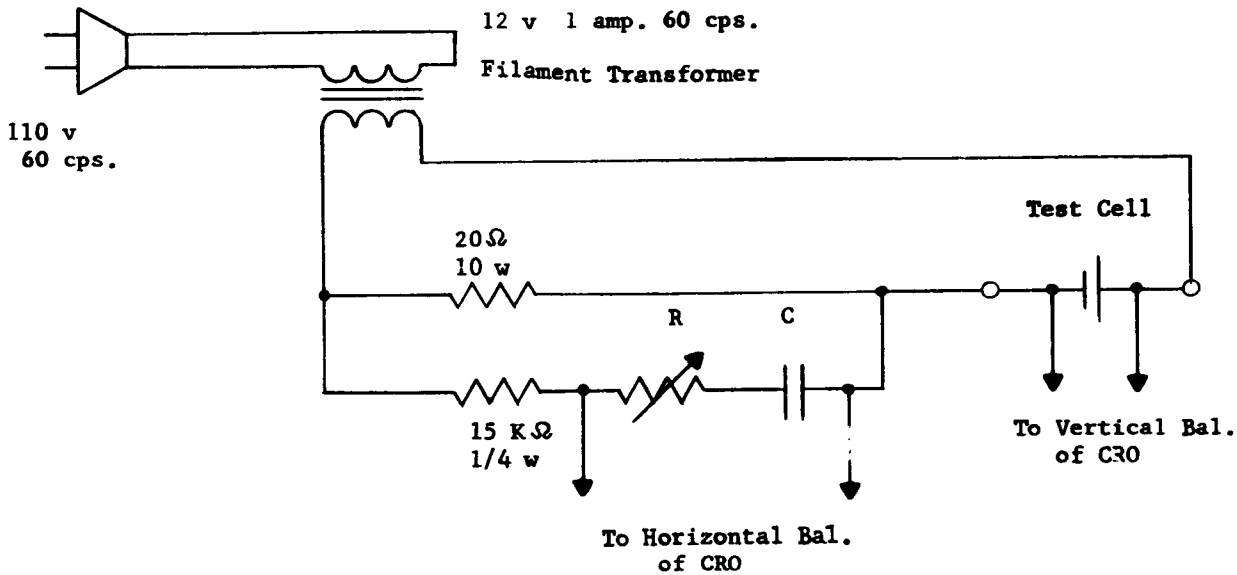

CRO = Tektronix 502

R = 0.1 to 9,999Ω Decade

X_c = 89 ± 1/2Ω @ 60 cps (30μfd)

Figure 15 Apparatus For Measuring Phase Shift at 60 cps.

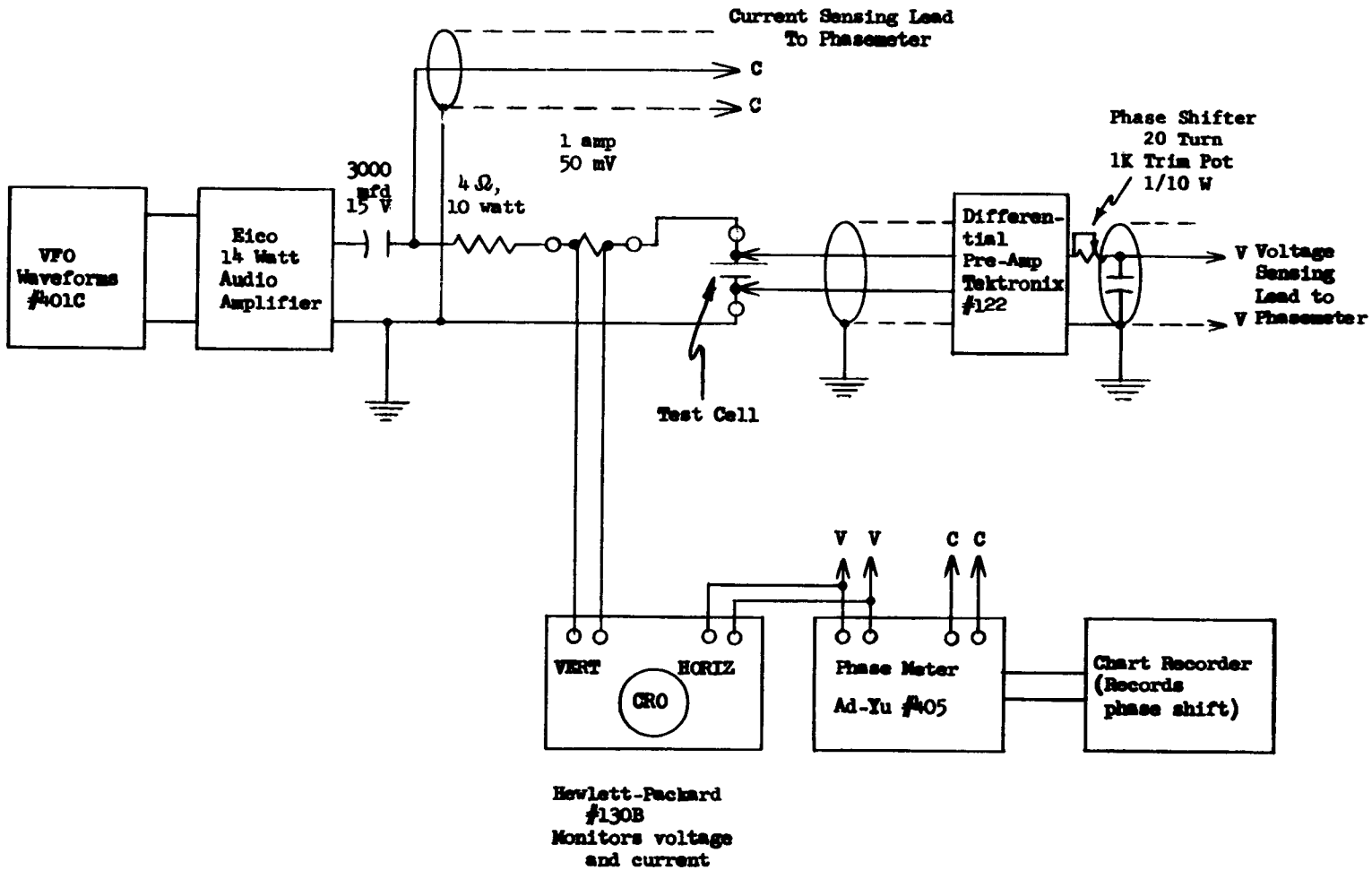

Figure 16 Diagram of Phase Measuring System

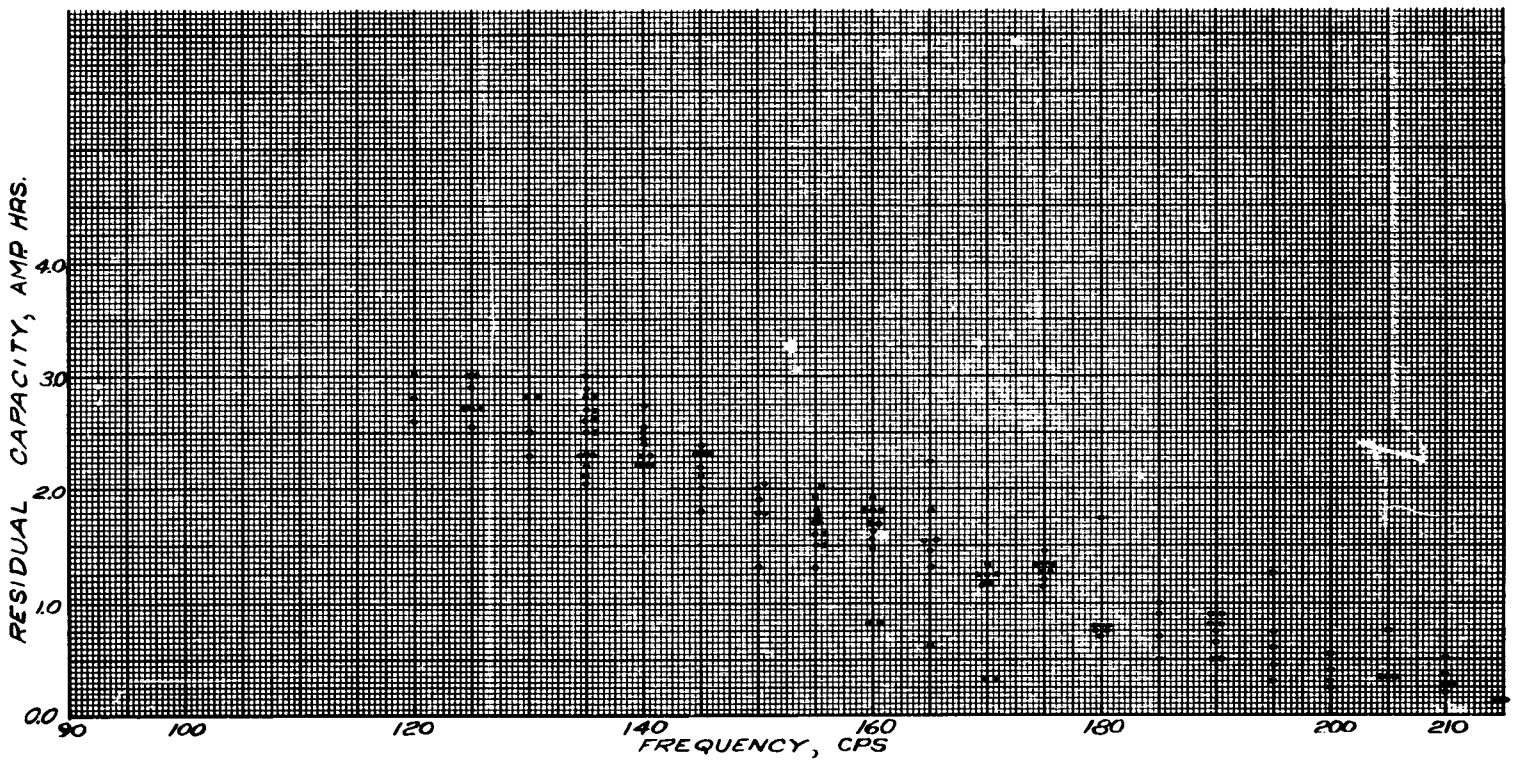

Figure 17 Resonant Frequency Vs. Residual Capacity

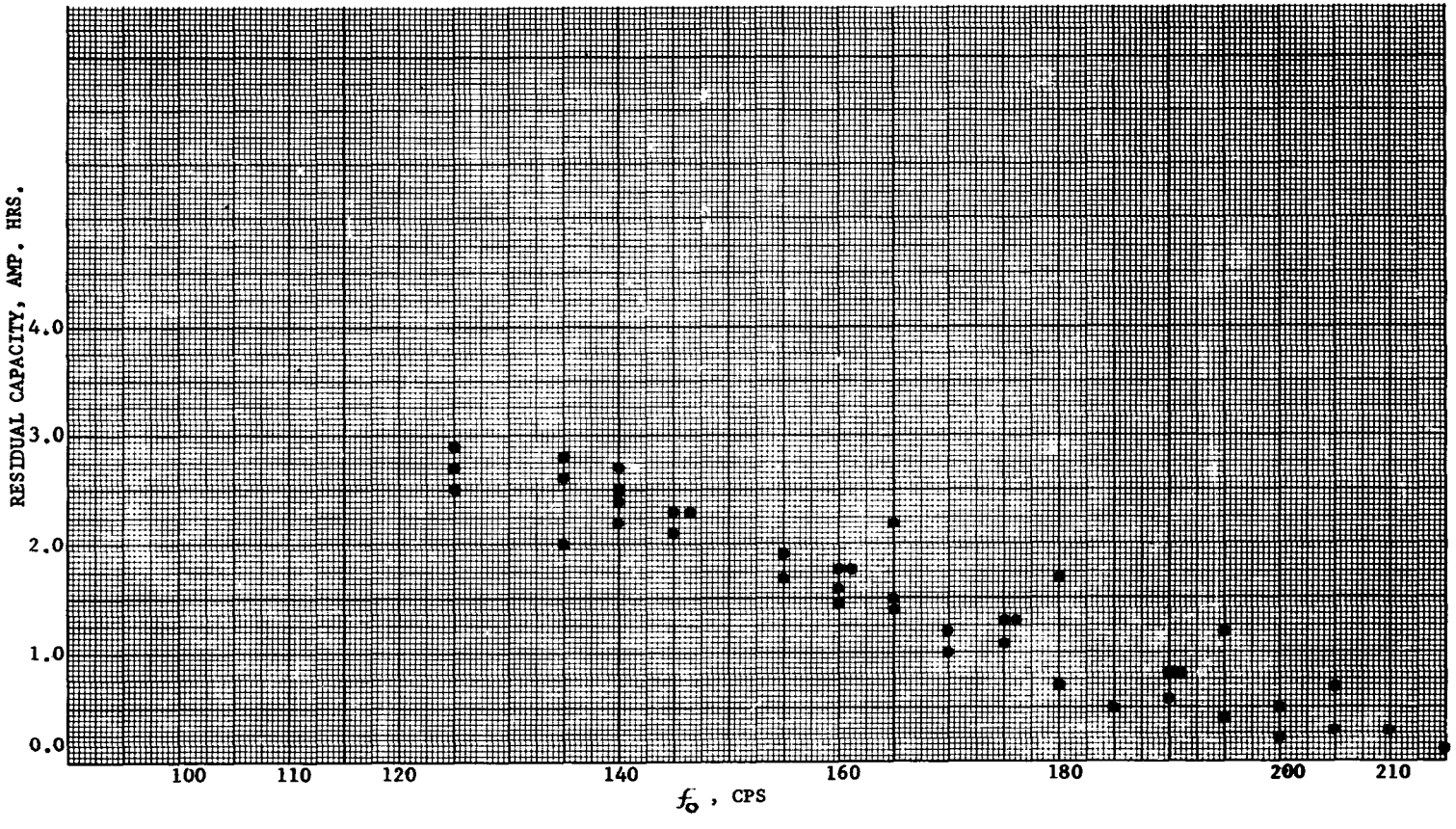

Figure 18 Resonant Frequency Vs. Residual Capacity

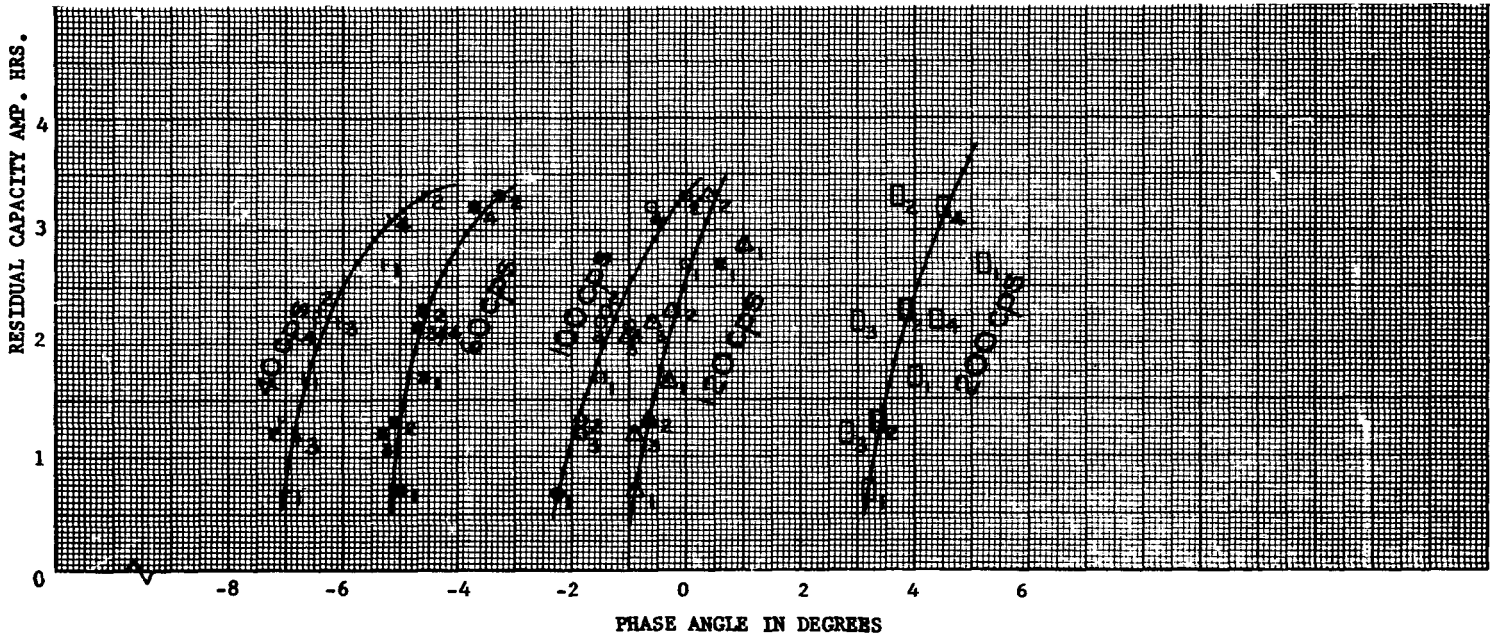

Figure 19 Phase Shift at Several Frequency Vs. Residual Capacity

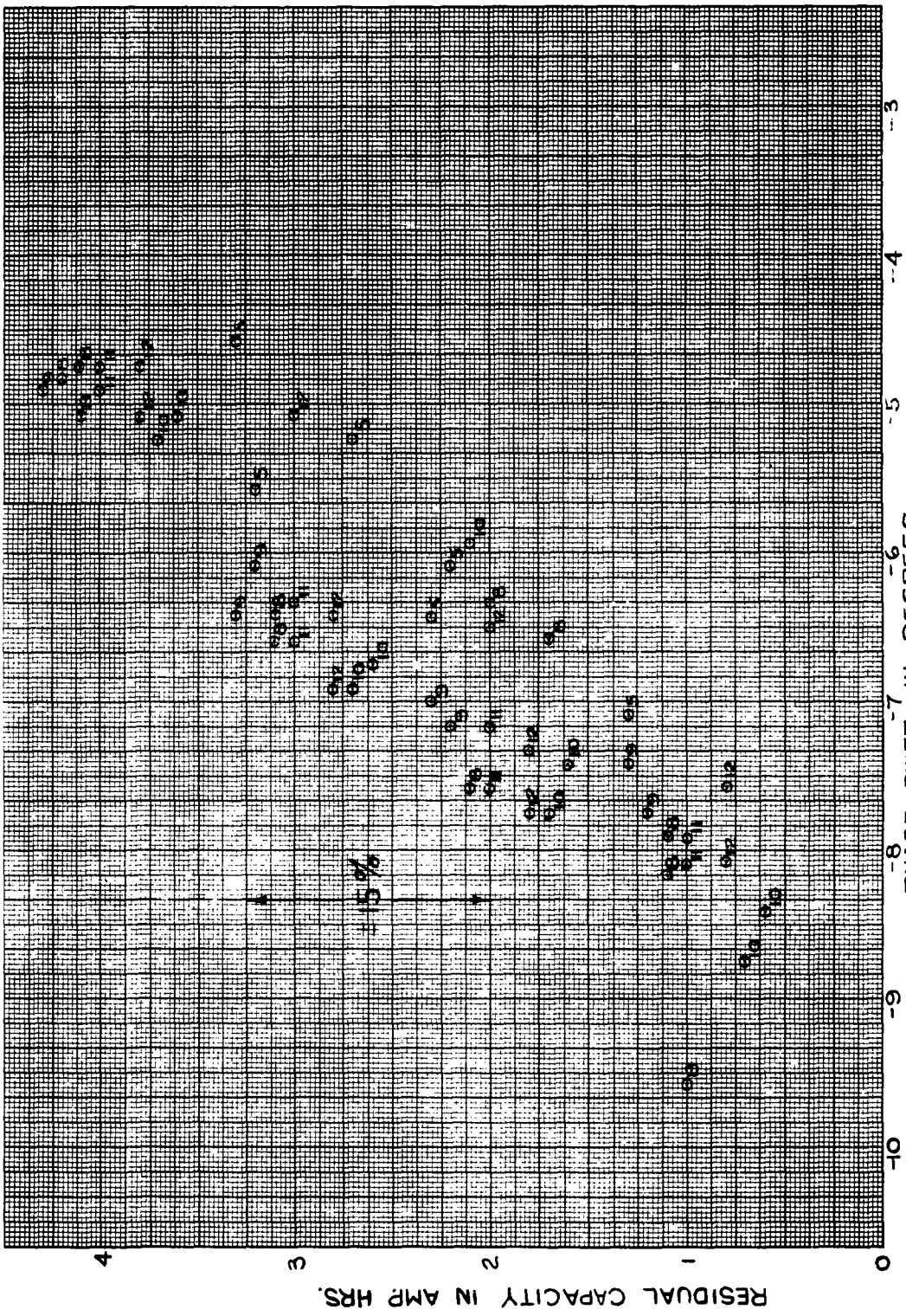

Figure 20 40 Cycle Phase Shift Vs. Residual Capacity

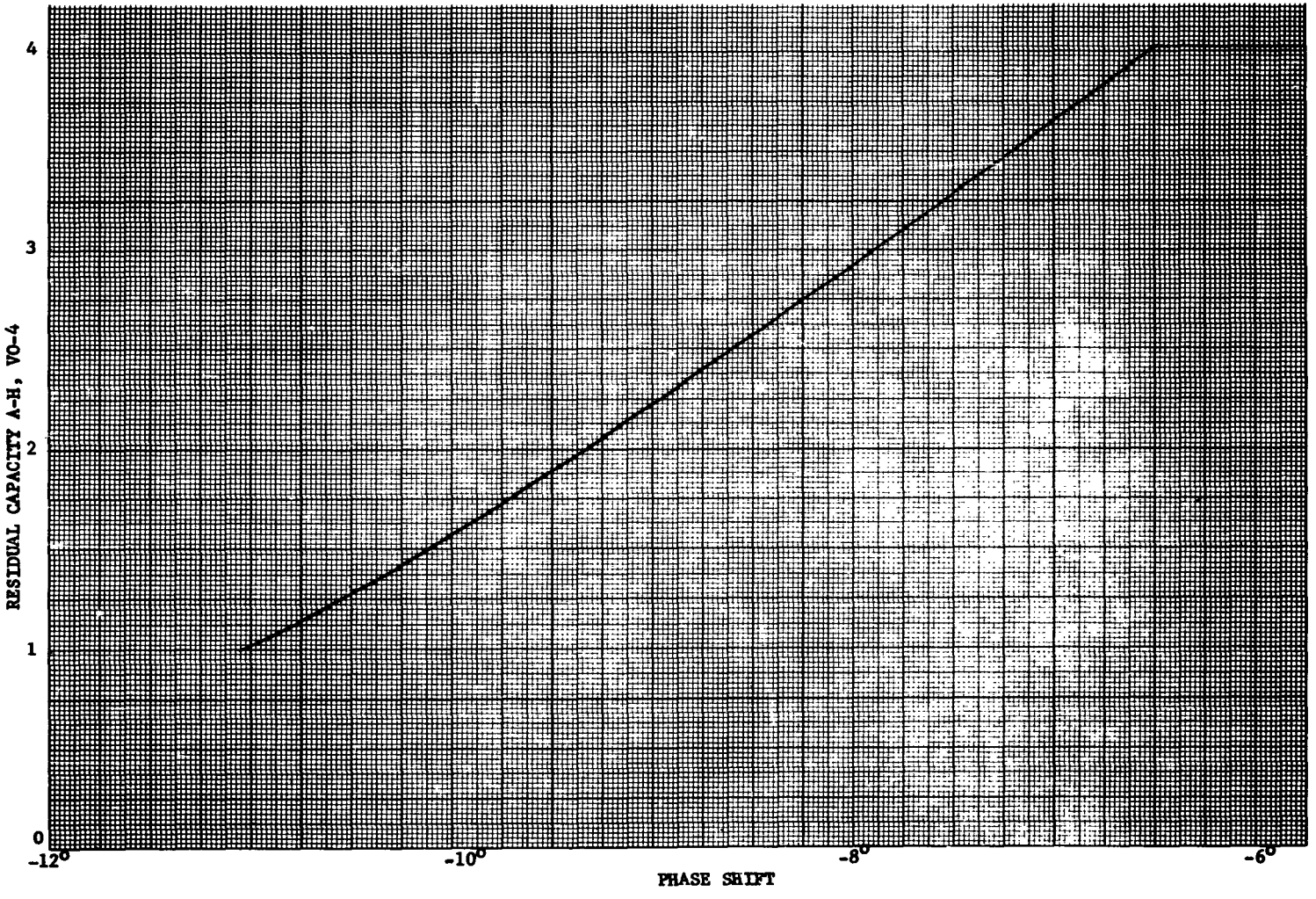

Figure 21A Calibration Curve at Room Temperature

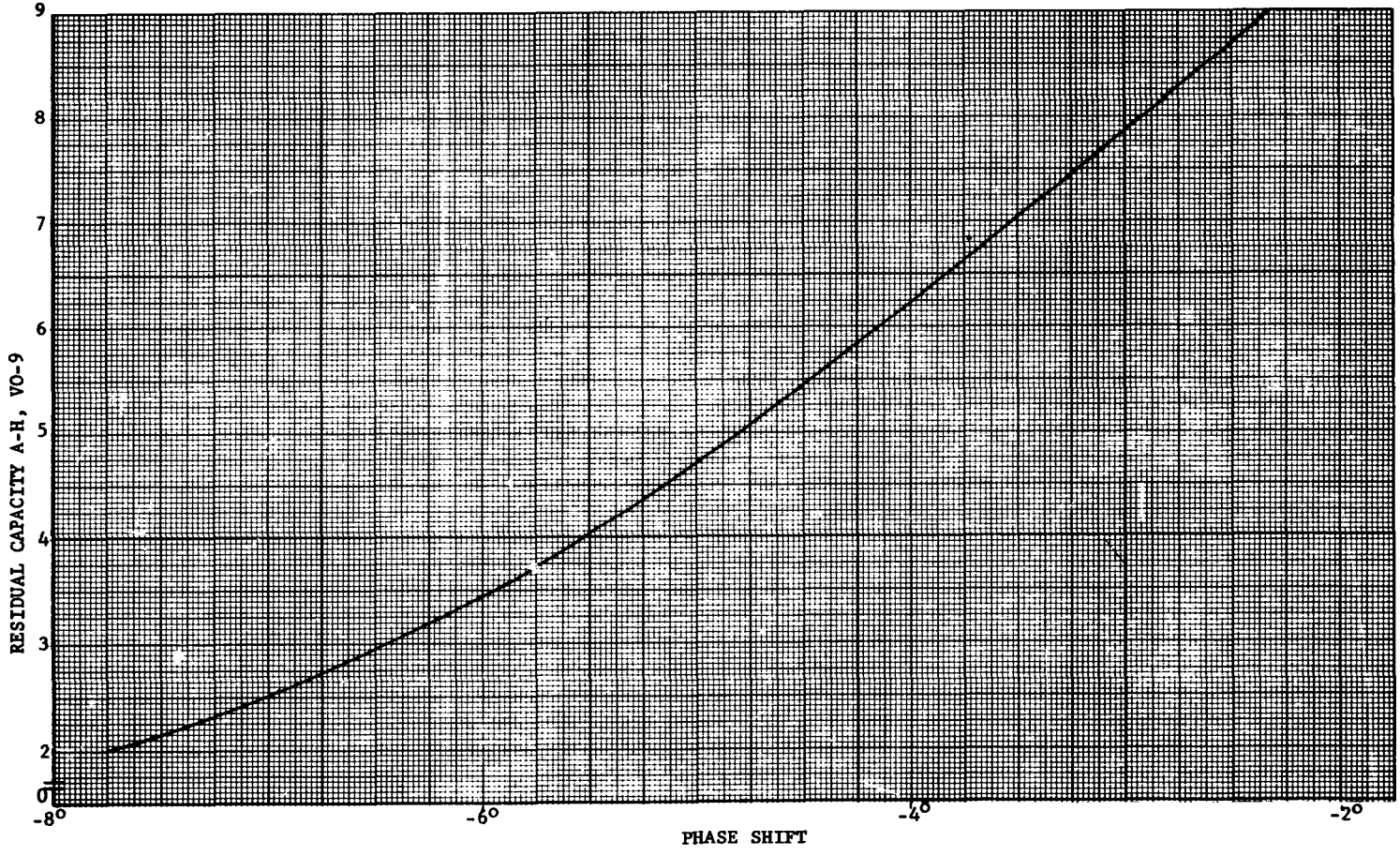

Figure 21B Calibration Curve at Room Temperature

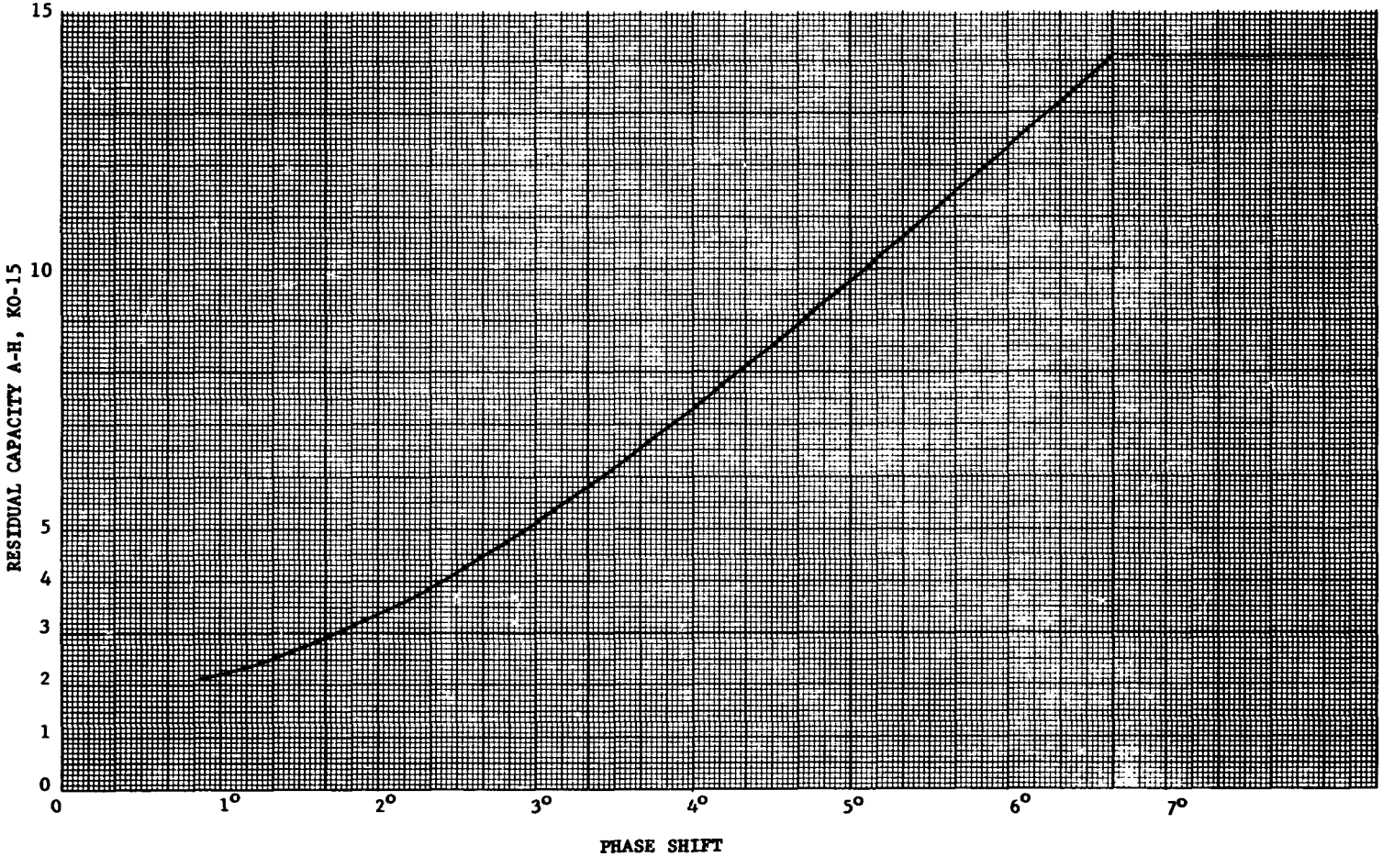

Figure 21C Calibration Curve at Room Temperature

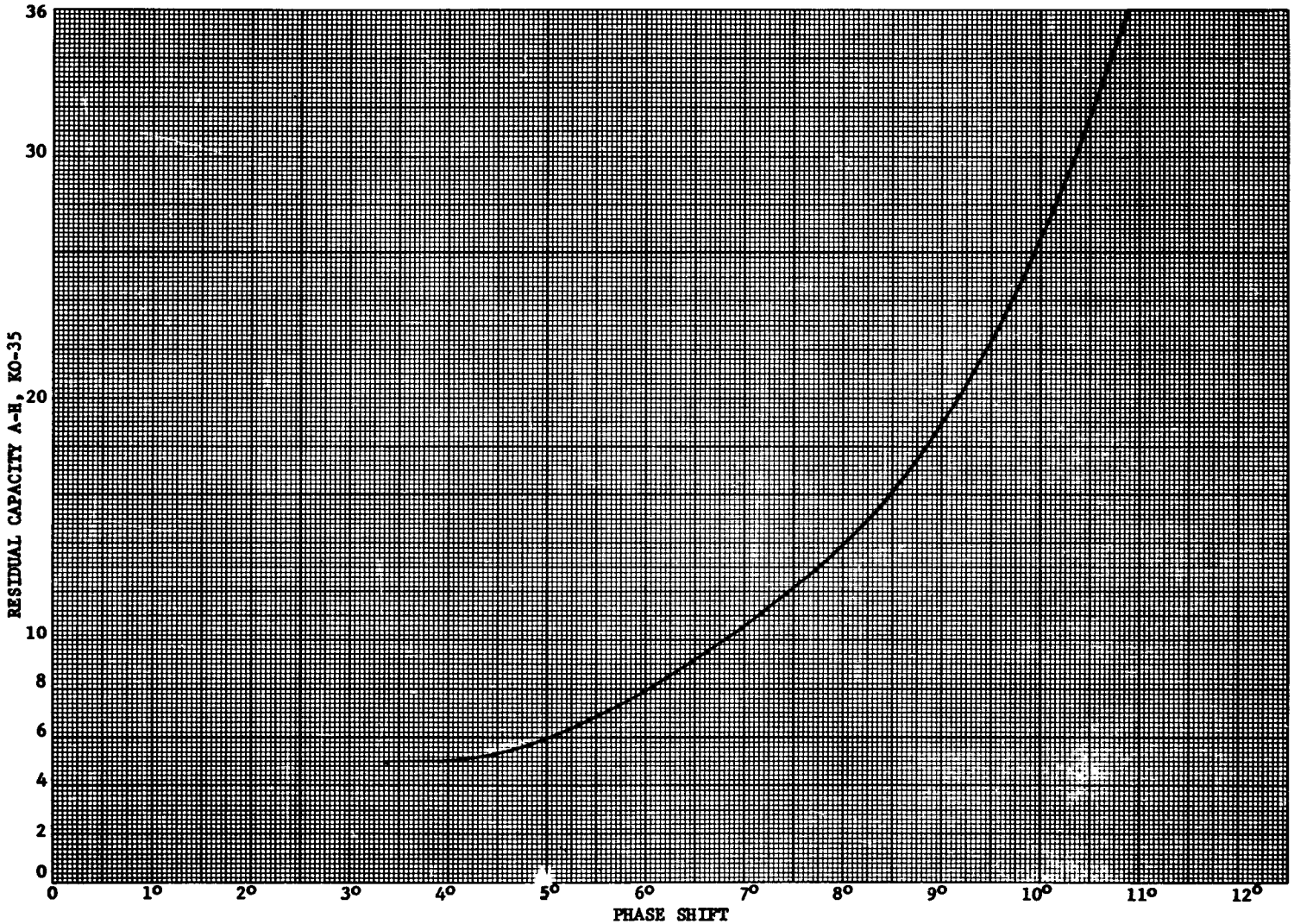

Figure 21D Calibration Curve at Room Temperature

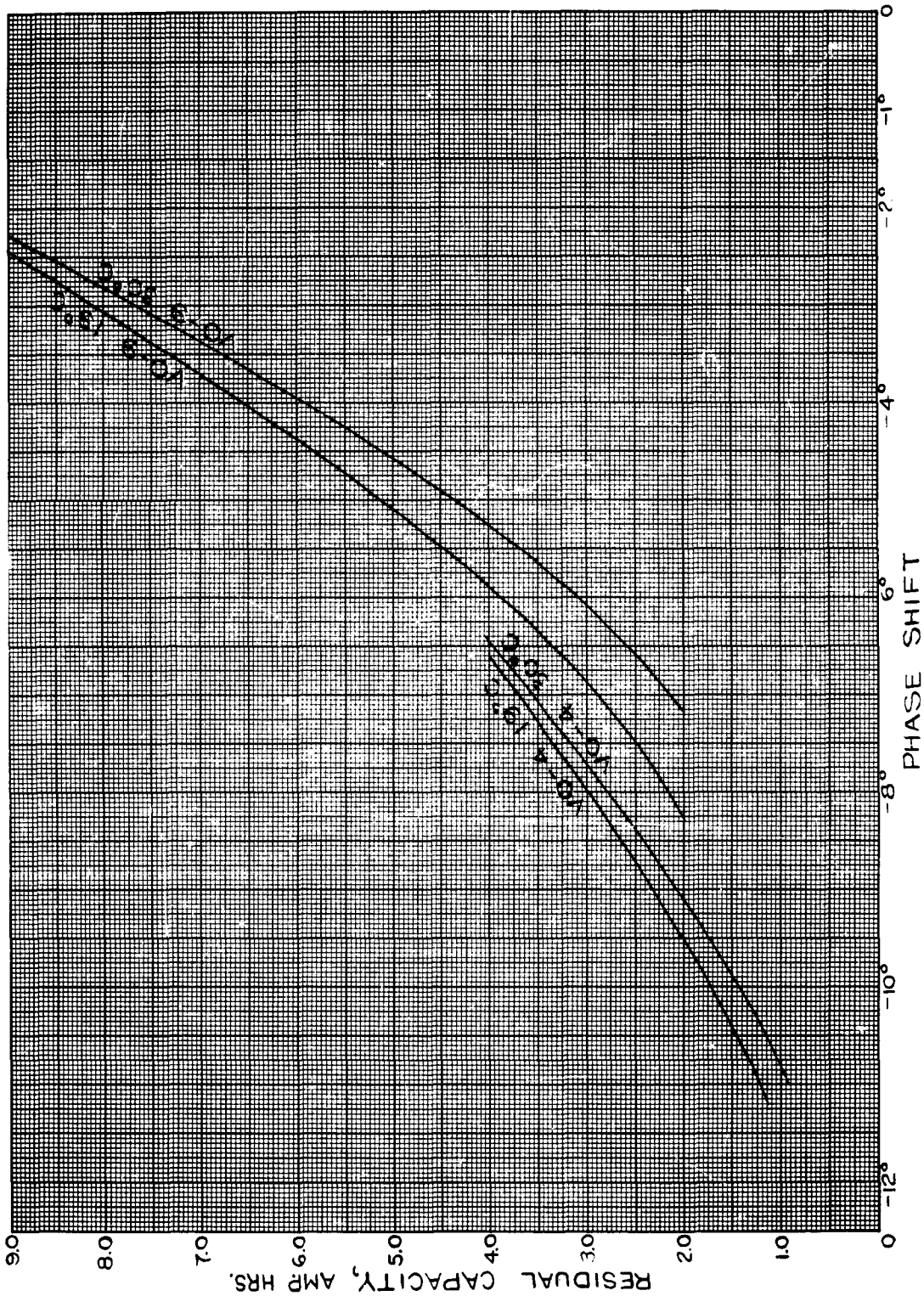

Figure 22 Calibration Curves at Fixed Temperatures

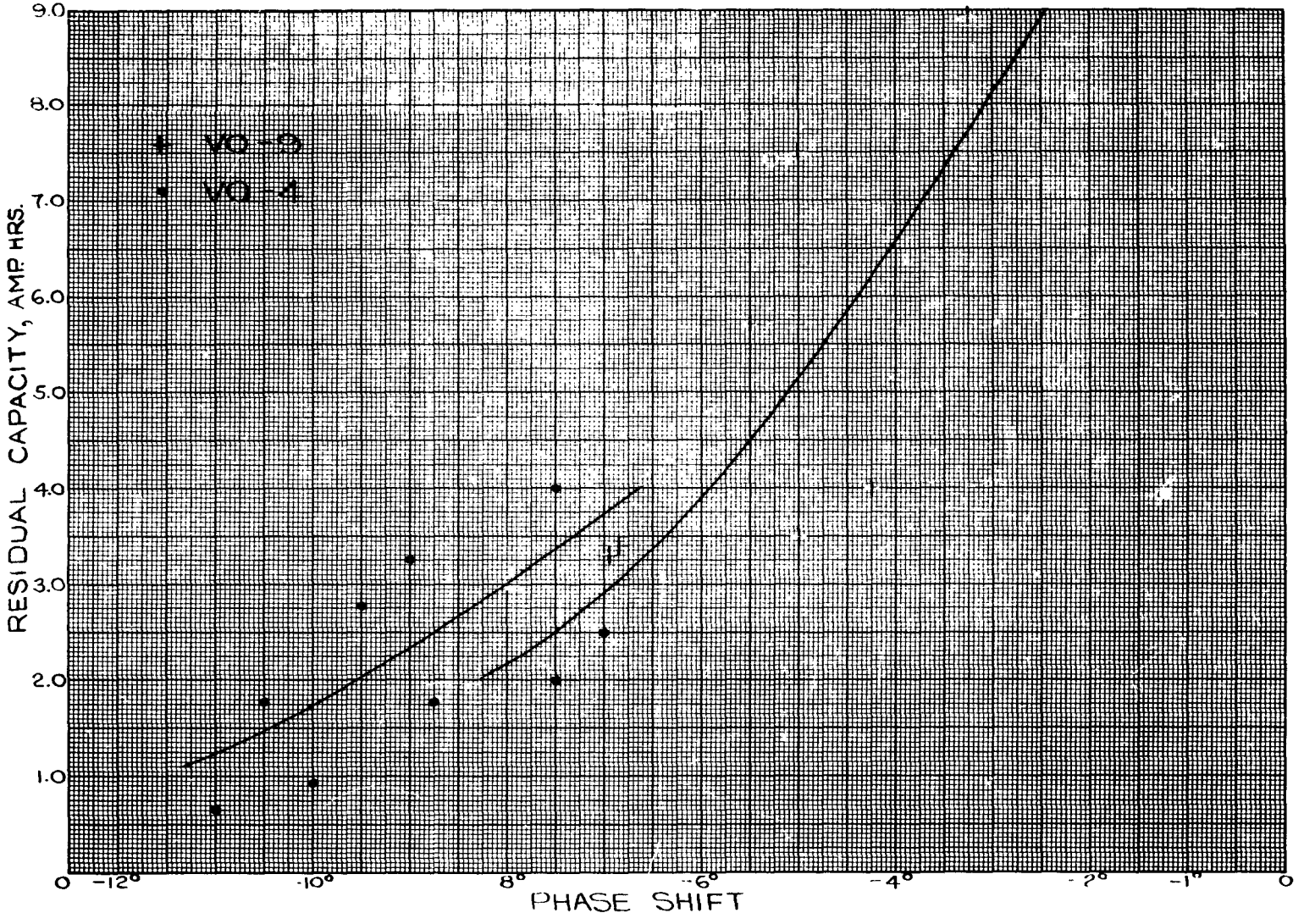

Figure 23 Calibration Curve Showing Extreme Points

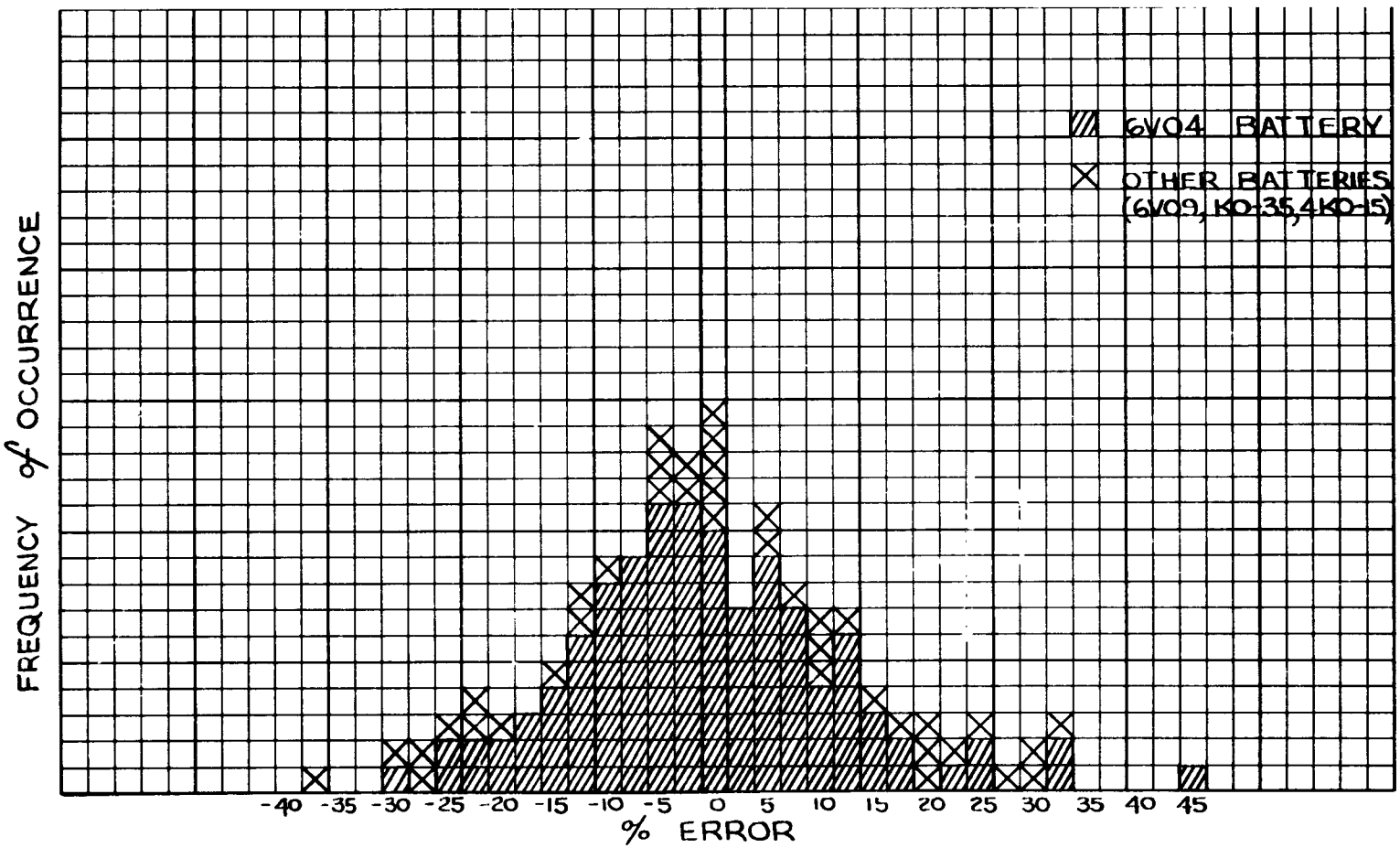

Figure 24 Distribution of Deviation, Histogram

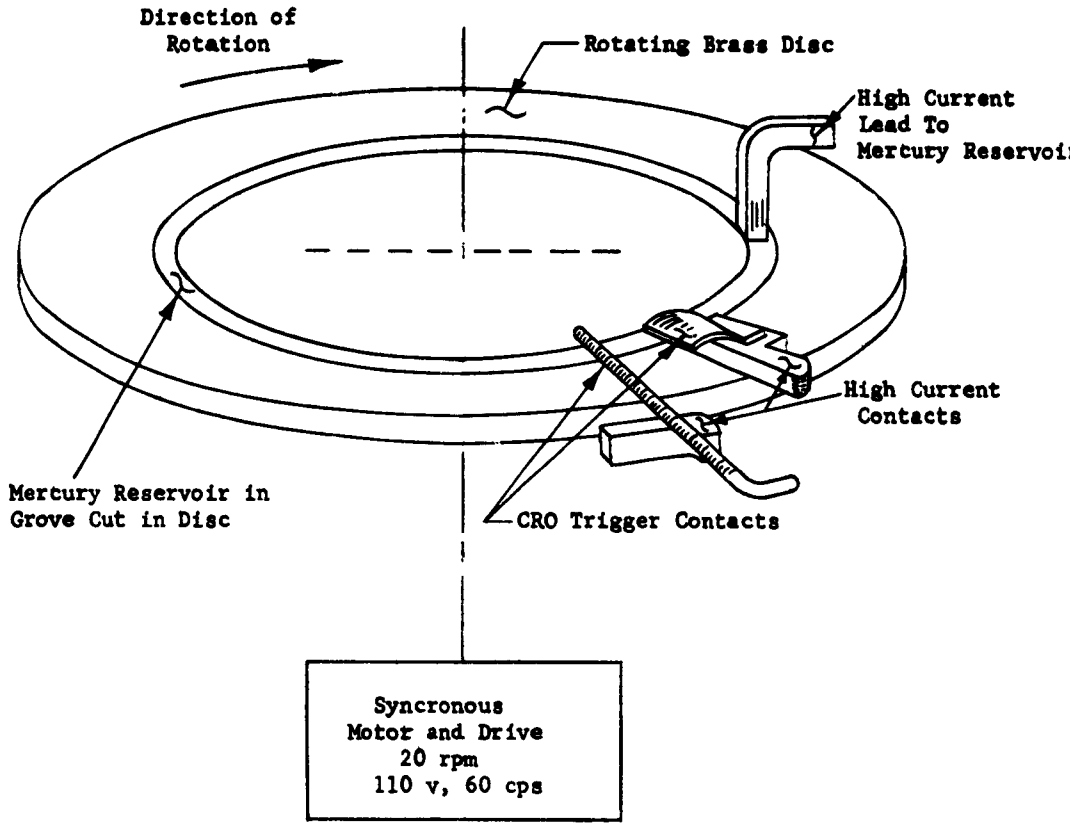

Figure 25 Mechanical High Current Switch

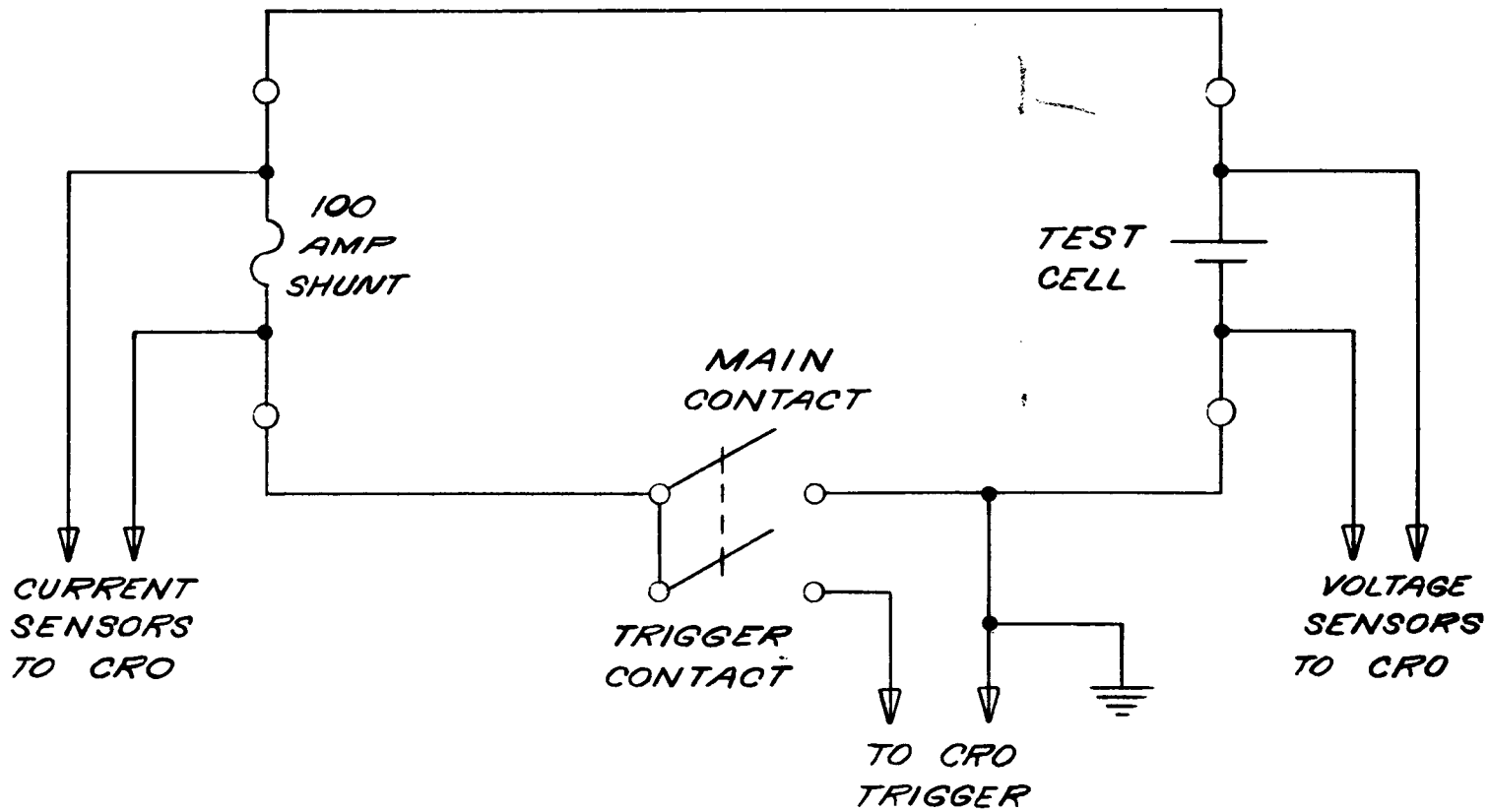

Figure 26 Wiring Diagram of Mechanical Switch

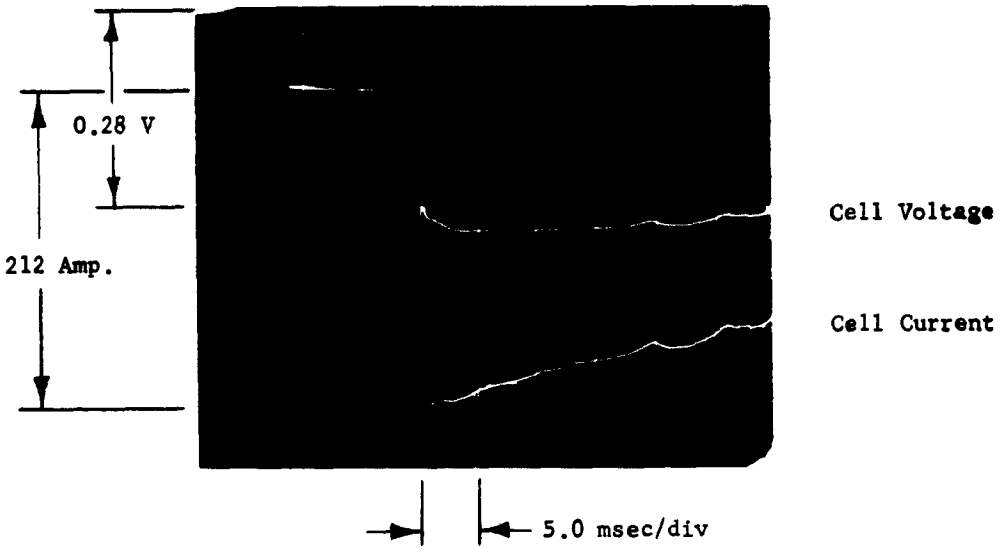

Current and voltage during high current pulse. Horizontal lines at left show open circuit voltage (upper) and zero current (lower) before switch is closed.

Figure 27 Oscilloscope Display To Measure Resistance During High Current Pulse

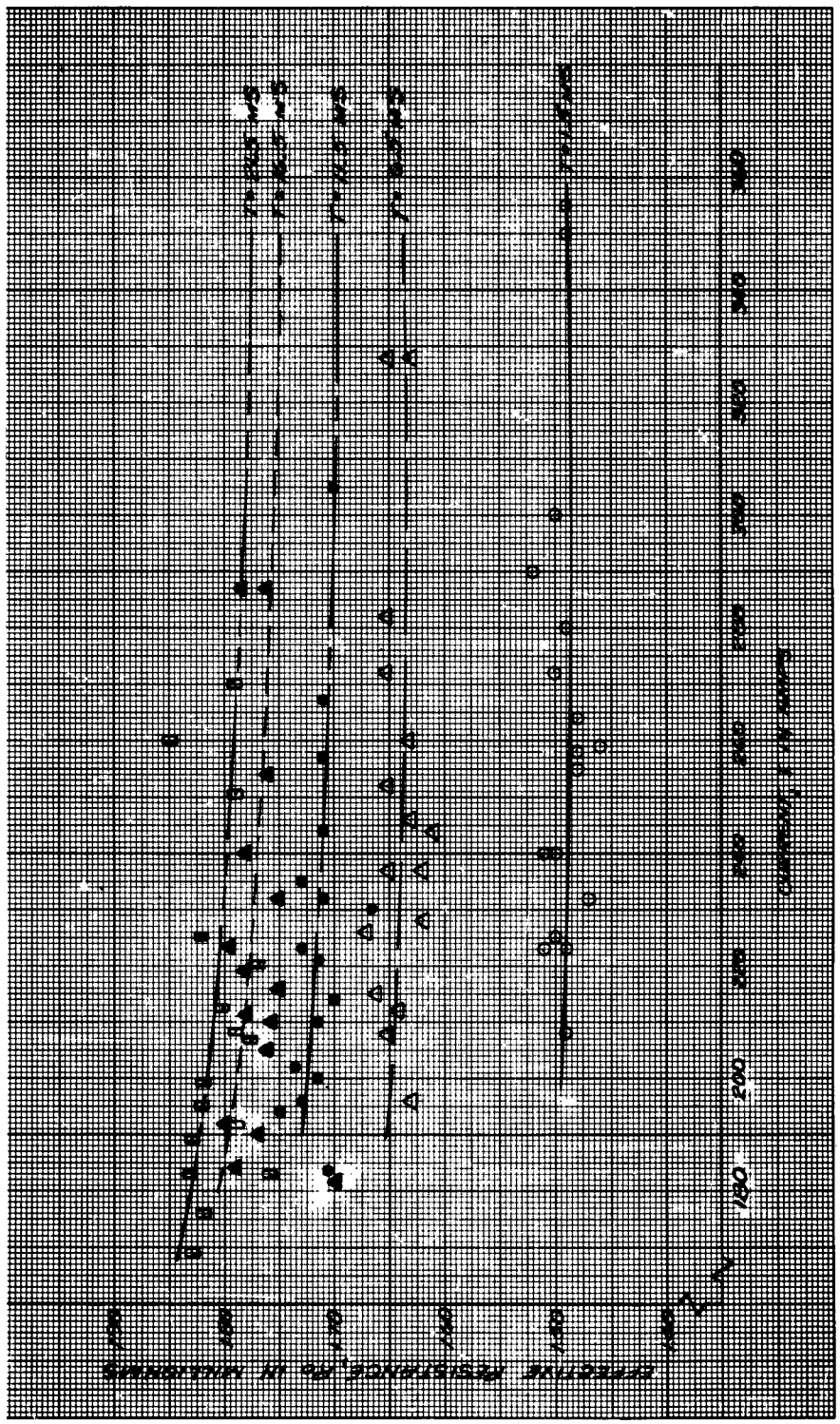

Figure 28 Effective Resistance Vs. Current and Time

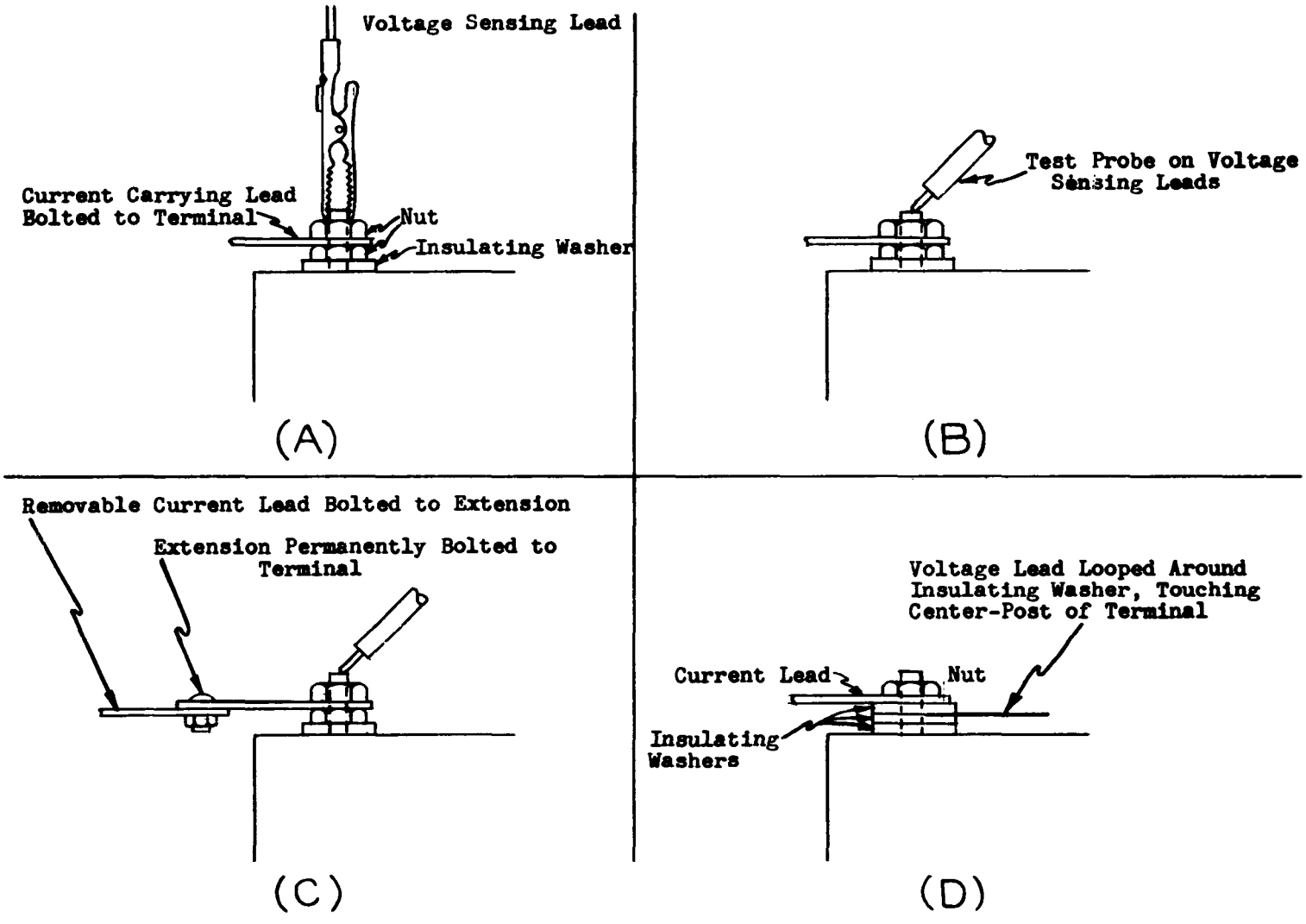

Figure 29 Four Methods of Connecting Voltage Leads to a Cell

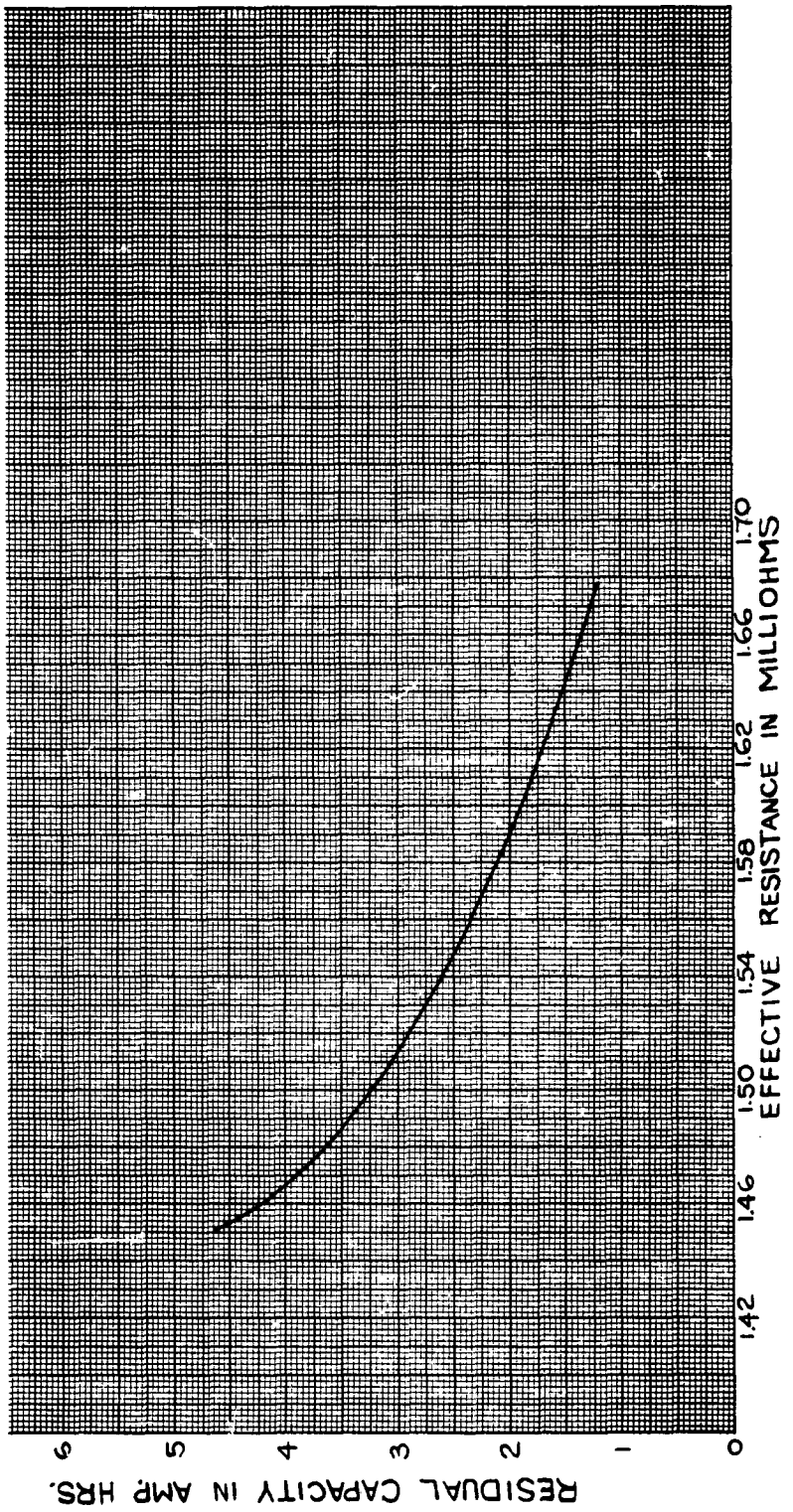

Figure 30 Average Curve of R_o Vs. R. C.

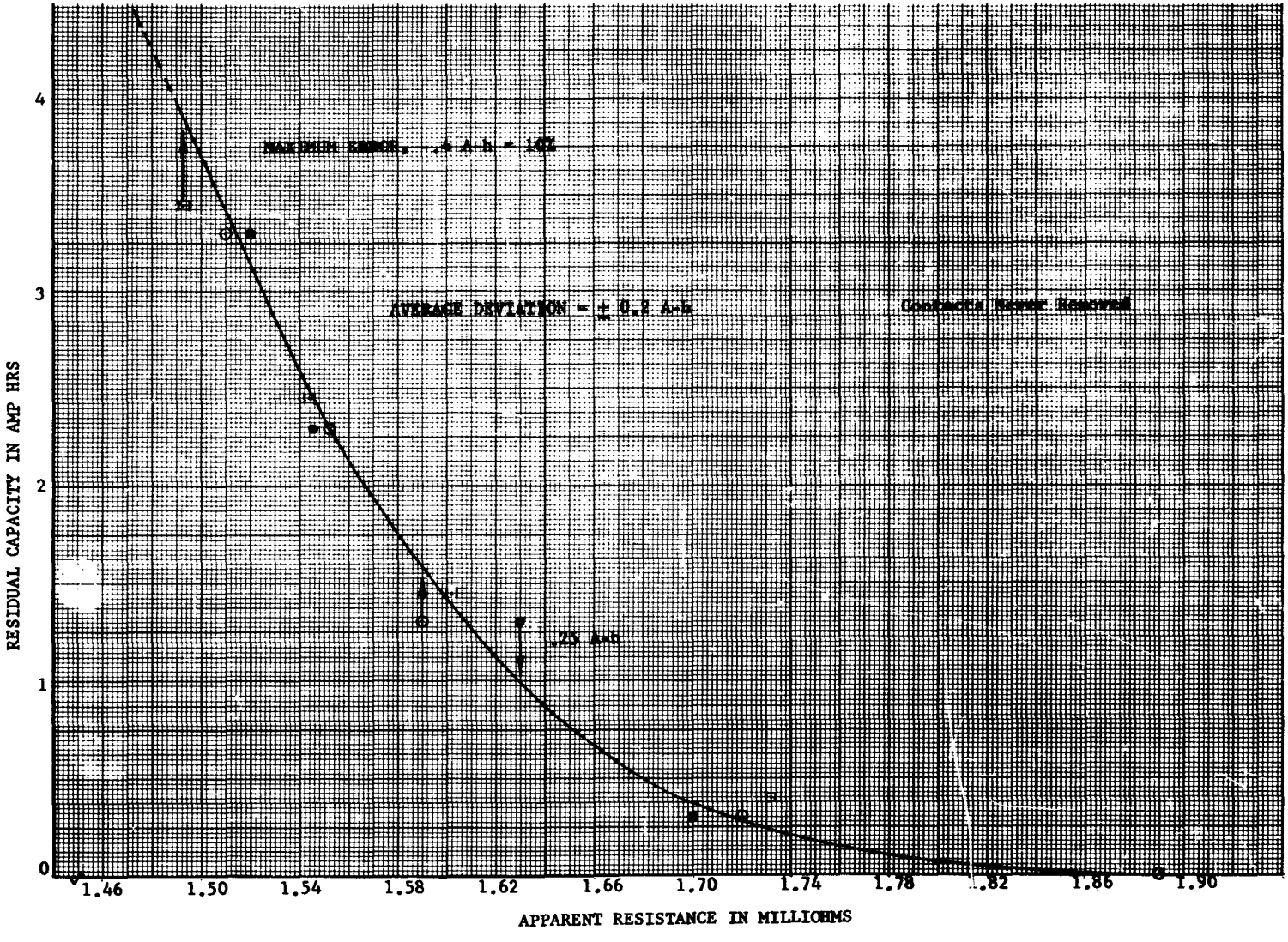

Figure 31 Resistance of Cell Permanently Connected to Apparatus

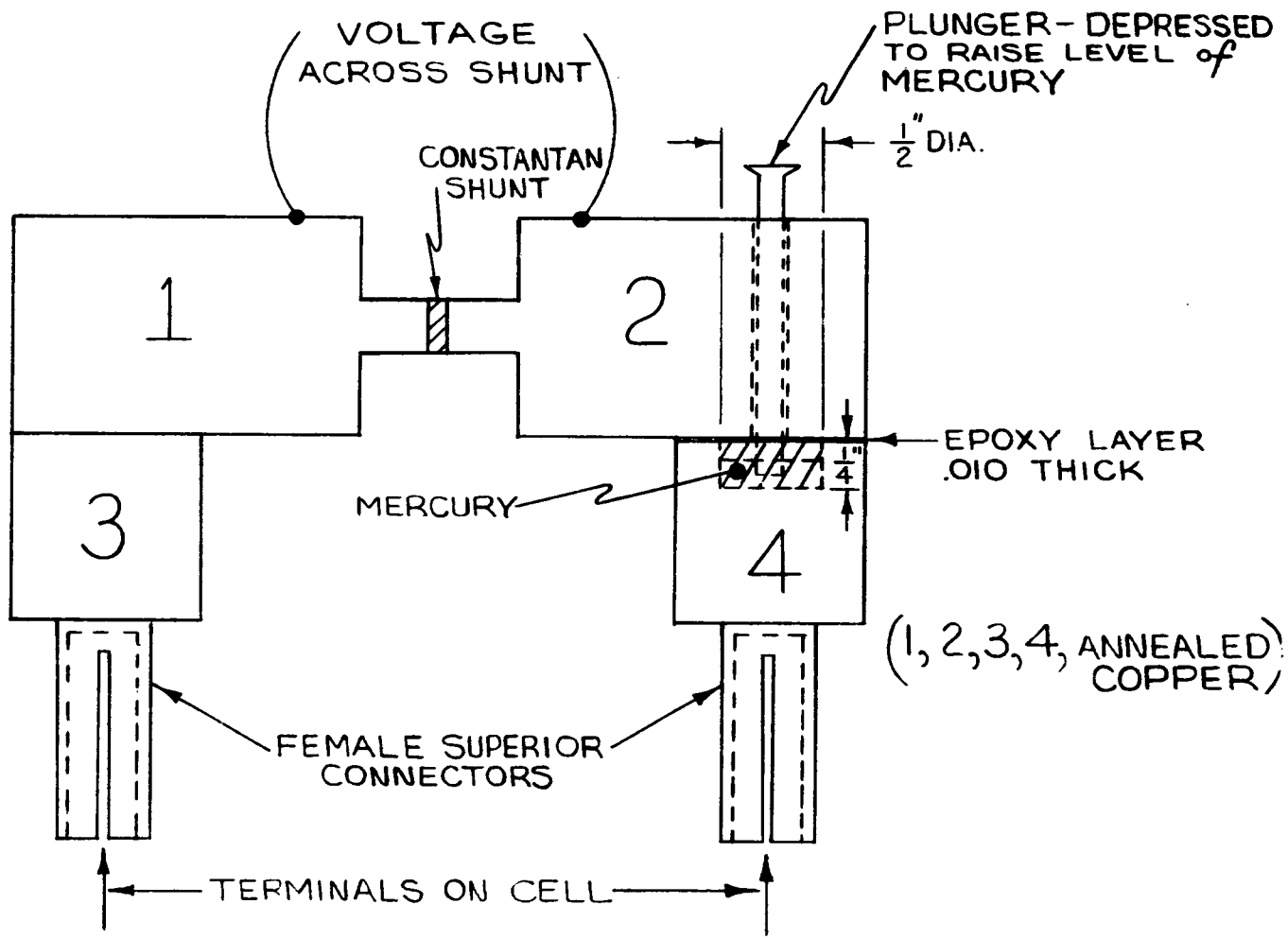

Figure 32 Design of Ultra-Low Resistance Switch

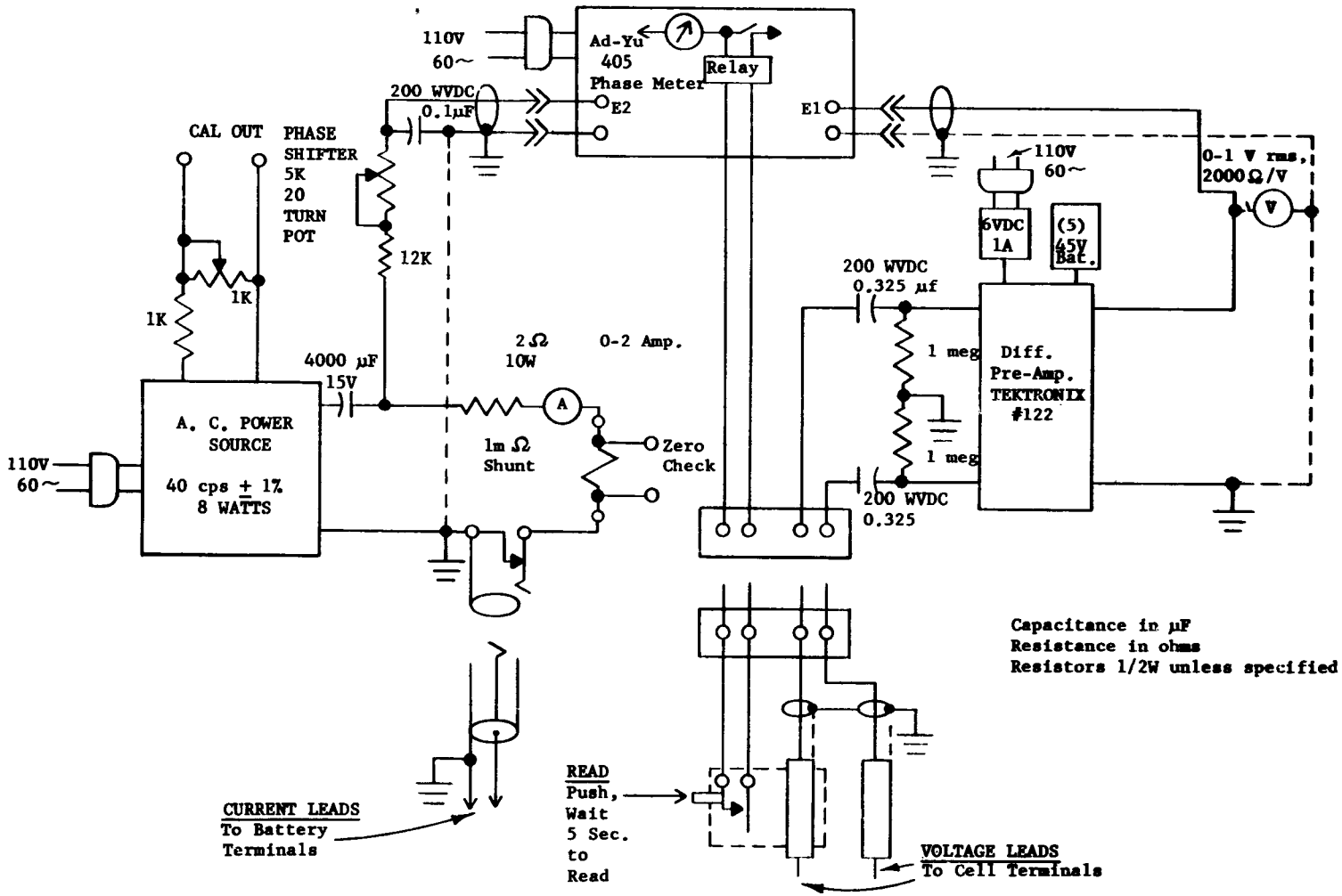

Figure 33 Block Diagram of Breadboard State of Charge Meter

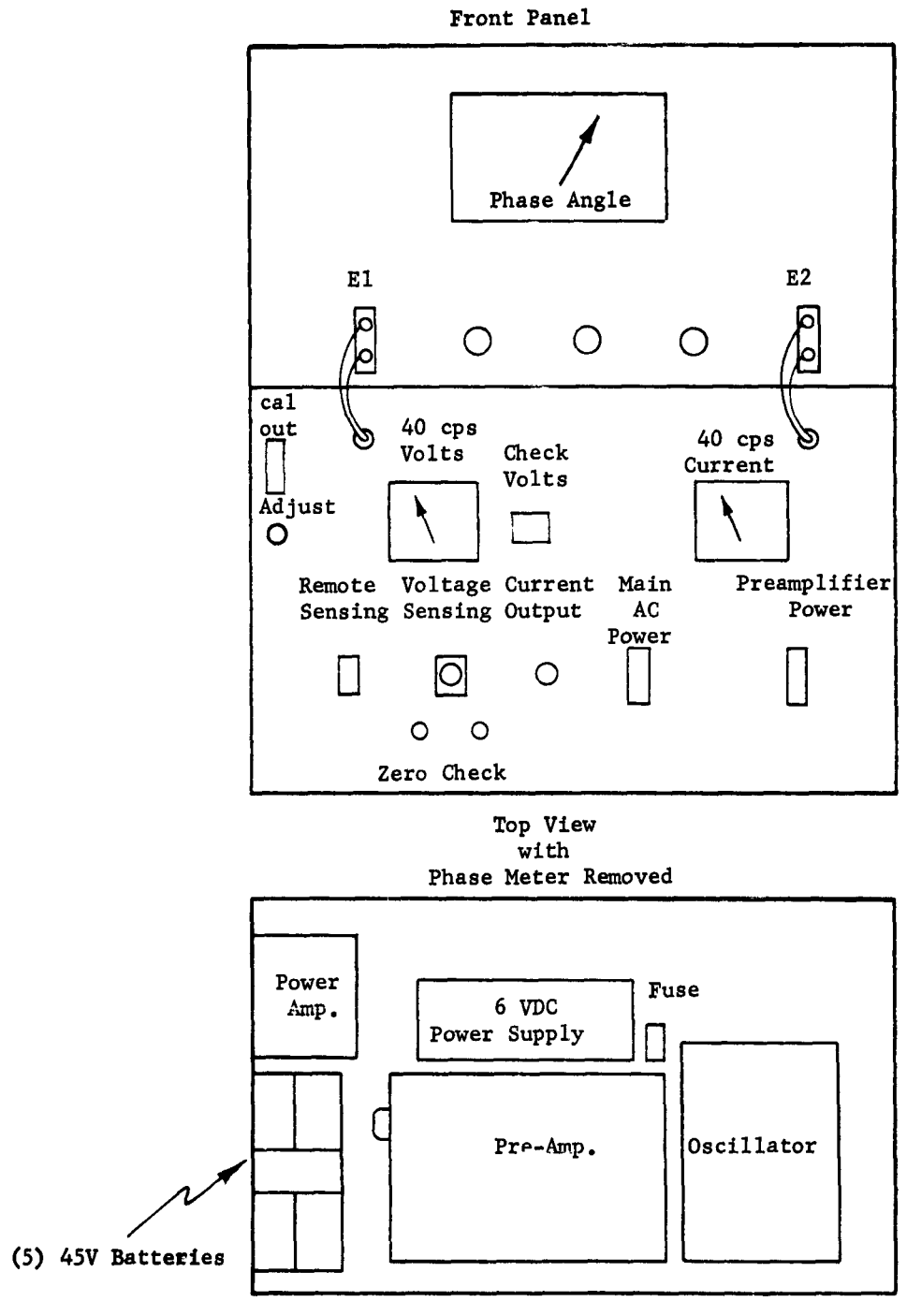

Figure 34 Layout of Breadboard State of Charge Meter

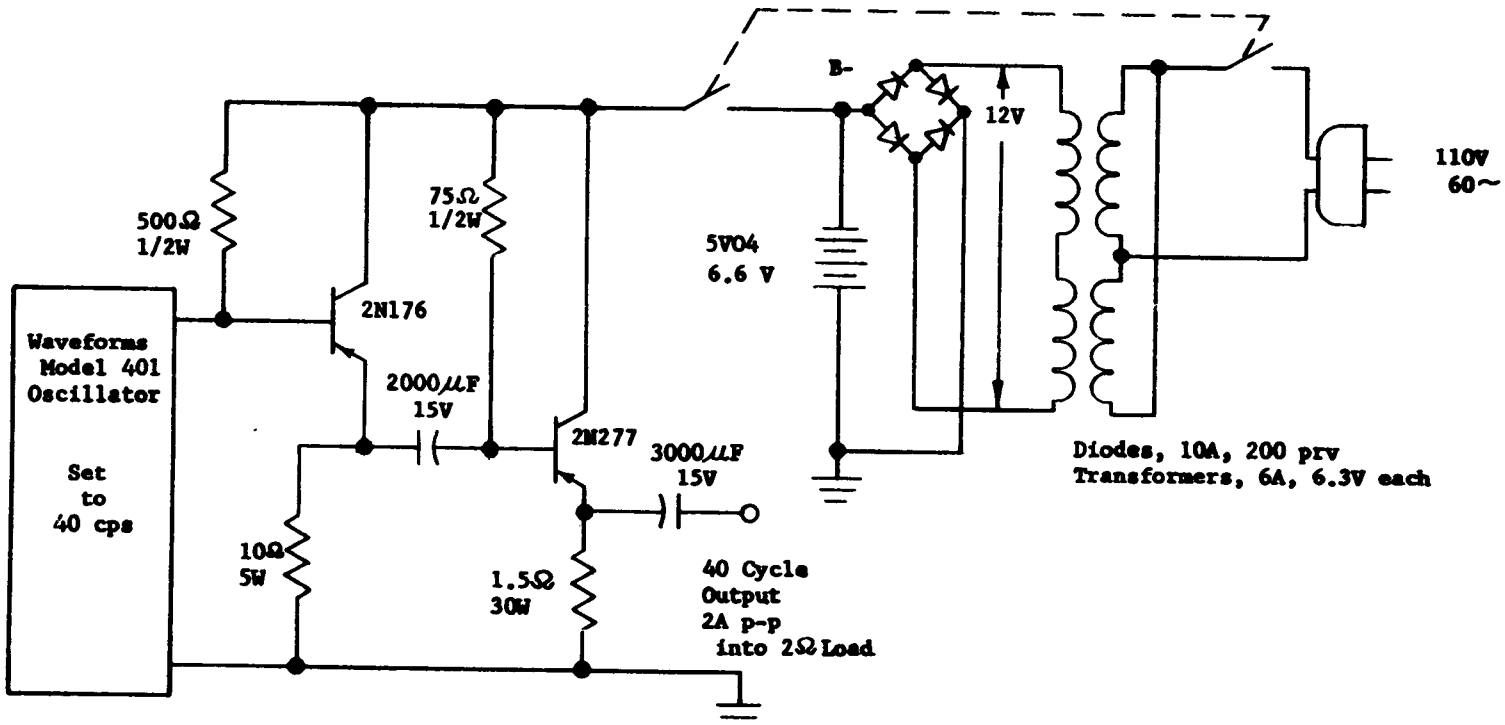

Figure 35 Schematic of 40 Cycle Power Amplifier

Aeronautical Systems Division, Dir./Aeromechanics. Flight Accessories Lab, Wright-Patterson AFB, Ohio.
Rpt. Nr. ASD-TDR-63-191. STATE OF CHARGE INDICATORS FOR ALKALINE BATTERIES. Final report, Feb. 63, 95p. incl. illus., tables, 5 refs.

Unclassified Report

The variations of several electrical properties of nickel cadmium cells with state of charge were studied to determine the suitability of any of these for measuring state of charge. Three methods were originally proposed: measurements of ohmic resistance, microsecond transients and double layer capacitance. During the investigations two additional parameters were measured, a.c. impedance and phase shift. Double layer capacitance and a.c. impedance and transient behavior are not useful properties for determining state of charge. A phase shift system is described which when properly calibrated predicted state of charge with an average deviation of ±10%. Ohmic resistance measured under correct conditions showed a closer correlation to state of charge but is difficult to measure.

UNCLASSIFIED

1. Charge indicators
2. Batteries and components
3. Alkaline cells
I. AFSC Project 8173
Task 817304
II. Contract AF 33 (657)-8130
III. Gulton Industries, Inc.
Metuchen, New Jersey
IV. M. Lurie, et al.
V. Aval fr OTS
VI. In ASTIA collection

Aeronautical Systems Division, Dir./Aeromechanics. Flight Accessories Lab, Wright-Patterson AFB, Ohio.
Rpt. Nr. ASD-TDR-63-191. STATE OF CHARGE INDICATORS FOR ALKALINE BATTERIES. Final report, Feb. 63, 95p. incl. illus., tables, 5 refs.

Unclassified Report

The variations of several electrical properties of nickel cadmium cells with state of charge were studied to determine the suitability of any of these for measuring state of charge. Three methods were originally proposed: measurements of ohmic resistance, microsecond transients and double layer capacitance. During the investigations two additional parameters were measured, a.c. impedance and phase shift. Double layer capacitance and a.c. impedance and transient behavior are not useful properties for determining state of charge. A phase shift system is described which when properly calibrated predicted state of charge with an average deviation of ±10%. Ohmic resistance measured under correct conditions showed a closer correlation to state of charge but is difficult to measure.

UNCLASSIFIED

1. Charge indicators
2. Batteries and components
3. Alkaline cells
I. AFSC Project 8173
Task 817304
II. Contract AF 33 (657)-8130
III. Gulton Industries, Inc.
Metuchen, New Jersey
IV. M. Lurie, et al.
V. Aval fr OTS
VI. In ASTIA collection

Aeronautical Systems Division, Dir./Aeromechanics. Flight Accessories Lab, Wright-Patterson AFB, Ohio.
Rpt. Nr. ASD-TDR-63-191. STATE OF CHARGE INDICATORS FOR ALKALINE BATTERIES. Final report, Feb. 63, 95p. incl. illus., tables, 5 refs.

Unclassified Report

The variations of several electrical properties of nickel cadmium cells with state of charge were studied to determine the suitability of any of these for measuring state of charge. Three methods were originally proposed: measurements of ohmic resistance, microsecond transients and double layer capacitance. During the investigations two additional parameters were measured, a.c. impedance and phase shift. Double layer capacitance and a.c. impedance and transient behavior are not useful properties for determining state of charge. A phase shift system is described which when properly calibrated predicted state of charge with an average deviation of ±10%. Ohmic resistance measured under correct conditions showed a closer correlation to state of charge but is difficult to measure.

UNCLASSIFIED

1. Charge indicators
2. Batteries and components
3. Alkaline cells
I. AFSC Project 8173
Task 817304
II. Contract AF 33 (657)-8130
III. Gulton Industries, Inc.
Metuchen, New Jersey
IV. M. Lurie, et al.
V. Aval fr OTS
VI. In ASTIA collection

Aeronautical Systems Division, Dir./Aeromechanics. Flight Accessories Lab, Wright-Patterson AFB, Ohio.
Rpt. Nr. ASD-TDR-63-191. STATE OF CHARGE INDICATORS FOR ALKALINE BATTERIES. Final report, Feb. 63, 95p. incl. illus., tables, 5 refs.

Unclassified Report

The variations of several electrical properties of nickel cadmium cells with state of charge were studied to determine the suitability of any of these for measuring state of charge. Three methods were originally proposed: measurements of ohmic resistance, microsecond transients and double layer capacitance. During the investigations two additional parameters were measured, a.c. impedance and phase shift. Double layer capacitance and a.c. impedance and transient behavior are not useful properties for determining state of charge. A phase shift system is described which when properly calibrated predicted state of charge with an average deviation of ±10%. Ohmic resistance measured under correct conditions showed a closer correlation to state of charge but is difficult to measure.

UNCLASSIFIED

1. Charge indicators
2. Batteries and components
3. Alkaline cells
I. AFSC Project 8173
Task 817304
II. Contract AF 33 (657)-8130
III. Gulton Industries, Inc.
Metuchen, New Jersey
IV. M. Lurie, et al.
V. Aval fr OTS
VI. In ASTIA collection